공학박사학위논문

Synthesis and Characterization of Organic/Inorganic Hybrid Ionogel Electrolytes Containing Crosslinkable Polysilsesquioxanes and Ionic Liquids for Lithium Battery Applications

폴리실세스퀴옥산 기반의 가교제와 이온성 액체를 포함하는 유/무기 복합 이온겔 전해질의 합성과 분석, 그리고 리튬 전지에의 응용

2016년 8월

서울대학교 대학원

화학생물공학부

이 진 홍

Synthesis and Characterization of Organic/Inorganic Hybrid Ionogel Electrolytes Containing Crosslinkable Polysilsesquioxanes and Ionic Liquids for Lithium Battery Applications

by

Jin Hong Lee

Adviser: Professor Yung-Eun Sung, Ph. D.

Submitted in Partial Fulfillment

of the Requirements for the Degree of

DOCTOR OF PHILOSOPHY

August, 2016

School of Chemical and Biological Engineering

College of Engineering

Graduate School

Seoul National University

Abstract

This study presents synthesis and characterization of organic/inorganic hybrid ionogel electrolytes containing cross-linkable silsesquioxanes and ionic liquids for lithium battery applications. Firstly, the synthesis of polysilsesquioxanes via a facile, base-catalysed system was used to obtain fully condensed, high molecular weight, ladder-like structured polysilsesquioxanes (LPMASQ) containing over one hundred methacryl moieties in a macromolecule. The fully condensed ladder-like structured LPMASQ provides imperceptible amounts of uncondensed silanol groups that only exist at the chain ends of the polymers. Due to the fully condensed structure, the LPMASQ provided good thermal and electrochemical stability and strong acid-resistance, which is an indispensable requirement for the ionogel electrolyte application. In addition, an abundance of the reactive methacryl pendant groups enhances the possibility that pendant groups meet each other and react to form covalent bonds. As a result, due to the unique structural feature, the fully condensed LPMASQ revealed the good efficiency for the inter-chain crosslinking reaction and achieved very fast gelation. A miniscule 2 wt % of LPMASQ was able to fully solidify the ionic liquid electrolyte solution to yield homogenous, pliant gels with high ionic conductivity and thermal stability. Lithium battery cell test performed with these hybrid gel

polymer electrolytes exhibited good Coulombic efficiency and cycling performance.

Secondly, a new series of inorganic-organic hybrid ionogel electrolytes consisting of an ionic liquid and synthesized ladder-like structured PEO-functionalized polysilsesquioxane with various PEO-copolymer compositions. By introducing the polyethylene oxide (PEO) groups at the molecular level to the inorganic polysilsesquioxane backbone and a thorough spectroscopic investigation into the ion conduction behavior of the hybrid ionogels as a function of PEO-copolymer composition, we were able to demonstrate how the PEO groups functioned to improve not only ionic conductivity, but their effects on optimal lithium ion battery performance at identical crosslinker concentration. In addition, we demonstrated that these hybrid ionogels revealed excellent thermal, electrochemical, and mechanical stability for improved safety in lithium ion battery cells.

Thirdly, a new methodology for fabrication of inorganic–organic hybrid ionogels and scaffolds was developed through facile crosslinking and solution extraction of a newly developed ionic polyhedral oligomeric silsesquioxane with inorganic core. Through design of various cationic tertiary amines as well of crosslinkable functional groups on each arm of the inorganic core, we were able to fabricate high performance ionogels with excellent electrochemical stability. The

well-defined, inter-connected, nano-sized pores and the unique ability to increase lithium transference led to exceptional lithium ion battery performance. Moreover, through solvent extraction of the liquid components, hybrid scaffolds with well-defined interconnected mesopores were utilized as heterogeneous catalysts for the CO_2-catalyzed cycloaddition of epoxides. Excellent catalytic performances, as well as highly efficient recyclability were observed when compared to other previous literature materials.

Finally, a novel ionic mixture of an imidazolium-based room temperature Ionic liquid containing ethylene oxide functionalized phosphite anion and a lithium salt that self-assembles into a smectic-ordered Ionic liquid crystal. The two key features in this study are the unique origin of the smectic order of the ionic mixtures and the facilitated ion transport behavior in the smectic ordered ionic liquid crystal. In fact, the ionic liquid crystals are self-assembled through Coulombic interactions between ion species, not through the hydrophilic-phobic interactions between charged ion heads and hydrophobic long alkyl pendants or the steric interaction between mesogenic moieties. Furthermore, the smectic order in the ionic crystal ionogel facilitates exceptional and remarkable ionic transport. Large ionic conductivity, viscoelastic robustness, and additional electrochemical stability of the Ionic liquid crystal ionogels provide promising opportunities for future electrochemical applications.

Keyword: Organic/Inorganic Hybrid, Gel polymer electrolyte, Ionic liquids, Ionogel, Silsesquioxane, Ionic liquid crystal, Lithium batteries.

Student Number: 2012-31301

TABLE OF CONTENT

Chapter 2

Preparation and Characterization of Hybrid Ionogel Electrolytes for High Temperature Lithium Battery Applications

Chapter 3

Ion Conduction Behavior in Chemically Cross-Linked Hybrid Ionogels: Effect of Free Dangling Oligo-PEOs

Chapter 4

Multifunctional Mesoporous Ionic Gels and Scaffolds Derived from Polyhedral Oligomeric Silsesquioxanes

Chapter 5

Facilitated Ion Transport in Smectic-like Ordered Ionic Liquid Crystals

List of Figures

List of Tables

Chapter 1

Introduction

1.1. Organic/Inorganic Hybrid Gel Polymer Electrolytes for Lithium Batteries

Over the past couple of decades, there have been immense research efforts to mitigate the safety concerns of liquid electrolytes in Li batteries, while maintaining practical battery performance. [1, 2] Liquid electrolytes, while inherently having large ionic conductivity, are comprised of lithium salts dissolved in flammable solvents, most commonly of the carbonate family. [3,4] These highly flammable solvents, coupled with the packaging issues arising from leakage of these solvents, have become key issues [1,2,5] for battery researchers as Li batteries have been considered the most practically viable power storage option for several applications not limited to cell phones, portable laptop computers and electronically powered vehicles. [5]

Two main strategies have been investigated to alleviate these safety concerns for the liquid electrolytes. First, to get rid of flammable solvents some approaches, such as blending polymers with lithium salts, have been performed as in the case of solid polymer electrolytes (SPE) [6–8]. Second, liquid electrolyte was solidified to form non-leaking gels, as appropriately the product was named gel polymer electrolytes (GPE). [9–11] Solid polymer electrolytes, while

completely free of solvents, usually suffer from low ionic conductivity (~10^{-5} S cm^{-1}) [6], due to severe restriction of the mobility of lithium ions in the solid state.

Gel polymer electrolytes can be further classified according to the method in which they are fabricated. Some GPEs are polymers swollen in electrolyte solutions (Figure 1.1), [9] with a great number of studies detailing the utility of using organic polymers, such as PVDF, PMMA, PVC, PAN, and some others as a matrix. [9,10] GPEs fabricated via this method provide good mechanical properties, while sacrificing ionic conductivity because of the large weight fraction of the organic polymer relative to the lithium salt needed to obtain gel properties. [11] Other GPEs are prepared through gelation of the liquid electrolyte in thermal- or photo-initiated processes using an oligomeric gelator with cross-linkable moieties, such as methacryl [12], acryl [13], or epoxy [14] derivatives. Although these GPEs have provided relatively larger ionic conductivity than all of the aforementioned polyelectrolytes, the contents of cross-linkable gelators, and their mechanical and thermal properties have remained issues for battery performance and stability.

Inorganic-organic hybrid materials, such as silicon-oxide based materials, have also been garnered great interest as support matrix for gel polymer electrolytes for their favorable properties; for instance, thermal stability, electrochemical stability and facile processing. [15–24] Several studies have

detailed the electrochemical studies and Li battery applications with chemically modified siloxanes, such as commercially available [RSiO1.5]n polysilsesquioxane-based ORMOCERS, [25] or [SiO2]n silica-based materials, as ionogel support matrix. [15–19] These approaches have either entailed the use of organic crosslinking functionalities or the in situ sol–gel gelation of liquid electrolyes using hydrolytic or non-hydrolytic sol–gel processes. [15–19] Notable studies by Vioux [17–19] and Panzer [15] groups have detailed the in situ gelation of ionic electrolytes to yield gel electrolyte with tunable flexibility. However, the fabrication of these gel electrolyte in situ sol–gel reactions may have a number of long-term problems in the solid state, as uncondensed silanol groups may produce water molecules through secondary condensations. Additionally, organic acids, such as formic acid, which are used for catalyzing the sol–gel hydrolysis-condensation rearrangements, may not be completely removed in vacuo, thus remaining as impurities. The long times (5 days~2 weeks) needed to solidify the ionic liquid in situ is also a process unfavorable for the industrial applications. [16]

Another class of hybrid gel polymer electrolytes includes composites of oxides particles. Functional silane-coated oxide-based nanoparticles, [26–29] which have been rigorously investigated by the Archer group, and ‘soggy sand’ electrolytes, which have been investigated by Bhattacharyya [30–32] are representative examples of such composites. Surface modification of oxide-based

nanoparticles coated with functional silanes (e.g., ionic liquid groups, oligo-polyethylene oxide groups, and single ion conducting groups) provides excellent electrochemical stability and mechanical robustness compared with the neat liquid electrolytes. [26] Soggy sands electrolytes, which comprise of oxide particles dispersed in non-aqueous liquid solutions, have also been widely investigated as structural supporting agents to solidify the liquid electrolytes. [30–33] However, for application in lithium ion battery, these hybrid gel polymer electrolytes should provide impeccable dispersion in liquid electrolytes to achieve well-defined homogeneous composites. Mechanical properties of these materials are still too low for such an application. These are issues that still need to be addressed and thoroughly investigated for practical lithium ion battery applications.

1.2. Ionic Liquid as Electrolytes for Lithium Batteries

Ionic liquids are a kind of molten salt composed of entirely ions but have melting point mostly below room temperature (Figure 1.2). [34] The salts are characterized by weak interactions due to the combination of a charge-delocalized anion and a large cation. [34, 35] Ionic liquids have been used in very wide application filed such as catalysis, separation, energy conversion, and storage for their excellent properties including insignificant vapor pressure, robust thermal

stability, wide electrochemical window, and designability [34-36].

In recent years, ionic liquids have been widely investigated as possible solutions for next generation of electrolytes in electrochemical cells due to their advantageous properties of high ionic conductivity, high electrochemical stability, non-flammability, negligible vapor pressure and high thermal stability. [35, 36] Despite these advantages over carbonate based lithium salt solutions, [37,38] ionic liquid electrolytes still face problems of leakage and high viscosity which has proved to be a serious concern for some applications, for instance in fully electronic or hybrid vehicles. [35] Moreover, ionic liquid electrolytes, while having inherently high ionic conductivity, are composed of lithium salts dissolved in quaternary ammonium-based ionic liquids, which leads to the well-known two-cation competition between the ionic liquid cation and lithium cation. [39] As such, the improvement in lithium mobility within ionic liquid solution to enhance lithium ion battery performance is still an ongoing challenge. Meanwhile, to solve the problem of leakage in ionic liquid electrolytes, GPEs composed of solidified ionic liquids, ionogels, have been pervasive in electrochemical device applications. To date, many ionogels have been fabricated using a variety of structural support materials, including polymers, colloidal particles, carbon nanotubes and cross-linkable small organic molecules. [40]

1.3. Motivation

Inorganic-organic hybrid electrolytes, such as sol-gel based solid polymer electrolytes and solidified ionic liquid ionogels, have been a hot topic of materials scientists for various electrochemical applications, including electrochromic devices, capacitors, and lithium ion batteries, because of their good thermal and electrochemical stabilities, and mechanical robustness. [7. 41-43] Several studies have detailed the electrochemical studies and Li battery applications with chemically modified siloxanes. However, the challenges of utilizing these sol-gel derived hybrid materials are the electrochemical instability of uncondensed silanol groups from uncontrolled siloxane structure, thus requiring substantial thermal treatments at elevated temperature. [42]

The literature survey indicated only one report for the use of silsesquioxanes as crosslinking moiety for the fabrication of GPEs. The study detailed the use of an amine-terminated butadiene crosslinked with an epoxy-functionalized T8 polyhedral silsesquioxane to make thermally ionic liquid gel. [44] However, the large POSS content and organic polymer required to gel the ionic liquid reduced the ionic conductivities. In another study, Li battery cell tests using an epoxy-functionalized cyclic siloxane thermally cured with only 2 wt % PS-co-P2VP (with respect to 1 M $LiPF_6$ electrolyte solution) has been reported.

[45] However, the use of multi-component crosslinking moieties, long times (~24 h) to fabricate these GPEs, coupled with the formation of considerable amounts of silanol groups after curing, make these GPEs tedious to prepare and unstable in the electrochemical cell performance.

Ladder-structured polysilsesquioxanes (LPSQ) belong to a unique class of polysilsesquioxanes in which the double stranded Si–O–Si siloxane structure is fully condensed in a polymeric network (Figure 1.3). [46–48] These polymeric materials offer enhanced processability, high solubility in a wide range of organic solvents and superior thermal and electrochemical stability [46–48].Conventional sol–gel derived random structured silsesquioxanes contain significant amounts of uncondensed silanol groups [49], which are electrochemically unstable at high voltages.[50] Moreover, these silanol groups undoubtedly cause siloxane structural change, especially at elevated temperatures, making sol–gel derived materials short-lived for device applications. [49] Recently, we developed a facile, one-pot synthesis of LPSQs utilising a base-catalysed system. [46–48] This method allowed the synthesis of fully condensed, high molecular weight LPSQs. Compared with other groups' syntheses of LPSQs [51,52], our method showed to be mass producible, making these materials highly applicable for industrial applications. For these reason, firstly we synthesized and characterized LPSQ with functional group, and then symmetrically studied on their application in

hybrid ionogel electrolyte for lithium batteries.

Polyhedral Oligomeric Silsesquioxanes, or more commonly known as POSS, are inorganic-organic hybrid materials with well-defined, inorganic siloxane polyhedral cores, with covalently bound organic functional groups stemming radially outwards. [53-56] The inner inorganic core is known as the smallest silica particle, as the free-volume of the POSS was reported to be as small as a sphere with diameter ~3 nm. [57] This nano-sized core and organic functional groups allows for solubility and/or impeccable dispersability in a wide variety of solvents. Moreover, through the myriad of organic functional groups that can be introduced, various functional materials can be fabricated through thermal or UV-initiated processes. Based on the understanding of unique features of POSS material, we fabricated a hybrid ionogel with a fully ionic group-substituted POSS. Examination of various properties including compatibility with ionic liquids, thermal, mechanical, electrochemical, and catalytic traits was conducted.

1.4. References

[1] J.-M. Tarascon and M. Armand, Nature (2001) 414, 359-367.

[2] N.-S. Choi, Z. Chen, S.A. Frruenberger, X. Ji, Y.-K. Sun, K. Amine, G. Yushin, L.F. Nazar, J. Cho, and P.G. Bruce, Angew. Chem. Int. Ed. (2012) 51, 9994-10024.

[3] K. Xu, Chem. Rev. (2004) 104, 4303-4417.

[4] Z. Chen, Y. Ren, A.N. Jansen, C.-K. Lin, W. Wang, and K. Amine, Nature Comm. (2013) 4:1513.

[5] A. Yoshino, Angew. Chem. Int. Ed. (2012) 51, 5798-5800.

[6] P. Lightfoot, M.A. Mehta, and P.G. Bruce, Science (1993) 262, 883-885.

[7] R. Bouchet, S. Maria, R. Meziane, A. Aboulaich, L. Lienafa, J.-P. Bonnet, T.N.T. Phan, D. Bertin, D. Gigmes, D. Devaux, R. Denoyel, and M. Armand, Nat. Mater. (2013) 12, 453-457.

[8] H. Kao and C.-L. Chen, Angew. Chem. Int. Ed. (2004) 43, 980-984.

[9] J.Y. Song, Y.Y. Wang, and C.C. Wan, J. Power Sources (1999) 77, 183-197.

[10] A.M. Stephan, Eur. Polym. J. (2006) 42, 21-42.

[11] A.M. Stephan and K.S. Nahm, Polymer (2006) 47, 5952-5964.

[12] D. Zhou, L.-Z. Fan, H. Fan, and Q. Shi, Electrochim. Acta (2013) 89, 334-338.

[13] J.-A. Choi, Y. Kang, H. Shim, D.W. Kim, H.-K. Song, and D.-W. Kim, J. Power Sources (2009) 189, 809-813.

[14] D. Saikia, H.-Y. Wu, Y.-C. Pan, C.-P. Lin, K.-P. Huang, K.-N. Chen, G.T.K. Fey, and H.-M. Kao, J. Power Sources (2011) 196, 2826-2834.

[15] A. I. Horowitz and M. J. Panzer, J. Mater. Chem. (2012) 22, 16534–16539.

[16] A. K. Gupta, M. P. Singh, R. K. Singh and S. Chandra, Dalton Trans., (2012) 41, 6362–6371.

[17] L. Viau, M.-A. Neouze, C. Biolley, S. Wolland, D. Brevet, P. Gaveau, P. Diudonne, A. Galarneau and A. Vioux, Chem. Mater. (2012) 24, 3128–3134.

[18] F. Gayet, L. Viau, F. Leroux, S. Monge, J.-J. Robin and A. Vioux, J. Mater. Chem. (2010) 20, 9456–9462.

[19] M.-A. Neouze, J.L. Bideau, P. Gaveau, S. Bellayer and A. Vioux, Chem. Mater. (2006) 18, 3931–3936.

[20] T. Echelmeyer, H. W. Meyer and L. Wullen, Chem. Mater. (2009) 21, 2280–2285.

[21] K. Matsumoto and T. Endo, Macromolecules (2009) 42, 4580–4584.

[22] R. K. Donato, L. Matejka, H. S. Schrekker, J. Plestil, A. Jigounov, J. Brus and M. Slouf, J. Mater. Chem. (2011) 21, 13801–13810.

[23] F. Gayet, L. Viau, F. Leroux, F. Mabille, S. Monge, J.-J. Robin and A.

Vioux, Chem. Mater. (2009), 21, 5575–5577.

[24] A. Vioux, L. Viau, S. Volland and J. L. Bideau, C.R. Chimie (2010) 13, 242–255.

[25] M. Popall, M. Andrei, J. Kappel, J. Kron, K. Olma and B. Olsowski, Electrochim. Acta (1998) 43, 1155–1161.

[26] Y. Lu, K. Korf, Y. Kambe, Z. Tu and L. A. Archer, Angew. Chem. Int. Ed. (2014) 53, 488–492.

[27] J. L. Schaefer, D. A. Yanga and L. A. Archer, Chem. Mater. (2013) 25, 834–839.

[28] Y. Lu, S. S. Moganty, J. L. Schaefer and L. A. Archer, J. Mater. Chem. (2012) 22, 4066–4072.

[29] S. S. Moganty, S. Srivastava, Y. Lu, J. L. Schaefer, S. A. Rizvi and L.A. Archer, Chem. Mater. (2012) 24, 1386–1392.

[30] S. K. Das, S. S. Mandal and A. J. Bhattacharyya, Energy Environ. Sci. (2011) 4, 139101399.

[31] M. Patel, M. Gnanavel and A. J. Bhattacharyya, J. Mater. Chem. (2011) 21, 17419–17424.

[32] S. K. Das and A. J. Bhattacharyya, J. Phys. Chem. C. (2009) 16, 6699–6705.

[33] C. Pfaffenhuber, M. Gobel, J. Popovic and J. Maier, Phys. Chem. Chem.

Phys. (2013) 15, 18318–18335.

[34] T. Welton, Chem. Rev. (1999) 99, 2071-2083.

[35] M. Armand, F. Endres, D. R. Macfarlane, H. Ohno, B. Scrosati, Nat. Mater. (2009) 8, 621-629.

[36] H. Niedemeyer, J. P. Hallett, I. J. Villar-Garcia, P. A. Hunt, T. Welton, Chem. Rev. (2012) 41, 7780-7802.

[37] K. Xu, Chem. Rev. (2004) 104, 4303–4417.

[38] Z. Chen, Y. Ren, A.N. Jansen, C.-K. Lin, W. Wang and K. Amine, Nat. Commun. (2013) 4, 1513.

[39] S.-Y. Lee, H.H. Yong, Y.J. Lee, S.K. Kim and S. Ahn, J. Phys. Chem. B (2005) 109, 13663-113667.

[40] D. M. Tigelaar, M. A. B. Meador and W. R. Bennet, Macromolecules (2007) 40, 4159–4164.

[41] Y. Lu, K. Korf, Y. Kambe, Z. Tu and L.A. Archer, Angew. Chem., Int. Ed. (2014) 53, 488.

[42] N. Boarett, A. Bittner, C. Brinkmann, B.-E. Olsowski, J. Schulz, M. Seyfried, K. Vezzu, M. Popall and V.D. Noto, Chem. Mater. (2014) 26, 6339.

[43] A. Guyomard-Lack, J. Abusleme, P. Soudan, B. Lestriez, D. Guyomard and J.L. Bideau, Adv. Energy Mater. (2014) 4, 1301570.

[44] M. Li, W. Ren, Y. Zhang, and Y. Zhang, J. Appl. Polym. Sci. (2012) 126, 273-279.

[45] S. Oh, D.W. Kim, C. Lee, M.-H. Lee, and Y. Kang, Electrochim. Acta (2011) 57, 46-51.

[46] S-S. Choi, H.S. Lee, S.S. Hwang, D.H. Choi, and K.-Y. Baek, J. Mater. Chem. (2010) 20, 9852-9854.

[47] A.S. Lee, S.-S. Choi, H.S. Lee, H.Y. Jeon, K.-Y. Baek, and S.S. Hwang, J. Polym. Sci. A. Polym. Chem. (2012) 50, 2653-4570.

[48] S.-S. Choi, A.S. Lee, H.S. Lee, H.Y. Jeon, K.-Y. Baek, D.H. Choi, and S.S. Hwang, J. Polym. Sci. A. Polym. Chem. (2011) 49, 5012-5018.

[49] K. Su, D.R. Buljalski, K. Eguchi, G.V. Gordon, D.L. Ou, P. Chevalier, S. Hu, and R.P. Boisvert, Chem. Mater. (2005) 17, 2520-2529.

[50] A. Walcarius, D. Mandler, J.A. Cox, M. Collinson, and O. Lev, J. Mater. Chem. (2005) 15, 3663-3689..

[51] Z.X. Zhang, J. Hao, P. Xie, X. Zhang, C.C. Han, and R. Zhang, Chem Mater. (2008) 20, 1322-1330.

[52] S. Chang, T. Matsumoto, H. Matsumoto, and M. Unno, Appl. Organometal. Chem. (2010) 24, 241-246.

[53] Z. Li, D. Wu, Y. Liang, R. Fu, K. Matyjaszewski, J. Am. Chem. Soc. (2014) 136, 4805-4808

[54] S. Wang, L. Tan, C. Zhang, I. Hussain, B. Tan, J. Mater. Chem. A (2015) 3, 6542-6548.

[55] A. S. Lee, S.-S. Choi, H. S. Lee, K.-Y. Baek, S. S. Hwang, Dalton Trans. 2012, 41, 10585-10588.

[56] M. Seino, W. Wang, J. E. Lofgreen, D. P. Puzzo, T. Manabe, G. A. Ozin, J. Am. Chem. Soc. 2011, 133, 18082-18085.

[57] D. B. Cordes, P. D. Lickiss, F. Rataboul, Chem. Rev. (2010) 110, 2081-2173.

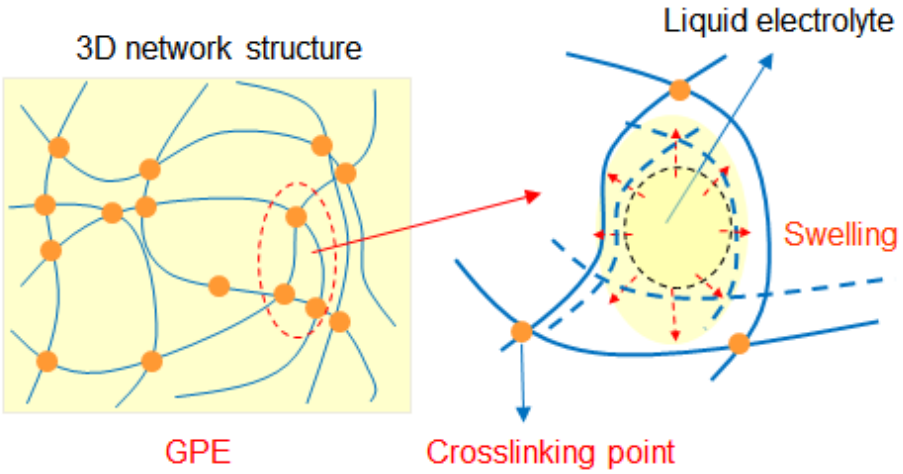

Figure 1.1. Schematic illustration of gel polymer electrolyte (GPE).

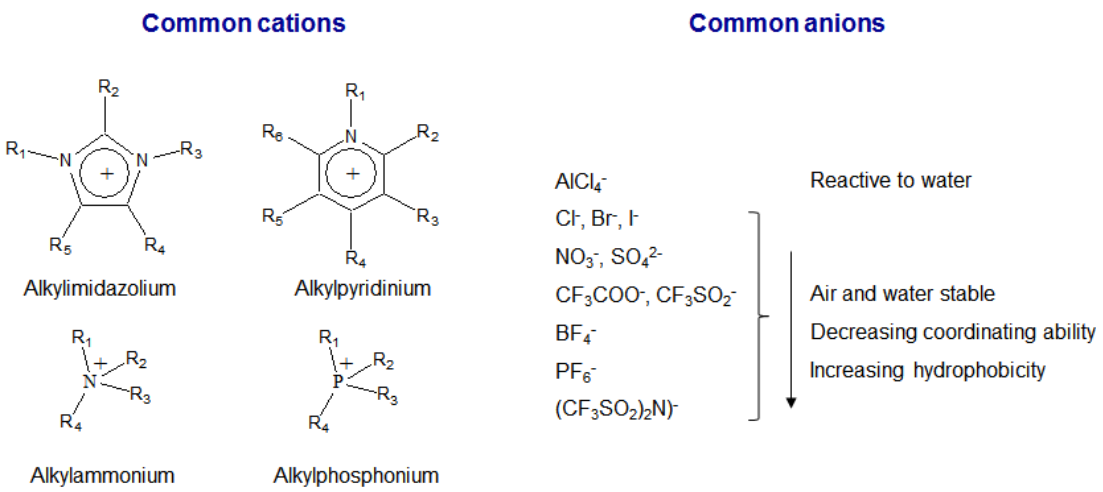

Figure 1.2. Typical ionic liquid molecular structures.

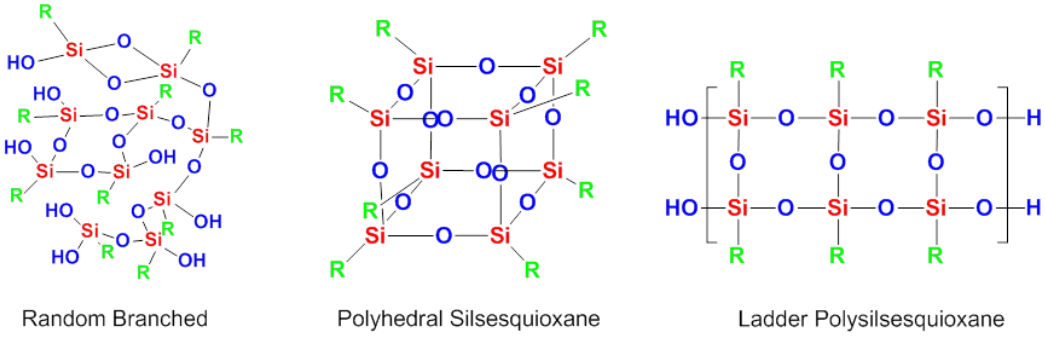

Figure 1.3. Various structures of polysilsesquioxanes.

Chapter 2

Preparation and Characterization of Hybrid Ionogel Electrolytes for High Temperature Lithium Battery Applications

2.1. Introduction

Lithium ion batteries are highly sought out as the energy storage solution for various applications ranging from portable electronic devices to hybrid vehicles. [1] And as these electronic devices have become more common in everyday human life, battery safety has become one of the key issues to be required along with high performance.[2,3] The need to fortify the safety of lithium ion batteries stems from the thermal instability of conventional commercial non-aqueous liquid electrolytes, as the volatile organic solvents under high temperature conditions renders volumetric expansion of cells and electrolyte leakage, which in turn leads to cell short circuit and possible explosions.[4,5] As such, the use of ionic liquids, and their solidified gel counterparts, so-called ‘ionogels’, have received much attention in recent years.[6-8]

Ionogels can be fabricated by a number of different methods which include swelling in physically crosslinked networks with polymers,[9] or chemical crosslinked through either UV / thermal treatment with multifunctional crosslinkable organic moieties. [10] While both methods have proved to be utile in various cases, the *in-situ* mix-and-cure system of utilizing multifunctional cross-linkers can be considered the most practical for device fabrication. To date,

a vast amount of literature studies have been devoted to study the various organic,[10] hybrid,[11,12] and inorganic[13] materials as ionic liquid crosslinkers for the fabrication of ionogels.

While these approaches have been proved to be extremely useful for the fabrication of gels and films, considerable amounts of matrix or crosslinking agent compared with the liquid electrolyte needed for the solidification of ionic liquids have had major depreciating effects on the electrochemical device performances. [14] Therefore, minimal use of the crosslinking agent, while maintaining non-flowing, solid-like behaviour, has remained a challenge for optimal electrochemical devices.

Polysilsesquioxanes (PSQs) with chemical formula [RSiO1.5] n are a class of inorganic–organic hybrid materials in which a silicon oxide network structure is equipped with an organic functionality. [15] There are three structural classes of PSQs, random-branched network, polyhedral cage and ladder-like polymers. Ionogels fabricated from random-branched structural PSQ-modified silica particles suffer from remnant silanol groups that will condense to form water molecules over time, making their applications in Li batteries practically infeasible.

Ladder-like structured polysilsesquioxanes (LPSQs) are a unique class of silsesquioxanes in which the siloxane bond is double stranded and the

organic functional groups are unidirectionally positioned to the siloxane bonds. [16–21] These materials exhibit enhanced solubility and superior thermal stability because of the imperceptible amount of silanol groups, which only reside at the polymer end groups. [16-21] The acid resistance and insensitivity to thermal history characters can also be said to be the highly attractive merits of these materials as polymer electrolytes. The polymeric nature of these materials allows for the introduction of several hundreds of organic moieties per polymer chain for a fast and easy curing process. [16, 17] Recently, our research group developed a facile, one-pot synthesis of LPSQs using a base-catalysed system. [16–19] The products of the synthesis were fully condensed high molecular weight LPSQs. Compared with the above approaches towards hybrid gel polymer electrolytes, these materials are highly soluble in non-aqueous electrolytes and ionic liquids, leading to high homogeneity, whereas they need only a small amount of gelator.

In this study, we synthesized a novel ladder-structured poly-(methacryloxypropyl)silsesquioxane (LPMASQ) following our method and used it as a cross-linker for an ionic liquid electrolyte, 1 M LiTFSI in N-butyl-N-methylpyrrolidinium bis(tri-fluoromethylsulfonyl)imide (BMPTFSI). Thermal cross-linking of the methacryl moieties of LPMASQ

resulted in homogeneous, non-leaking hybrid ionogels. The thermal, mechanical and flame-retardant properties of these inorganic–organic hybrid gel polymer electrolytes were examined and Li battery cells were fabricated to test their applications as thermally stable and high performance ionogels.

2.2. Experimental

Materials

3-methacryloxypropyltrimethoxysilane (Shin-Etsu, 98%) and ethyl acetate (J.T. Baker, HPLC grade) were distilled over CaH_2 prior to use. Potassium carbonate (Daejung) was dried at 40 °C. THF (J.T. Baker, HPLC grade) was distilled over sodium. Azobisisobutyronitrile (Daejung) was recrystallised from methanol. Lithium bis(trifluoromethylsulfonyl)imide (LiTFSI) (Aldrich, 99.9%, battery grade), 1-methylpyrrolidine (Aldrich, 98%), 1-iodobutane (Aldrich, 99%) and all other solvents were used as received.

Synthesis of LPMASQ

LPMASQ was synthesized following a known literature procedure. [37–40] In a typical experiment, potassium carbonate, K_2CO_3 (0.04 g, 0.29 mmol) was dissolved in deionised H_2O (4.8 mL, 0.27 mol) and 8 g of THF was added. To this solution, 3-methacryloxypropyltrimethoxysilane (19.9 mL, 0.08 mol) was added dropwise under nitrogen flow. The solution was

magnetically stirred for 10 days when the molecular weight reached its maximum value. After partial evaporation of THF, the resinous material was dissolved in dichloromethane and extracted several times with water. Collection of the organic layers followed by drying of the organic layer over anhydrous magnesium sulphate and evaporation of the solvent under reduced pressure yielded a transparent liquid with medium viscosity (15.2 g, 95% crude yield). LPMASQ was found to have excellent solubility in the majority of organic solvents.

^{1}H NMR ($CDCl_3$) (δ, ppm): (0.48–0.78, $SiC\mathit{H}_2CH_2CH_2OCOCCH_2CH_3$),

(1.5–1.75, $SiCH_2C\mathit{H}_2CH_2OCOCCH_2CH_3$),

(3.9–4.1, $iCH_2CH_2C\mathit{H}_2OCOCCH_2CH_3$), (5.4, 5.9, $SiCH_2CH_2CH_2OCOCC\mathit{H}_2CH_3$),

(1.75–1.85, $SiCH_2CH_2CH_2OCOCCH_2C\mathit{H}_3$),

^{13}C NMR ($CDCl_3$) (δ, ppm): (7.6–10.3, $Si\mathit{C}H_2CH_2CH_2OCOCCH_2CH_3$),

(17.5–18.5, $SiCH_2CH_2CH_2OCOCCH_2CH_3$),

(21.2–22.4, $SiCH_2\mathit{C}H_2CH_2OCOCCH_2CH_3$),

(65.4–66.8, $SiCH_2CH_2\mathit{C}H_2OCOCCH_2CH_3$),

(124.4–126.1, $SiCH_2CH_2CH_2OCOC\mathit{C}H_2CH_3$),

(135.5–136.9, $SiCH_2CH_2CH_2OCO\mathit{C}CH_2CH_3$),

(166.6–168.6, $SiCH_2CH_2CH_2OCOCCH_2CH_3$),

^{29}Si NMR (ppm): –65 to –68 ppm,

M_w = 26,000 g mol^{-1}, M_w/M_n = 2.1

Synthesis of *N*-butyl-*N*-methyl pyrrolidinium bis (trifluoromethylsulfonyl) imide

Synthesis of BMPTFSI was performed following literature procedure.[43] In a dry 500 mL round-bottom flask, stoichiometric amounts of 1-methylpyrrolidine (50 g, 0.59 mol) and 1-iodobutane (108 g, 0.59 mol) in 250 mL of ethyl acetate were magnetically stirred at room temperature for 24 h. The product was repeatedly washed with ethyl acetate and filtered until pure white salt of BMPI was obtained. BMPI was then dissolved in deionized water and mixed with a stoichiometric amount of LiTFSI dissolved in deionized water. The organic phase was extracted with methylene chloride and subsequently dried at 100 °C for 24 h to remove any residual water. The resulting BMP–TFSI had H_2O content of less than 100 ppm as measured with the Karl Fischer method.

Preparation of Inorganic–Organic Hybrid Ionogel Electrolytes

In an inert, argon-charged glove, solutions with various amounts of LPMASQ in 1M LiTFSI in BMPTFSI were prepared in glass vial. An amount of 1 wt % (relative to LPMASQ) of AIBN as thermal initiator was added to this solution. After taking the solutions out of the glove box, samples were sonicated and shaken for 10 min or until the solution was homogenous. Then, the samples were directly taken to an oven preset at 70 °C for 3 h. The hybrid ionogels were named as HI-2 and HI-5 for ionogels containing 2 and 5 wt % of LPMASQ, respectively.

Characterization

Fourier transform infrared spectra were measured with a Perkin-Elmer FT-IR system Spectrum-GX. Number average molecular weight (M_n) and molecular weight distributions (M_w/M_n) of polymers were measured using JASCO PU-2080 plus SEC system equipped with refractive index detector (RI-2031 plus), UV detector (λ = 254 nm, UV-2075 plus) and Viscotek SLS apparatus using THF as the mobile phase at 40 °C with a flow rate of 1 mL min^{-1}. The samples were separated through four columns (Shodex-GPC KF-802, KF-803, KF-804, and KF-805). ^{1}H-NMR and ^{29}Si

NMR spectra were recorded in $CDCl_3$ at 25 °C using a Varian Unity INOVA (^{1}H: 300 MHz, ^{29}Si: 59.6 MHz). Thermal gravimetric analysis was carried out with TA instrument (TGA 2950) at heating rate of 10 °C min^{-1} under N_2 atmosphere.

Rheological properties were examined using a rheometer (Advanced Rheometric Expansion System, ARES) instrument with cone-plate geometry (25 mm diameter). All rheological measurements were performed in the linear viscoelastic region under nitrogen atmosphere.

The ionic conductivity was determined using a complex impedance analyzer (Bio-Logics, VMP3) over frequency range from 1 Hz to 1 MHz at AC amplitude of 10 mV. The electrochemical stability of the gel polymer electrolytes was examined using a linear sweep voltammetry system. In the experiments, a stainless steel working electrode was used with lithium metal as both the counter and reference electrodes. The voltage was swept at a scan rate of 1.0 mV s^{-1}. The time evolution dependence of interfacial resistance between the lithium metal and the ionogel was measured through monitoring the AC impedance response over the frequency range from 100 KHz to 10 MHz of the Li/HI-2/Li symmetric cells. Electrochemical measurements of the gel polymer electrolyte were conducted using 2032 coin cells consisting of a separator, Li metal and a $LiFePO_4$ cathode (90 wt %

$LiFePO_4$, 5 wt % carbon black, 5 wt % PVDF). All the cells were assembled in argon-charged glove box. After fabrication, the cells with pre-gel solution were subjected to thermal cross-linking for 3 h at 70 °C. The galvanostatic charge-discharge experiments were carried out with voltage range of 2.5–4.2 V using a battery cycler (Wonatech, WBCS3000) in various temperatures.

2.3. Results and Discussion

The structure of LPMASQ synthesized according to Figure 2.1 was analyzed by 1HNMR, ^{13}C NMR, ^{29}Si NMR, FT-IR, GPC, and TGA techniques. The LPMASQ was observed as a transparent and resinous liquid with a weight averaged molecular weight of 26 000 g mol^{-1}. ^{1}H NMR (Figure. 2.2(a)) revealed the appropriate peaks for the methacryloxypropyl groups and revealed that no unhydrolysed methoxy or uncondensed silanol groups were remaining. Furthermore, ^{29}Si NMR results (Figure 2.2(b)) showed a monomodal peak centred at -68 ppm, which was assigned to the T3 (alkyl-Si(OSi–)3) structure, [24] indicative of fully condensed siloxane structures. No peaks were found at -58 ppm, belonging to T2 (alkyl-Si(OSi–)2OH) uncondensed silicons. [24] FT-IR analyses (Figure. 2.3) also showed that no silanol groups were present, as no discernible peaks at 3500 or 960 cm^{-1} were observed, and the doubly split siloxane peaks at 1040 and 1150 cm^{-1} indicated a ladder-like polymeric structure. [22-24] TGA thermograms of LPMASQ showed no secondary condensations indicative of the absence of uncondensed silanol groups (Figure. 2.4) and gave an initial degradation temperature at 380 ^{o}C, exhibiting superior thermal stability. It should be noted that the fully condensed LPMASQ exhibits excellent chemical resistance

to acids that may be due to the lithium salts under humid conditions, [24] and is insensitive to thermal history, [24] making LPSQ materials highly attractive as polymeric electrolytes.

The obtained LPMASQ was then dissolved in an ionic liquid solution of 1M LiTFSI in BMPTFSI with various amounts of AIBN as thermal initiator. Through mild thermal treatment at 70 °C, non-leaking, homogenous hybrid ionogels were able to be easily processed as free-standing gels. We expected the LPMASQ network being formed after crosslinking was loose enough to facilitate high lithium mobility within the LPMASQ network. The obtained hybrid ionogels were HI-2, HI-5 containing 2 and 5 wt % of LPMASQ, respectively.

Through extensive pre-trials, we observed that LPMASQ was capable of completely solidifying BMPTFSI, even at an exceeding low concentration of 2 wt % (HI-2). As shown in Figure. 2.5, the peaks assigned to the C=C bonds at 1635 cm^{-1} completely disappeared after curing process, demonstrating that the cross-linking reaction was completed. The inset photograph in Figure 2.5 shows that the ionic liquid electrolyte was completely solidified after thermal curing. Similar to our previous study, [16] we demonstrated that LPMASQ was able to produce mechanically pliant and non-flowing gel polymer electrolytes using only a mere 2 wt % of gelator. This stable formation of homogenous ionogels led us to hypothesize optimal electrochemical performance with these hybrid ionogels.

Rheological examinations of gel polymer electrolytes and hybrid ionogels have recently observed as an efficient method to elucidate the mechanical properties of such soft materials. [25–30] Figure 2.6(a) presents the changes of dynamic viscoelastic properties of neat BMPTFSI and hybrid ionogels as a function of angular frequency. For the neat BMPTFSI, the loss modulus G″ was found greater than storage modulus G′. Both dynamic moduli values exhibited power law dependency over the experimental range, which is a typical rheological characteristic of a viscous fluid. [30, 31] These results clearly demonstrate the dynamic shift from liquid to solid-like state; predominantly elastic behaviour with only minimal addition of LPMASQ due to the well-developed network structure. Meanwhile, with increasing LPMASQ concentration, the network structure becomes denser, resulting in an increase in the gel rigidity, as evident by the increase in dynamic modulus order. Furthermore, as shown in Figure 2.6(b), the thermal scanning rheological observation for hybrid ionogel HI-2 showed that storage modulus values were stable as temperatures exceeding 250 °C.

Thermal stability of electrolytes is a critical requirement for their safety and stability in lithium ion battery applications. The TGA thermograms of LPMASQ, BMPTFSI and two kinds of prepared hybrid ionogels are presented in Figure 2.7(a) As shown, the initial degradation

temperature of LPMASQ and BMPTFSI are very similar (~400 °C), but LPMASQ left residual silica at temperatures exceeding 500 °C. The residual mass of the hybrid ionogels at various concentrations also correlated well with the LPMASQ concentration as ionogels with larger LPMASQ concentration gave greater residual mass at 800 °C. Given the exceeding high initial degradation temperature of these hybrid ionogels, it can be said that these materials exhibit superior thermal stability. Moreover, thermal shrinkage tests with the neat ionic liquid compared with HI-2 impregnated polypropylene (PP) separator were conducted at 150 ^{o}C for 30 minutes (Figure 2.7(b)). As shown, the neat ionic liquid impregnated PP separator showed significant shrinkage, while the HI-2 impregnated PP separator showed exceptionally low thermal shrinkage, indicating that these hybrid ionogels have superior thermal and thermo-mechanical properties for use at elevated temperatures.

The temperature dependency of ionic conductivity of gel polymer electrolytes produced with various amounts of cross-linker was examined via AC impedance spectroscopy technique. The ionic conductivity (σ) of an electrolyte can be described using the following equation. [32]

$$\sigma\,(T) = \Sigma\, n \times q \times \mu$$

where n is the number of charge carriers, q is the charge on the charge carrier, and μ is the mobility of charge carriers. Hybrid ionogels fabricated through the gelation of liquid electrolyte can provide good mechanical properties, though at the cost of sacrificing ionic conductivity. The ionic mobility (μ) correlated to the diffusion of ions is hindered when compared with the 1M LiTFSI in BMPTFSI electrolyte due to the formation of a network structure. Furthermore, a decrease in the number of the charge carrier (n) per unit volume of electrolyte, caused by the introduction of the crosslinking agent, is also a contributing factor for the restricted ionic conductivity. A notable advantage of this work is the gelation of ionic liquid with 2 wt % LPMASQ. Due to the minimal amount of gelator content used to fabricate these free-standing hybrid ionogels, high ionic conductivity similar to the neat BMPTFSI was expected. As shown in Figure 2.8, a decrease in ionic conductivity was observed for hybrid ionogels with increasing the amounts of LPMASQ. However, the ionic conductivity of HI-2 was observed as 0.79 mS cm^{-1} at 30 °C, which is in close proximity to the ionic conductivity of the neat ionic liquid electrolyte (0.96 mS cm^{-1}). In addition, we plotted the ionic conductivities of a commercially available organic-based crosslinker (Ethoxylated trimethylolpropane triacrylate : ETPTA) utilized in several previous studies. [33] As shown, the high amounts of ETPTA required for full solidification of 1M

LiTFSI BMPTFSI led to the drastic decrease in ionic conductivities and subsequent poor cell performance to be discussed later. The electrochemical stability of electrolytes over the operating voltage of a lithium-ion battery is also an important requirement for practical battery operation. The linear sweep voltammetry (LSV) measurements were performed in the potential between 3.0 and 7.0 V (V vs. Li/ Li^+) under various temperature conditions. As shown in Figure 2.9, upon the voltage sweep, the onset of the oxidation current increase, which is related to the electrochemical oxidative decomposition of electrolyte shifted closer to 5.0 V with increasing temperature. Greater slopes of I-E diagrams were also observed at higher temperatures, indicating that oxidation current depends on the test temperature. However, no significant oxidation current was observed below 5.0 V even at elevated temperatures, demonstrating that obtained gel polymer electrolytes were electrochemically stable up to 5.0 V, which could be applied to high-voltage lithium batteries over a wide temperature range.

To evaluate the compatibility of Li metal electrodes with hybrid ionogels, the interfacial resistance of Li/HI-2/Li test cell was monitored during a period of 25 days. Figure. 2.10(a) shows the time evolution of the AC impedance spectra under open-circuit potential conditions. The intercept with the Z_{real} axis at high frequency presents the bulk resistance (R_s), which remained stable and constant with the storage time, confirming the stability of ionogels against the lithium

metal. In comparison, the mid-frequency semicircle associated with the interfacial resistance (R_{int}) gradually increased with time until a steady state was reached. Such a response could be explained by the formation of the passivation layer on the lithium metal electrode surface that suppresses continuous electrochemical reactions between the lithium metal electrode and electrolyte, resulting in the stabilization after a few days of storage. [34, 35] The electrochemical behaviour of the hybrid ionogel toward lithium metal was further investigated with running a cyclic voltammetry (CV) of a symmetrical Li/HI-2/Li cell. As Figure 2.10(b) reveals, the cell exhibited reversible redox process with high coulombic efficiency, and the peak current of CV profile tended to decrease with increase in cycle number. These results also confirm the stabilization at the interface, suggesting that the compatibility of the ionogel towards the lithium metal electrode is sufficient for application in lithium batteries.

To characterize electrochemical performance of hybrid ionogels, we fabricated coin cells using $LiFePO_4$ as the cathode and metallic lithium counter electrodes assembled with HI-2 (98 wt % of ionic liquid containing 2 wt % LPMASQ). Figure 2.11(a) presents the discharge capacity of the cells at various temperatures. In the examination, the cells were charged at a constant current density of 0.1 C (1 C rate corresponded to a current density of 155.1 mA g^{-1}) and discharged at various current densities in a voltage range of 2.5–4.2 V. As shown,

the cells delivered stable discharge capacity upon repeated cycling at various current rates. However, the discharge capacity and voltage of cells gradually decreased when the discharging current density rate increased. This lower discharge capacity is attributed to the increase in cell polarization caused by the poor kinetics at the electrode-electrolyte interface. [36] With increasing temperature, as expected, discharge capacity of cell increased. For instance, in the initial cycle at 50 °C, the discharge capacity with a current density of 0.5 C was 88.3 mAh g^{-1}, whereas cells cycled at 90 °C delivered a greater discharge capacity of 156.2 mAh g^{-1}, which is close to the theoretical discharge capacity of the cathode active material in this potential region (170 mAh g^{-1} for $LiFePO_4$).

Typical discharge profiles of the cell fabricated with HI-2 at various temperatures with 0.1C charge-0.1C discharge are displayed in Figure 2.11(b). In general, a flat voltage plateau at approximately 3.4 V (vs. Li/Li^+) corresponds to the conversion between $LiFePO_4$ and $FePO_4$. [36, 37] A well-defined voltage plateau was observed above 50 °C, whereas the truncated flat voltage region and the voltage drops were observed at 30 °C. These results clearly show that the limited conversion process is mainly due to the low diffusion of lithium-ion in both electrolytes and cathode material, indicating sufficient mobility of lithium ions is required to maintain electrochemical performance of batteries.

The cycling stability of the cells at 90 °C was evaluated further through measurement of discharge capacity. The cells were charged at a current density of 0.2 C and discharged at a 0.5 C. Figure 2.12(a) shows the cycling performance of cell made with our hybrid ionogels and the discharge profiles at various cycles, in comparison with the cells made with a well-known organic crosslinker, ETPTA-based ionogel. [33] The cells containing HI-2 ionogels exhibited relatively stable cycling performance. In addition, the discharge capacities for HI-2 were comparable to cells containing the liquid 1M LiTFSI BMPTFSI. The discharge capacity was able to maintain a value of 147.1 mAh g^{-1} after 50 cycles, which was 94.9% of its largest discharge capacity and the columbic efficiency of the system was found above 98% with the exception of cell activation. Moreover, no obvious change in the charge/discharge profiles or significant capacity decay were observed, confirming the thermal stability and electrochemical stability of the ionogels. In comparison, the cells containing organic crosslinker ETPTA-based ionogel exhibited a rapid capacity loss over repeatable cycling process and the discharge capacity decreased to 118.7 mA g^{-1}. That was capacity retention of 82.7%, the greatest discharge capacity after being cycled merely for 50 times. It should be noted that HI-2 was able to fully solidify the ionic liquid at a mere 2 wt %, whereas the organic ionogel fabricated with ETPTA required a high concentration of cross-linker (15 wt %), which caused the significantly lower

ionic conductivity compared with HI-2. (Figure 2.8) Therefore, the improved electrochemical performances of the cell with ionogels could be ascribed to the less dense network-structure formed by LPMASQ, which could help to minimize the depreciation of the lithium-ion diffusion of the gel polymer electrolyte, resulting in enhanced electrochemical performances.

2.4. Conclusion

An inorganic–organic hybrid ionogel electrolyte was successfully prepared via thermal initiation of a polymeric poly (methacryloxypropyl)silsesquioxane (LPMASQ) for preparation of an ionic liquid solution. The fully condensed LPMASQ revealed good thermal stability beyond 400 °C, good solubility in an ionic liquid solution. A minuscule 2 wt% of LPMASQ was able to fully solidify the ionic liquid solution to yield homogeneous, pliant gels with stable wide electrochemical window and high ionic conductivity on par with the neat ionic liquid. The lithium ion battery cell test performed with these hybrid gel polymer electrolytes exhibited good Coulombic efficiency and battery cell performance at elevated temperature. The facile, mass producible synthetic route towards LPMASQ and preparation of hybrid ionogel, the minuscule 2 wt% required to gel an electrolyte solution, fast curing kinetics as well as good Li battery cell performance make these materials highly promising products for future industrial battery applications.

2.5. References

[1] A. Yoshino, The birth of the lithium ion battery, Angew. Chem., Int. Ed. (2012) 51, 5798–5800.

[2] J.-M. Tarascon and M. Armand, Nature (2001) 414, 359–367.

[3] N.-S. Choi, Z. Chen, S. A. Fruenberger, X. Ji, Y.-K. Sun, K. Amine, G. Yushin, L. F. Nazar, J. Cho and P. G. Bruce, Angew. Chem., Int. Ed. (2012) 51, 9994–10024.

[4] Z. Chen, Y. Ren, A. N. Jansen, C.-K. Lin, W. Wang and K. Amine, Nat. Commun. (2013) 4, 1513-1521.

[5] K. Xu, Chem. Rev. (2004) 104, 4303–4417.

[6] M. P. Singh, R. K. Singh and S. Chandra, Prog. Mater. Sci. (2014) 64, 73–120.

[7] A. I. Horowitz and M. J. Panzer, J. Mater. Chem. (2012) 22, 16534–16539.

[8] A. K. Gupta, M. P. Singh, R. K. Singh and S. Chandra, Dalton Trans. (2012) 41, 6362–6371.

[9] A. M. Stephan, Review on gel polymer electrolytes for lithium batteries, Eur. Polym. J. (2006) 42, 21–42.

[10] A. M. Stephan and K. S. Nahm, Polymer (2006) 47, 5952–5964.

[11] J.H. Lee, A.S. Lee, J.C. Lee, S.M. Hong, S.S. Hwang and C.M. Koo, J.

Mater. Chem. A. (2015) 3, 2226-2233.

[12] A.S. Lee, J.H. Lee, S.M. Hong, J.C. Lee, S.S. Hwang and C.M. Koo, RSC Adv. (2015) 5, 94241-94247.

[13] F. Gayet, L. Viau, F. Leroux, S. Monge, J. J. Robin and A. Vioux, J. Mater. Chem. (2010) 20, 9456–9462.

[14] D. M. Tigelaar, M. A. B. Meador and W. R. Bennet, Macromolecules, (2007) 40, 4159–4164..

[15] R. H. Baney, M. Itoh, A. Sakakibara and T. Suzuki, Chem. Rev. (1995) 95, 1409–1430.

[16]. A. S. Lee, J. H. Lee, J.-C. Lee, S. M. Hong, S. S. Hwang and C. M. Koo, J. Mater. Chem. A. (2014) 2, 1277–1283.

[17] A. S. Lee, S. S. Choi, H. S. Lee, H. Y. Jeon, K. Y. Baek and S. S. Hwang, J. Polym. Sci. Part A: Polym. Chem. (2012) 50, 4563–4570.

[18] S. S. Choi, A. S. Lee, H. S. Lee, H. Y. Jeon, K. Y. Baek and S. S. Hwang, J. Polym. Sci. Part A: Polym. Chem. (2011) 49, 5012–5018.

[19] S. S. Choi, H. S. Lee, S. S. Hwang, D. H. Choi and K. Y. Baek, J. Mater. Chem. (2010) 20, 9852–9854.

[20] Z. X. Zhang, J. Hao, P. Xie, X. Zhang, C. C. Han and R. Zhang, Chem Mater. (2008) 20, 1322–1330.

[21] S. Chang, T. Matsumoto, H. Matsumoto and M. Unno, Appl. Organometal.

Chem. (2010) 24, 241–246.

[22] M. Patel, M. Gnanavel and A. J. Bhattacharyya, J. Mater. Chem. (2011) 21, 17419–17424.

[23] S. K. Das and A. J. Bhattacharyya, J. Phys. Chem. C. (2009) 16, 6699–6705.

[24] C. Pfaffenhuber, M. Gobel, J. Popovic and J. Maier, Phys. Chem. Chem. Phys. (2013) 15, 18318–18335.

[25] Y. Lu, K. Korf, Y. Kambe, Z. Tu and L. A. Archer, Angew. Chem. Int. Ed. (2014) 53, 488–492.

[26] J. L. Schaefer, D. A. Yanga and L. A. Archer, Chem. Mater. (2013) 25, 834–839.

[27] Y. Lu, S. S. Moganty, J. L. Schaefer and L. A. Archer, J. Mater. Chem. (2012) 22, 4066–4072.

[28] S. S. Moganty, S. Srivastava, Y. Lu, J. L. Schaefer, S. A. Rizvi and L.A. Archer, Chem. Mater. (2012) 24, 1386–1392.

[29] S. K. Das, S. S. Mandal and A. J. Bhattacharyya, Energy Environ. Sci., (2011) 4, 139101399.

[30] M. Patel, M. Gnanavel and A. J. Bhattacharyya, J. Mater. Chem. (2011) 21, 17419–17424. 30.

[31] S. K. Das and A. J. Bhattacharyya, J. Phys. Chem. C. (2009) 16, 6699–

6705. 36.

[32] D.-G. Kim, J. Shim, J. H. Lee, S.-J. Kwon, J.-H. Baik and J.-C. Lee, Polymer (2013) 21, 2812–5820.

[33] M. Li, W. Ren, Y. Zhang and Y. Zhang, J. Appl. Polym. Sci. (2012) 126, 273–279..

[34] M. A. Navarra, J. Manzi, L. Lombardo, S. Panero and B. Scrosati, ChemSusChem. (2011) 4, 125–130.

[35] V. Gentili, S. Panero, P. Reale and B. Scrosati, J. Power Source, 170 (2007) 185–190.

[36] M. Wetjen, M. A. Navarra, S. Panero, S. Passerini, B. Scrosati and J. Hassoun, ChemSusChem., 6 (2013) 1037–1043.

[37] L.-X. Yuan, Z.-H. Wang, W.-X. Zhang, X.-L. Hu, J.-T. Chen, Y.-H. Huang and J. B. Goodenough, Energy Environ. Sci. (2011) 4, 269–284.

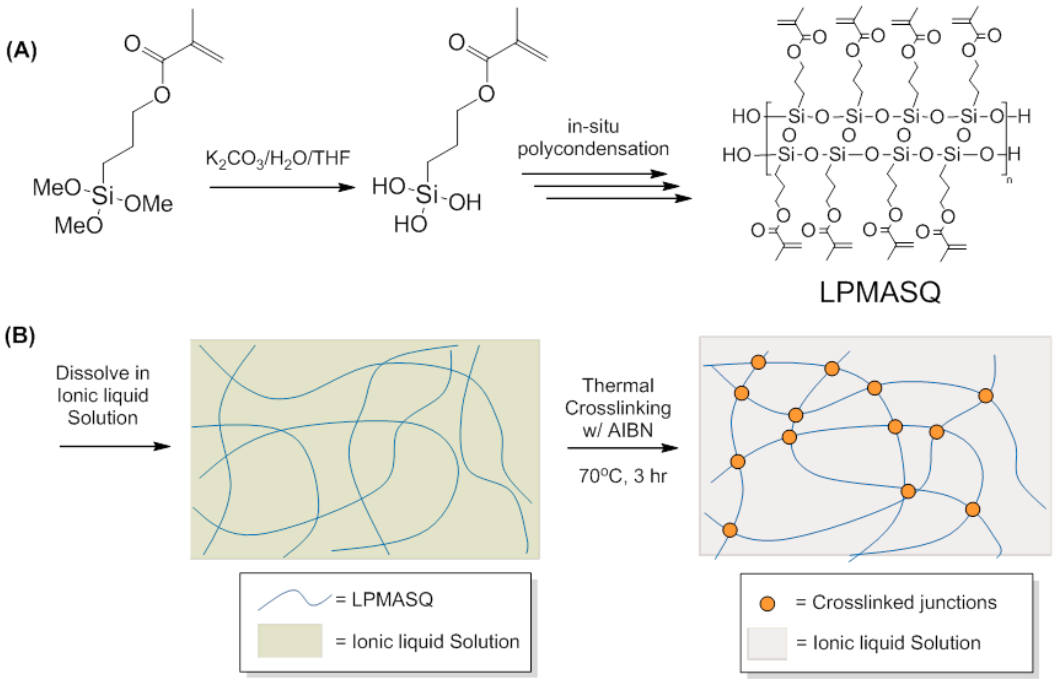

Figure 2.1. (A) Synthesis of the LPMASQ, (B) Preparation of hybrid ionogel fabrication

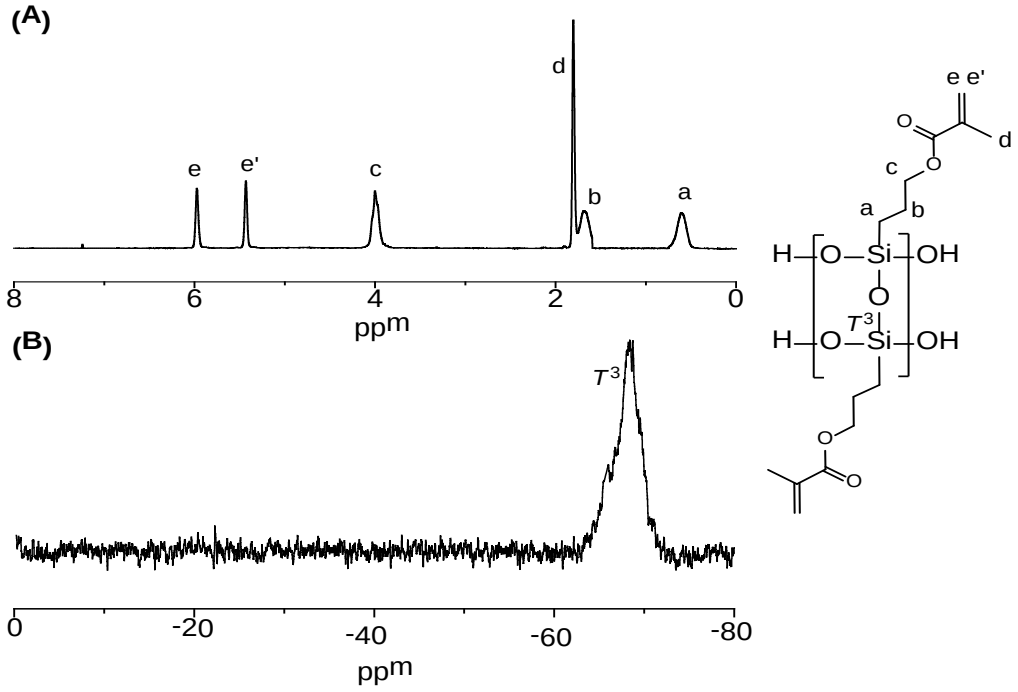

Figure 2.2. (A) ^{1}H NMR, (B) ^{29}Si NMR spectra for LPMASQ

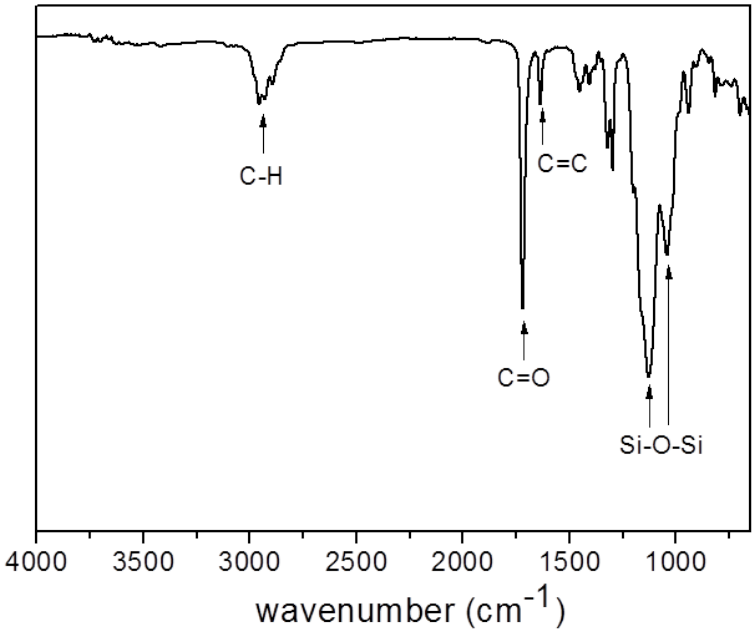

Figure 2.3. FT-IR Spectrum for LPMASQ

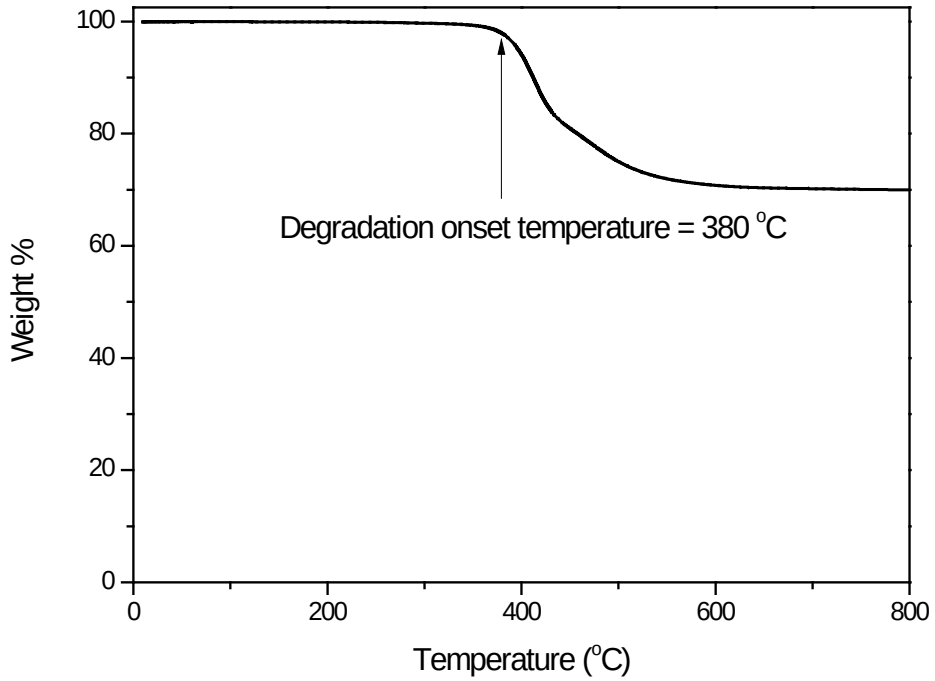

Figure 2.4. TGA thermograms of LPMASQ (under N_2, heating rate= 10 °C/min)

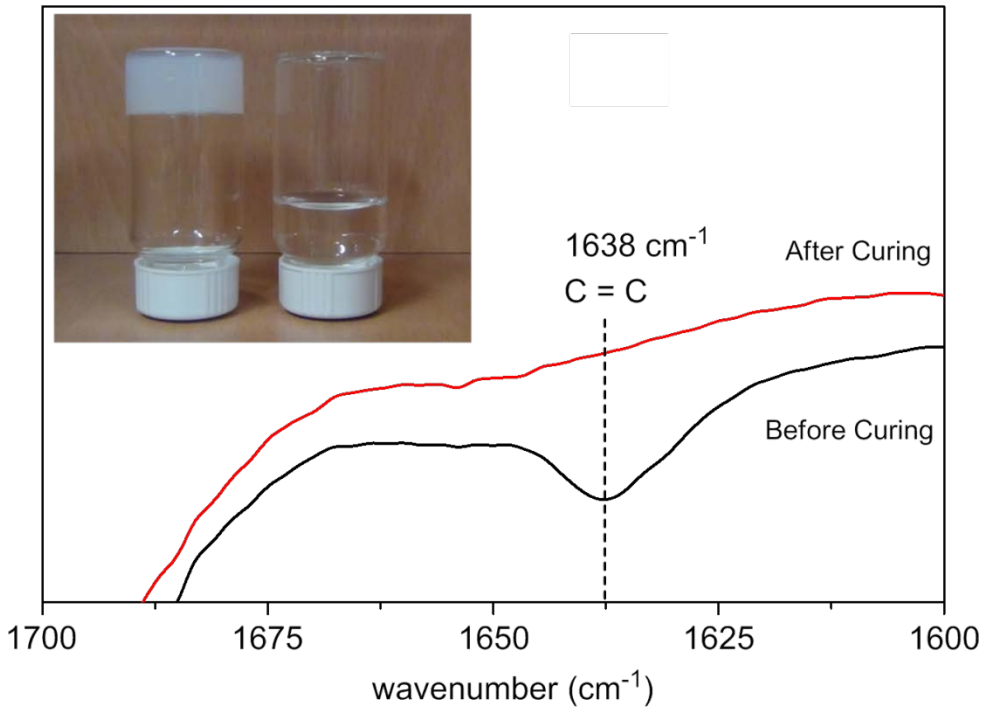

Figure 2.5. FTIR spectra of hybrid ionogel HI-5 before and after thermalcuring with an inset photograph.

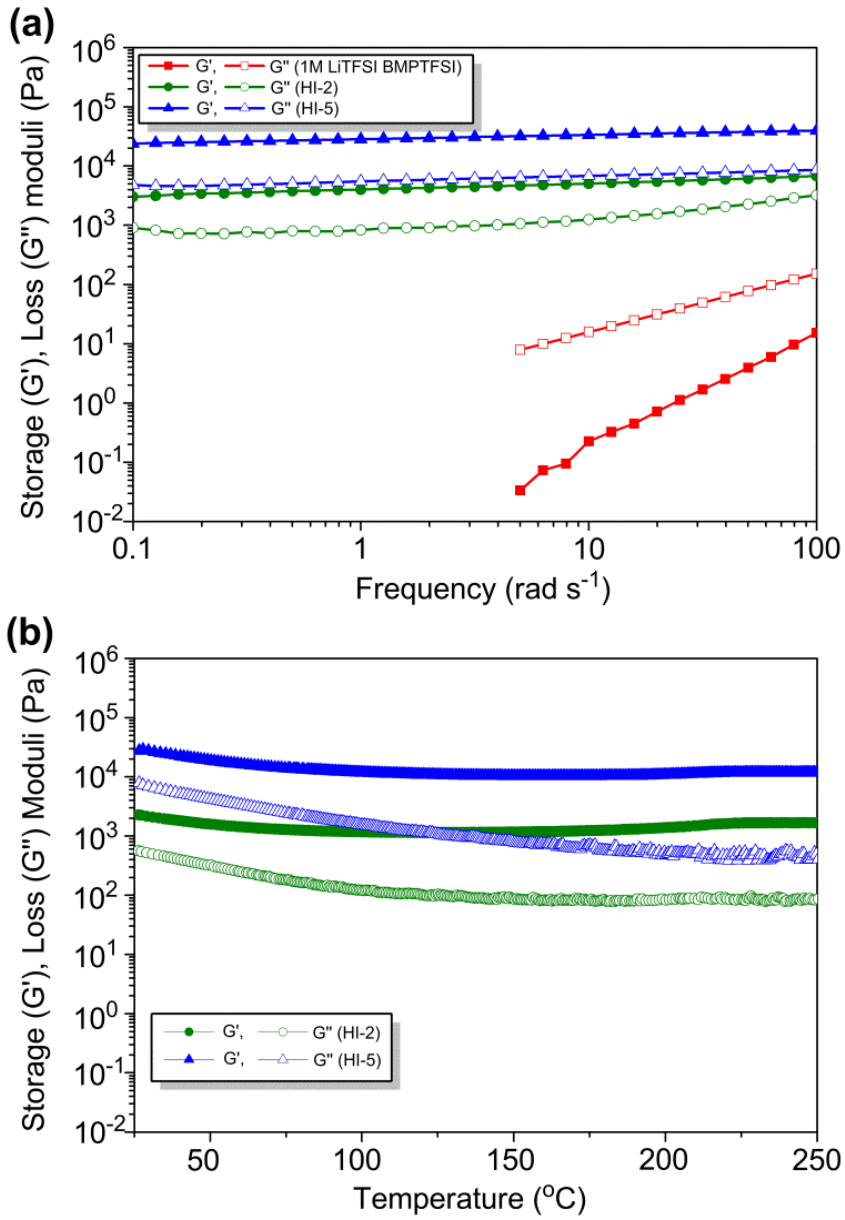

Figure 2.6. Rheological properties of hybrid ionogels (a) frequency sweep (b) temperature sweep.

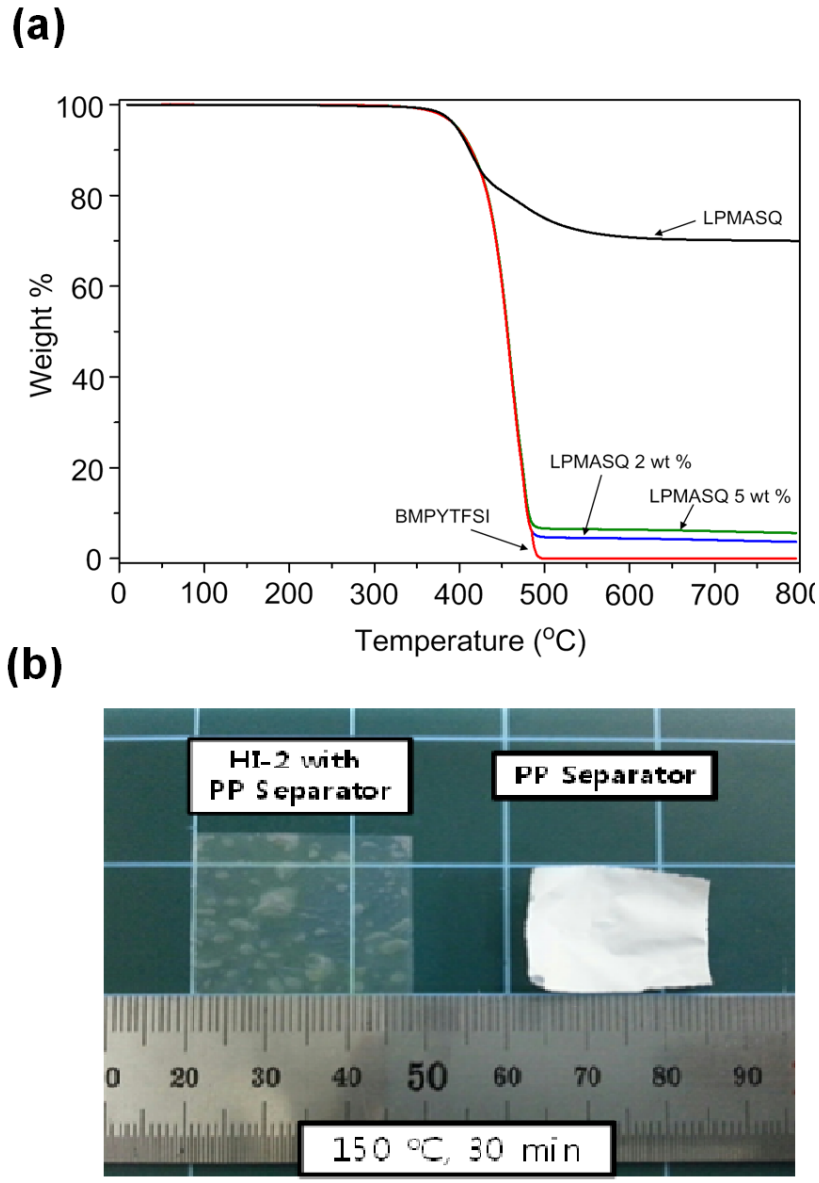

Figure 2.7. (a) TGA thermograms of BMPTFSI, LPMASQ, and hybrid ionogels, (b) Thermal shrinkage tests with neat ionic liquid and HI-2 impregnated polypropylene separators

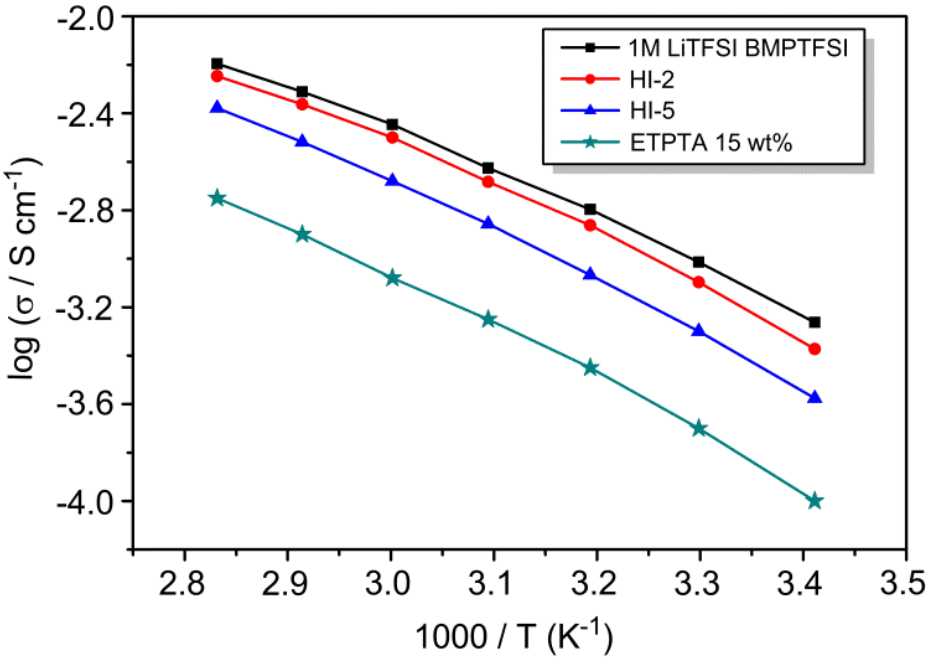

Figure 2.8. Temperature dependency of ionic conductivities of hybrid ionogels.

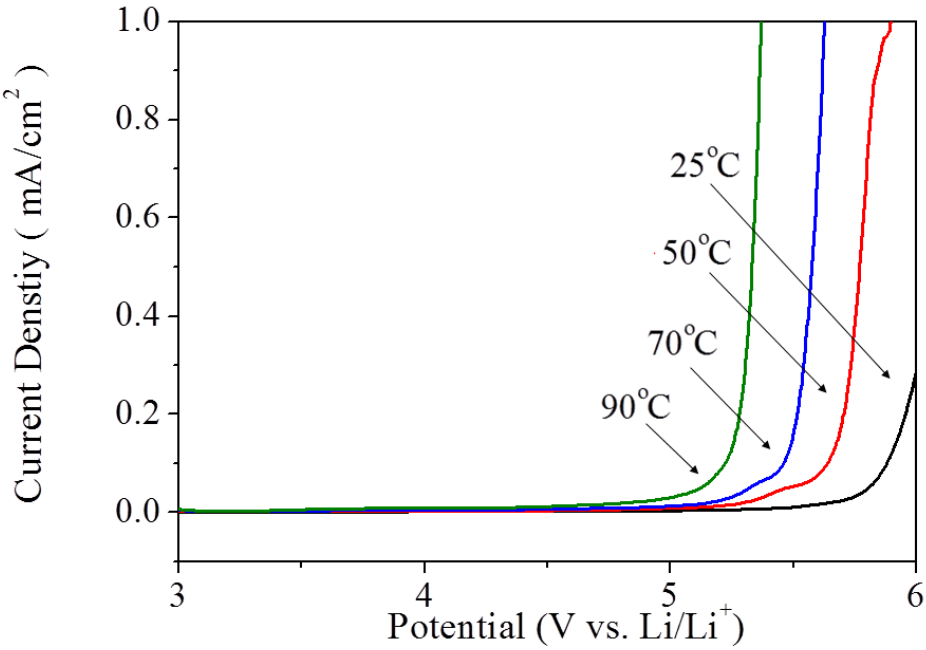

Figure 2.9. Linear sweep voltamagrams of hybrid ionogel HI-2 at various temperatures

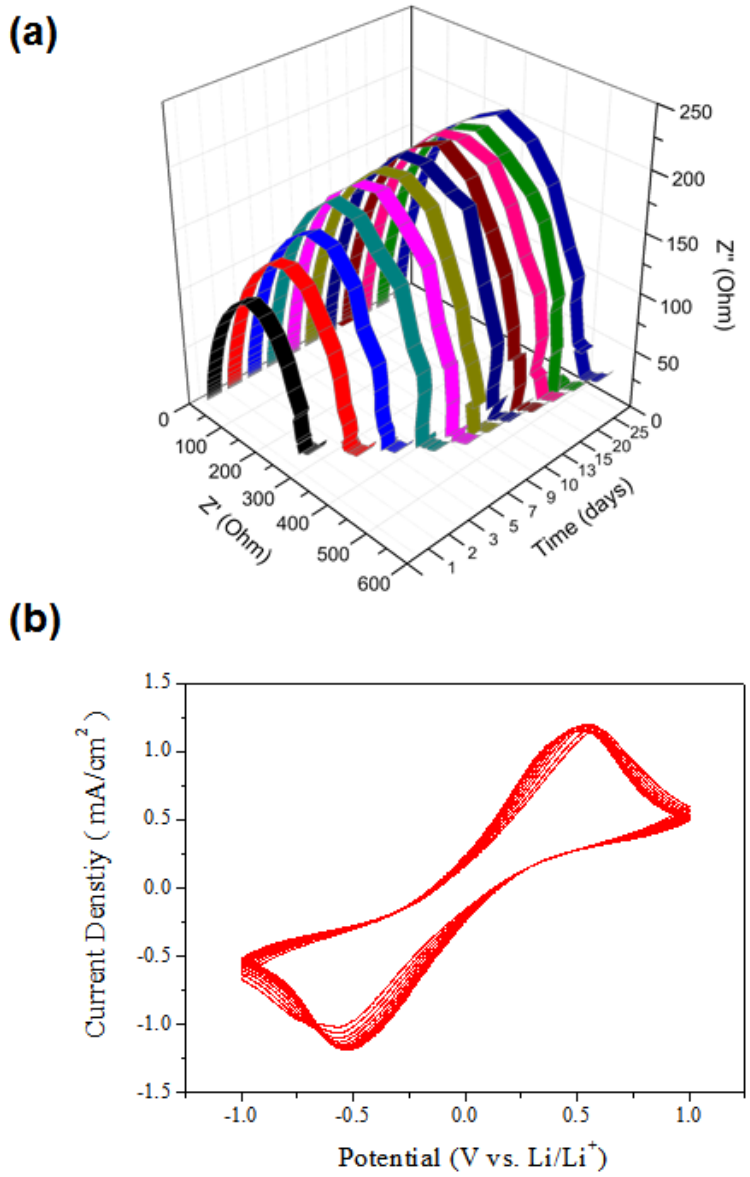

Figure 2.10. (a) Nyquist plot of AC impedance for a Li/HI-2/Li cell, (b) Cyclic Voltammogram for a symmetrical Li/HI-2/Li cell

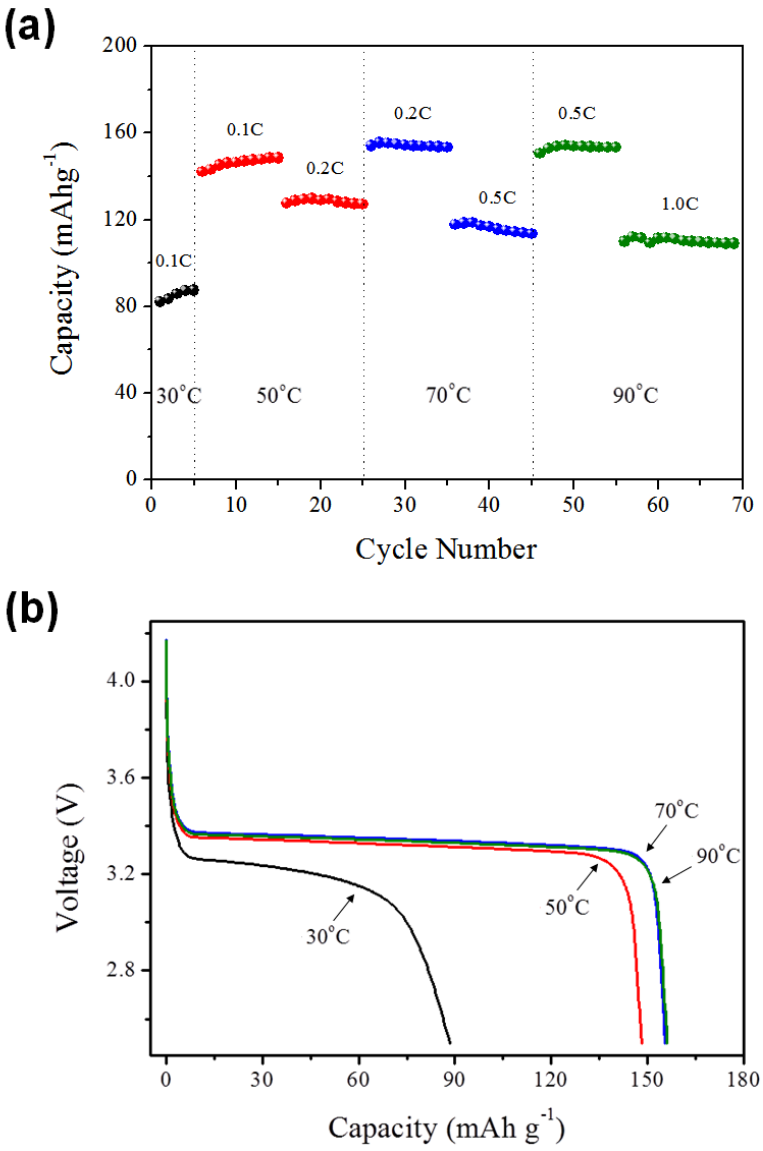

Figure 2.11. (a) Discharge capacity at various temperatures and C-rates for LiFePO4/HI-2/Li Cells, (b) representative discharge profile under different temperatures for LiFePO4/HI-2/Li cells cycled under 0.1C charge-0.1C discharge conditions

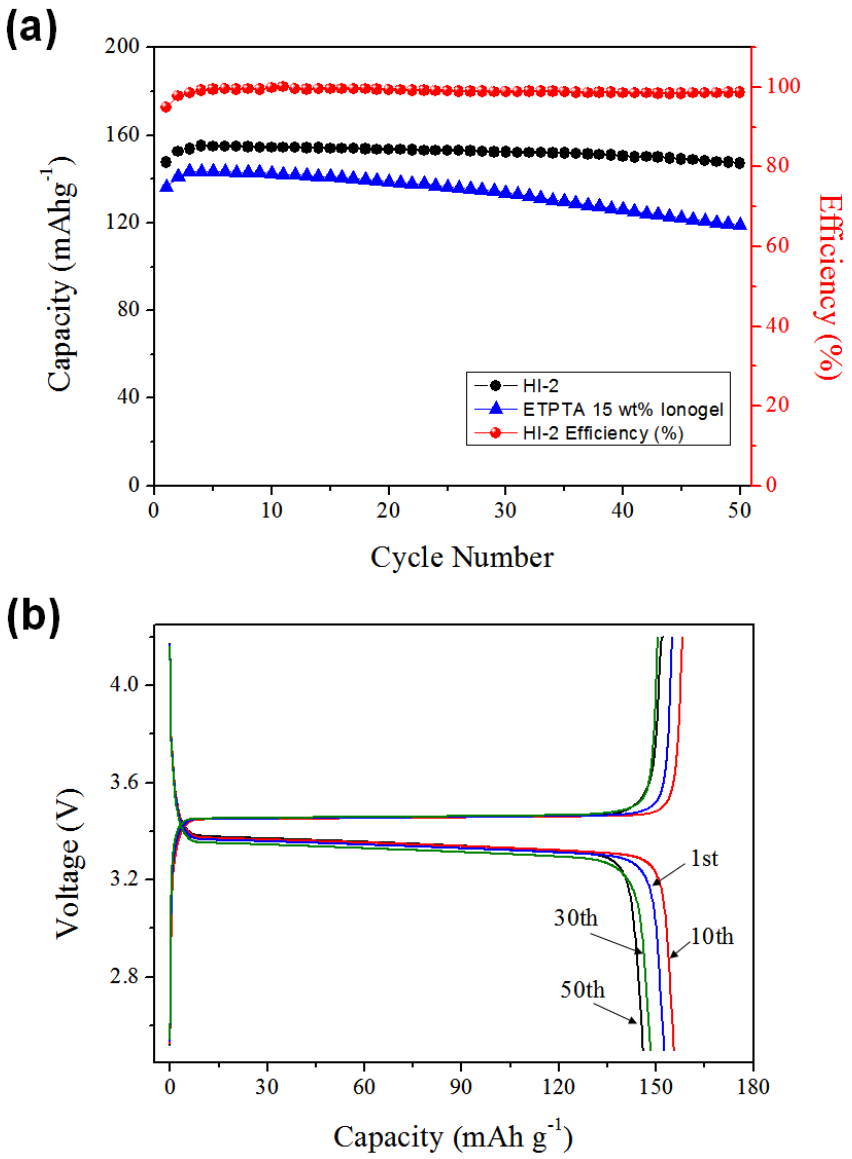

Figure 2.12. (a) Cyclability of HI-2 compared with a conventional organic ionogel fabricated with ETPTA, (b) representative discharge profiles for HI-2.

Chapter 3

Ion Conduction Behavior in Chemically Cross-Linked Hybrid Ionogels: Effect of Free Dangling Oligo-PEOs

3.1. Introduction

With the ever increasing demand for the next generation of electrochemical cells to achieve better performance, the safety issues often arising from the thermal and mechanical stability of organic liquid electrolytes are overlooked. [1, 2] With the applications requiring high performance electrochemical cells in electronic devices, such as laptop computers, mobile phones and hybrid/fully electronic vehicles, all being used in close range by humans, safety concerns over electrolyte leakage and thermal expansion have been well documented. [3, 4] Further exacerbating of this issue is the flammability of electrolyte solutions, which are comprised of lithium salts dissolved in highly flammable carbonate-based organic solvents. [5, 6]

To alleviate the above safety concerns, ionogels have recently garnered great interest in the academic community. Ionogels are defined as ion-conducting liquids solidified through physical or chemical crosslinking, usually with cross-linkable polymeric gelators. [7–9] Through tuning of both the content and composition of the solidifying gelator, various ionogels have been fabricated and their usage for practical electrochemical performance was confirmed. [10–12] However, even these ionogels crosslinked with organic gelator materials lacked

the necessary thermal and mechanical properties, leading to excess use of crosslinking materials, invariably depreciating ion mobility and electrochemical performance. [13, 14]

The hybridization of the crosslinking matrix network to attain hybrid ionogels has also been a booming field of interest to alleviate the above concerns of low thermal, mechanical and ion transport properties. The gelation of ion-conducting solutions with various inorganic-organic hybrid materials, such as ORMOCERs, [15] inorganic oxides [16–18] and polysilsesquioxanes [10] have extensively been investigated. However, many of these approaches have entailed the use of organic moiety for only crosslinking function. Additionally, inorganic oxides, such as nano-sized silica and alumina particles, have shown great promise because of their ability to gel ion-conducting solutions through the aggregation of inorganic networks, following the Derjaguin-Landau-Verwey-Overbeek (DLVO) theory. [19] In their pioneering works, Archer group [11, 12, 20, 21] have investigated hybrid ionogels gelled through silane surface-modified metal oxides. Through surface treatment of ionic liquid groups, oligo-ethylene oxide groups and single ion-conducting groups, all functioning to improve the electrical properties of the hybrid ionogels, these hybrid ionogels have greatly been improved in thermal stability, mechanical properties and ion mobility. However, these hybrid ionogels still suffer from the fact that they can only be dispersed

inhomogeneously in ion-conducting solutions, [18, 22] and that the degree of control over mechanical properties is low compared with those of chemically crosslinked hybrid ionogels.

In our previous study, we investigated hybrid gel polymer electrolytes and hybrid ionogels fabricated with a methacryloxypropyl-functionalized ladder-structured polysilsesquioxane homopolymer. Ladder-structured polysilsesquioxanes, [10, 23] which are comprised of an inorganic Si–O–Si ladder backbone with radial organic functional groups, exhibited high solubility in various ion-conducting solutions, thus, we were able to tune the mechanical properties such that liquid-like ionic conductivity was able to be attained without sacrificing gel robustness.

In this study, we sought out to investigate the effect of free dangling oligomeric PEO groups copolymerized with methacryloxypropyl groups at various comonomer ratios on the ion conduction behavior of chemically crosslinked hybrid ionogels. We stipulated that through introduction of the free dangling oligomeric PEO groups into the inorganic ladderstructured backbone at the molecular level, the inorganic backbone would function as support for mechanical robustness, whereas the PEO groups would contribute to enhance ion conduction behavior through an in-depth spectroscopic analysis of these PEGylated hybrid ionogels compared with our previously studied hybrid ionogels.

3.2. Experimental

Materials

2-[methoxy(polyethyleneoxy)propyl]trimethoxysilane (Gelest, 90%), 3-methacryloxypropyltrimethoxysilane (Shin-Etsu, 98%) and ethyl acetate (J.T. Baker, HPLC grade) were distilled over CaH2 prior to use. Potassium carbonate (Daejung) was dried at 40 °C. THF (J.T. Baker, HPLC grade) was distilled over sodium. Azobisisobutyronitrile (Daejung Chemicals, 99%) was recrys-tallized from solution in methanol. Lithium bis(trifluoromethylsulfonyl)imide (LiTFSI) (Aldrich, 99.9%, battery grade) and N-butyl-N-methylpyrrolidinium bis(trifluoromethylsulfonyl)imide (BMPTFSI) (C-TRI, 99.9%) were used after drying in a vacuum oven and storing in an argon-charged glove box.

Synthesis of LPEOMASQ Series.

LPEOMASQ was synthesized following a modified literature procedure. [24, 25] In a typical experiment, potassium carbonate, K_2CO_3 (0.04 g, 0.29 mmol), was dissolved in deionized H_2O (4.8 ml, 0.27 mol), then 8 g of THF was added. To this solution, 3-methacryloxypropyltrimethoxysilane (9.9 ml, 0.04 mol) and 2-

[methoxy(polyethyleneoxy)propyl]trimethoxysilane (19 ml, 0.04 mol) were added dropwise under nitrogen flow. The solution was magnetically stirred for 10 days when the molecular weight reached its maximum value. After partial evaporation of THF, the resinous material was dissolved in dichloro-methane and extracted several times with water. Collection of organic layer followed by drying over anhydrous magnesium sulphate and evaporation of the solvent under reduced pressure yielded a trans-parent liquid with medium viscosity (22 g, 92% crude yield). LPEOMASQ was found to have excellent solubility in the majority of organic solvents of medium to high polarity. LPEOMASQs with 3 different methacryloxypropyl : polyethyleneoxide mol ratios of 25 : 75, 50 : 50 and 75 : 25, were synthesized via simply varying the initial feed comonomer ratio. The samples were named LPEOMASQ25, LPEOMASQ50 and LPEOMASQ75 according to the PEO-copolymer composition percentage.

^{1}H NMR ($CDCl_3$) (δ, ppm): 0.35–0.45 (m, $Si(CH_2CH_2CH_2OCOCCH_2CH_3$,

$SiCH_2CH_2CH_2O(CH_2CH_2O)_{6\text{-}9}CH_3$, 4H),

1.8–1.9 (m, $Si(CH_2CH_2CH_2OCOCCH_2CH_3$,

$SiCH_2CH_2CH_2O(CH_2CH_2O)_{6\text{-}9}CH_3$, 4H),

1.95–2.05 (m, $Si(CH_2CH_2CH_2OCOCCH_2CH_3$, 3H),

3.15–3.3 (m, $Si(CH_2CH_2CH_2OCOCCH_2CH_3$,

$SiCH_2CH_2CH_2O(CH_2CH_2O)_{6\text{-}9}CH_3$, 4H),

3.7–3.8 (m, $SiCH_2CH_2CH_2O(CH_2CH_2O)_{6\text{-}9}CH_3$, 30H),

4.08–4.16 (m, $SiCH_2CH_2CH_2O(CH_2CH_2O)_{6\text{-}9}CH_3$, 3H),

5.3–6.1 (m, $Si(CH_2CH_2CH_2OCOCCH_2CH_3$, 2H)

^{29}Si NMR (ppm): –68 ~ –70 ppm,

Mw = 24.3 k.

Characterization.

Fourier transform infrared spectra were measured with a Perkin-Elmer FT-IR system Spectrum-GX on cast KBr plates. Raman spectra were obtained with a Renishaw InVia spectrometer equipped with 633 nm HeNe laser. Weight averaged molecular weight (Mw) and molecular weight distributions (Mw/Mn) of polymers were determined using JASCO PU-2080 plus SEC system equipped with refractive index detector (RI-2031 plus), UV detector (λ = 254 nm, UV-2075 plus) and Viscotek SLS apparatus with THF as the mobile phase at 40 °C and a flow rate of 1 mL min^{-1}. The samples were separated through four columns (Shodex-

GPC KF-802, KF-803, KF-804, KF-805). Solution-state 1H-NMR and 29Si NMR spectra were recorded in CDCl3 at 25 °C using Varian Unity INOVA system (1H: 300 MHz, ^{29}Si: 59.6 MHz). Solid-state ^{7}Li NMR and ^{19}F NMR spectra were obtained on a Varian INOVA (^{1}H: 400 MHz, ^{7}Li: 155.45 MHz, ^{19}F: 376.3 MHz) with spinning frequency held constant at 10 kHz with a pulse delay time of 4 s. Samples were packed into 7.5 mm zirconia rotors and sealed with KeI-F short caps. Thermal gravimetric analysis was carried out with TA instrument (TGA 2950) at heating rate of 10 °C min^{-1} under N_2 atmosphere. Rheological properties were examined using a rheometer (Advanced Rheometric Expansion System, ARES) instrument with cone–plate geometry (25 mm diameter). All rheological measurements were performed in the linear viscoelastic region under N_2 atmosphere. The ionic conductivity was determined using a complex impedance analyzer (Bio-Logics, VMP3) over frequency range from 1 Hz to 1 MHz at AC amplitude of 10 mV. The electrochemical stability of the ionogel electrolytes was examined with a linear sweep voltammetry system. In the experiments, a stainless steel working electrode was used with lithium metal as both the counter and reference electrodes. The voltage was swept at a scan rate of 1.0 mV s^{-1}. Electrochemical measurements of the hybrid ionogel polymer electrolytes were conducted using 2032 coin cells consisting of a separator, Li metal and LiFePO4 (90 wt % $LiFePO_4$, 5 wt % carbon black, and 5 wt % PVDF) electrodes. All the

cells were assembled in argon-charged glove box. After fabrication, the cells containing pre-gel solutions were subjected to thermal cross-linking for 3 h at 70°C. The galvanostatic charge-discharge experiments were carried out in a voltage range of 2.5–4.2 V using a battery cycler (Wonatech, WBCS3000) at 50 °C.

3.3. Results and Discussion

PEO-functionalized ladder-structured polysilsesquioxanes were synthesized according to our previous method. [24,25] A basecatalyzed aqueous sol–gel reaction was conducted in which various comonomer compositions of 25 : 75, 50 : 50 and 75 : 25 for 2-[methoxy(polyethyleneoxy)propyl]trimethoxysilane and 3-methacryloxypropyltrimethoxysilane were hydrolyzed and condensed in-situ. (Figure 3.1(a)) The hybrid polymers products were named as LPEOMASQ25, LPEOMASQ50 and LPEOMASQ75 according to the PEO comonomer percentage. Through design of the comonomers, cross-linkable ladder structured polysilsesquioxanes with free dangling PEO groups were introduced at molecular level. These LPEOMASQ compounds were then used to crosslink ionic liquid solutions of 1 M LiTFSI in BMPTFSI at a low concentration of 5 wt %.

The characterization of the LPEOMASQ compounds were conducted with ^{1}H NMR, ^{29}Si NMR and FTIR techniques, as shown in Figure 3.2. ^{1}H NMR spectroscopy of LPEOMASQ compounds showed that the methacryloxypropyl groups and PEG groups were introduced based on their initial comonomer ratio as indicated by the increasing large signal at 3.7 ppm, attributed to the ethylene oxide proton when the PEG-ratio from LPEOMASQ25 to LPEOMASQ75 increased.

Moreover, no discernible peaks were observed at 5.0 ppm, attributed to the uncondensed silanol Si–OH end groups. [26] Moreover, ^{29}Si NMR results revealed the presence of two large signals centred at –67 and –69 ppm, attributed to the fully condensed T3 Si–O–Si structure of Si–methacryloxypropyl- (Si-MMA) and 2-[methoxy(polyethyleneoxy)propyl (Si–PEG) groups, respectively. [27] As shown, the relative intensity of the T3 for Si–PEG at –69 ppm (assigned as X) increased when the PEG-ratio increased from LPEOMASQ25 to LPEOMASQ75, and the relative integrative ratio between the T3 for Si-PEG at –69 ppm (assigned as X) and the T3 for Si–methacryloxypropyl at –67 ppm (assigned as Y) reflected the initial comonomer feed ratio. Additionally, noteworthy are the lack of signals near –58 ppm, which are the charcateristics chemical shifts for the uncondensed T2 alkyl-silicons, as this provides additional evidence for the fully condensed, ladder-like structure of LPEOMASQ compounds. FT-IR spectra revealed the presence of C=O, C=C and Si–O–Si bands centred at 1745 cm^{-1}, 1638 cm^{-1}, and 1050 cm^{-1}, 1100 cm^{-1}, respectively.

The hybrid ionogels were prepared via a thermal-curing process. The unsaturated vinyl groups of methacryloxypropyl moieties in ladder-like poly(methacryloxypropyl-copolyethyleneoxide) silsesqui-oxane (LPEOMASQ) were crosslinked in an ionic liquid solution of 1 M LiTFSI in BMPTFSI to form a

polymeric network structure at 70 °C, resulting in mechanically stable and homogeneous ionogels. As shown in Figure 3.3(a), the disappearance of peaks assigned to C=C bonds at 1638 cm^{-1} was determined with FT-IR examination after thermal treatment.

Furthermore, the dynamic viscoelastic properties of the thermally cured hybrid ionogels as a function of frequency are presented in Figure 3.3(b). For the test, we fabricated the PEGlyated hybrid ionogels with equal concentrations (5 wt %) of LPEOMASQs to eliminate mitigating factors of crosslinker concentration. For all ionogel samples, the response of dynamic modulus was observed as nearly independent of the applied frequency and the elastic modulus G′ was greater than storage modulus G″, indicating pre-dominantly solid-like viscoelastic behavior. [28, 29] Moreover, the effect of increasing PEO content was to plasticize the hybrid ionogel, as LPEOMASQ75 5 wt% exhibited the lowest modulus and LPMASQ 5 wt%, which has no PEO groups, giving the highest modulus values across all frequencies. This was in due part to the free-dangling oligomeric PEO groups, which at room temperature existed in the melt-phase given the liquid state of the neat PEGylated LPSQs. Moreover, given that all of the LPEOMASQ gels exhibited solid-like behaviour, even the low MMA content of LPEOMASQ25 contained enough crosslinking functionality for obtaining

mechanically robust hybrid gels.

Figure 3.4 compares the measured ionic conductivities as a function of temperature. As presented, gelation of ionic liquids provided an undeniable depreciating effect on ionic conductivity, whereas, enabling mechanical support and dimensional stability. Such decreased ionic conductivity (σ) of the electrolyte can be described using the following equation:

$$\sigma\ (T) = \Sigma\ n \times q \times \mu$$

where n is the number of charge carriers, q is the charge on the charge carrier and μ is the mobility of charge carriers. [30] The decrease in ionic mobility and the number of ions per unit volume of electrolyte, caused by the introduction of the crosslinking agent, is attributed to the deteriorated ionic conductivity. Interestingly, the incorporation of ethylene oxide groups into network structure led to the increase in ionic conductivity. Moreover, we observed that the ionic conductivity continuously increased with in-creasing the content of ethylene oxide groups. It should be noted that the cross-linker contents were identical in ionogel systems, held constant at 5 wt %. Considering the number of charge carrier was invariant,

the observed ion transport behavior could be explained by the change in mobility of charged species. We speculated that the efficient diffusion of ions in PEGylated network structure correlates with the ability of ion dissociation and conduction, which facilitates ion transport. [31, 32]

As such, we conducted solid-state ^{7}Li NMR single-pulse experiments, comparing the neat ionic liquid with various hybrid ionogels (as shown in Figure 3.5(a)) to probe the ability of ion dissociation and conduction of lithium ions. As shown, while the neat IL showed a very sharp peak attributed to the lithium cation derived from the lithium salt dissolved in IL, the ^{7}Li NMR linewidth for the hybrid ionogels revealed a noticeable degree of decrease, or sharpening effect, as the PEO comonomer content increased from 0% (LPMASQ) to 75% (LPEOMASQ75). This point was further explored through comparison of the temperature dependent solid-state ^{7}Li NMR spectra of LPMASQ and LPEOMASQ75 (Figure 3.5(b)), indicating a rapid sharpening of Li^{+} peak starting around 35 °C, correlating to the melt phase state of the ionic liquid confined in the hybrid matrix. [9] It was clear from these NMR observations that the effect of free dangling PEGs on the lithium salt was pronounced in effectively dissociating the TFSI anion from lithium cation. This was a noteworthy result, as the effect was only previously demonstrated with zwitterionic compounds and single-ion conducting compounds, which functioned to completely immobilize the anion.33

Further distinguishing from these previous results is the low concentration of cross-linker (5 wt %) required to fully gel the liquid solution due to the hybrid inorganic backbone delivering mechanical robustness further, showcasing the inherent high and effective ion conduction behavior of these hybrid PEGylated ionogels for practical commercial performance.

Moreover, solid-state ^{19}F NMR single-pulse experiments with the PEGylated hybrid ionogels (Figure. 3.6(a)) revealed similar peak sharpening effect as the fluorine atoms derived from the TFSI anions were more dissociated for those hybrid gels containing greater concentration of PEO groups. To better understand the observed intermolecular interaction, we characterized the extent of ion pair formation using Raman analysis. It has previously reported that the strong Raman bands at 742 and 748 cm^{-1} correspond to free or dissociated $TFSI^-$ ions and bonded or associated Li^+ $TFSI^-$ ion pairs, respectively. [34,35] As shown in Figure 3.6(b), we observed changes in Li^+ coordination with PEO concentration that may possibly contribute to an increase in ionic mobility. It can be clearly seen that there was a weak interaction in LPEOMASQ ionogels over the non-PEO containing LPMSASQ ionogel counterpart, which caused an increase in ionic mobility, and thus enhanced ionic conductivity.

Before evaluation of the ionogels electrochemical performances, we assessed electrochemical stability using linear sweep voltammometry (LSV) examinations.

No abrupt rise in oxidative current related to the electrochemical decomposition of electrolyte was detected below 5.0 V in the anodic sweep (Figure 3.7(a)), demonstrating that the prepared ionogels were electrochemically stable up to 5.0 V, which could be used in high-voltage lithium batteries. Additionally, we investigated the thermal stability of ionogels. As depicted in Figure 3.7(b), these ionogels exhibited excellent thermal stability with no thermal degradation at temperatures exceeding 350 °C. Moreover, this high thermal stability of indistinguishable decomposition of residual silanol groups, thus full condensation of the Si–O–Si backbone, rendered high electro-chemical stability of PEGylated hybrid ionogels.

We fabricated LiFePO4/lithium cells assembled with hybrid ionogels (95 wt % of BMPTFSI ionic liquid containing 5 wt % cross-linker) to characterize the electrochemical performance of hybrid PEGylated ionogels. Figure 3.8(a) presents the rate capabilities of the cells with various cross-linker systems. For the test, the cells were charged at a constant current density of 0.1 C (1 C rate corresponded to a current density of 155.1 mA g^{-1}) and discharged at various current densities in a voltage range of 2.5–4.2 V. At a low current rate of 0.1 C, the reversible discharge capacity of LPEOMASQ hybrid ionogels was 148.9 mAh g^{-1}, which is slightly larger than those of cells containing ionogel without PEO groups (LPMASQ). However, upon an increase in the current rate, the LPEOMASQ PEGylated hybrid

ionogels containing cells exhibited improvement in capacity retention. For instance, the cell fabricated with LPEOMASQ ionogel retained 47.2% of its initial capacity, whereas the cell containing LPMASQ ionogel retained 33.1% at a current rate of 0.5 C. In general, rate capability of cell suffers from poor kinetics at the electrode-electrolyte interface. [36] As expected, the capacity degradation was closely coupled with ion transport of different electrolyte systems. We stipulated from these observations that the enhanced electrochemical performance achieved in this work is due partly to the incorporation of free dangling PEO groups to the network structure, promoting transport of lithium ions' heightened ability to dissociate from the anion, thereby alleviating the ohmic polarization loss of the cell. [37]

The cycling performance of cells was evaluated further through measurement of discharge capacities in which the cells were charged at a current density of 0.1 C and discharged at 0.1 C. Figure 3.8(b) presents the charge/discharge capacity and Columbic efficiency as a function of cycle number. As shown, the cycling behaviors of cells containing LPEOMASQ hybrid ionogels were more stable in the following cycles. In the initial stages of cycling, reversible discharge capacities reached 148.2 mAh g^{-1}, which was close to the cells fabricated with the liquid 1 M LiTFSI BMPTFSI (Figure. 3.9). The retained discharge capacity was obtained as 136.6 mAh g^{-1} after 50 cycles and the Columbic efficiency of the

system was observed to be nearly 99%. In addition, a well-defined voltage plateau around 3.4 V (vs. Li/Li^+), associated to the lithium insertion/extraction into cathode materials, indicates a highly maintained and repeatable process, [38] confirming the sufficient mobility of lithium ions and electrochemical stability of these PEGylated hybrid ionogels. Therefore, we clearly demonstrated that the incorporation of PEO groups into the network structure could help facile ion transport of hybrid ionogels, resulting in improvement of electrochemical performance.

3.4. Conclusion

In conclusion, we synthesized a series of PEGylated ladder-structured polysilsesquioxanes with various PEG to methacryloxypropyl copolymer ratios. Chemical crosslinking of methacryl groups in 1 M LiTFSI N-butyl-N-methylpyrrolidinium bis(trifluoromethylsulfonyl)imide ionic liquid solution at a low concentra-tion of 5 wt % yielded PEGylated hybrid ionogels. Through an in-depth spectroscopic investigation of the ion conduction behavior of these PEGylated hybrid ionogels and comparison with hybrid ionogels without PEG groups, we were able to demonstrate how enhancement in lithium ion battery performance for PEGylated hybrid iongels could be achieved at identical crosslinker concentrations.

3.5. References

[1] J. M. Tarascon and M. Armand, Nature (2001) 414, 359-367.

[2] N.-S. Choi, Z. Chen, S. A. Freunberger, X. Ji, Y.-K. Sun, K. Amine, G. Yushin, L. F. Nazar, J. Cho and P. G. Bruce, Angew. Chem. Int. Ed. (2012) 51, 9994-10024.

[3] E. Quartarone and P. Mustarelli, Chem. Soc. Rev. (2011) 40, 2525-2540.

[4] Y. Wang and W.-H. Zhong, ChemElectroChem (2015), 2, 22-36.

[5] K. Xu, Chem. Rev. (2004) 104, 4303-4418.

[6] Z. Chen, Y. Ren, A. N. Jansen, C.-k. Lin, W. Weng and K. Amine, Nat. Commun. (2013) 4, 1513.

[7] J. Le Bideau, L. Viau and A. Vioux, Chem. Soc. Rev. (2011) 40, 907-925.

[8] S. A. M. Noor, P. M. Bayley, M. Forsyth and D. R. MacFarlane, Electrochim. Acta (2013) 91, 219-226.

[9] M. P. Singh, R. K. Singh and S. Chandra, Prog. Mater. Sci. (2014) 64, 73-120.

[10]. J. H. Lee, A. S. Lee, J.-C. Lee, S. M. Hong, S. S. Hwang and C. M. Koo, J. Mater. Chem. A (2015) 3, 2226-2233.

[11] Y. Lu, K. Korf, Y. Kambe, Z. Tu and L. A. Archer, Angew. Chem. Int. Ed., (2014) 53, 488-492.

[12] Y. Lu, S. S. Moganty, J. L. Schaefer and L. A. Archer, J. Mater. Chem. (2012) 22, 4066-4072.

[13] J.-A. Choi, Y. Kang and D.-W. Kim, Electrochim. Acta (2013) 89, 359-364.

[14] C. Liao, X.-G. Sun and S. Dai, Electrochim. Acta (2013) 87, 889-894.

[15] M. Popall, M. Andrei, J. Kappel, J. Kron, K. Olma and B. Olsowski, Electrochim. Acta (1998) 43, 1155-1161.

[16] A. I. Horowitz and M. J. Panzer, J. Mater. Chem. (2012) 22, 16534-16539.

[17] L. Viau, M.-A. Néouze, C. Biolley, S. Volland, D. Brevet, P. Gaveau, P. Dieudonné, A. Galarneau and A. Vioux, Chem. Mater. (2012) 24, 3128-3134.

[18] F. Gayet, L. Viau, F. Leroux, S. Monge, J.-J. Robin and A. Vioux, J. Mater. Chem. (2010) 20, 9456-9462.

[19] H. K. Christenson, J. Chem. Soc., Faraday Trans. (1984) 80, 1933-1946.

[20] J. L. Schaefer, D. A. Yanga and L. A. Archer, Chem. Mater. (2013) 25, 834-839.

[21] S. S. Moganty, S. Srivastava, Y. Lu, J. L. Schaefer, S. A. Rizvi and L. A. Archer, Chem. Mater. (2012) 24, 1386-1392.

[22] M.-A. Néouze, J. L. Bideau, P. Gaveau, S. Bellayer and A. Vioux, Chem. Mater. (2006) 18, 3931-3936.

[23] A. S. Soo Lee, J. H. Lee, J.-C. Lee, S. M. Hong, S. S. Hwang and C. M.

Koo, J. Mater. Chem. A (2014) 2, 1277-1283.

[24] A. S. Lee, Y. Y. Jo, H. Jeon, S.-S. Choi, K.-Y. Baek and S. S. Hwang, Polymer, (2015) 68, 140-146.

[25] A. S. Lee, S. S. Choi, S. J. Song, K. Y. Baek and S. S. Hwang, RSC Adv., (2014) 4, 56532-56538.

[26] A. S. S. Lee, S.-S. Choi, H. S. Lee, H. Y. Jeon, K.-Y. Baek and S. S. Hwang, J. Polym. Sci., Part A: Polym. Chem. (2012) 50, 4563-4570.

[27] S. S. Choi, A. S. Lee, H. S. Lee, H. Y. Jeon, K. Y. Baek, D. H. Choi and S. S. Hwang, J. Polym. Sci., Part A: Polym. Chem. (2011) 49, 5012-5018.

[28] M. Patel, M. Gnanavel and A. J. Bhattacharyya, J. Mater. Chem. (2011) 21, 17419-17424.

[29] M. Patel and A. J. Bhattacharyya, Energy Environ. Sci. (2011) 4, 429-432.

[30] S.-J. Kwon, D.-G. Kim, J. Shim, J. H. Lee, J.-H. Baik and J.-C. Lee, Polymer (2014) 55, 2799-2808.

[31] D. Zhou, Y.-B. He, R. Liu, M. Liu, H. Du, B. Li, Q. Cai, Q.-H. Yang and F. Kang, Adv. Energy Mater. (2015) 5.

[32] F. Croce, M. L. Focarete, J. Hassoun, I. Meschini and B. Scrosati, Energy Environ. Sci. (2011) 4, 921-927.

[33] C. Tiyapiboonchaiya, J. M. Pringle, J. Sun, N. Byrne, P. C. Howlett, D. R. MacFarlane and M. Forsyth, Nat. Mater (2004) 3, 29-32.

[34] L. J. Hardwick, M. Holzapfel, A. Wokaun and P. Novák, J. Raman Spectrosc. (2007) 38, 110-112.

[35] M. J. Monteiro, F. F. C. Bazito, L. J. A. Siqueira, M. C. C. Ribeiro and R. M. Torresi, J. Phys. Chem. B (2008) 112, 2102-2109.

[36] M. Wetjen, M. A. Navarra, S. Panero, S. Passerini, B. Scrosati and J. Hassoun, ChemSusChem (2013) 6, 1037-1043.

[37] S.-H. Kim, K.-H. Choi, S.-J. Cho, E.-H. Kil and S.-Y. Lee, J. Mater. Chem. A (2013) 1, 4949-4955.

[38] L.-X. Yuan, Z.-H. Wang, W.-X. Zhang, X.-L. Hu, J.-T. Chen, Y.-H. Huang and J. B. Goodenough, Energy Environ. Sci. (2011) 4, 269-284.

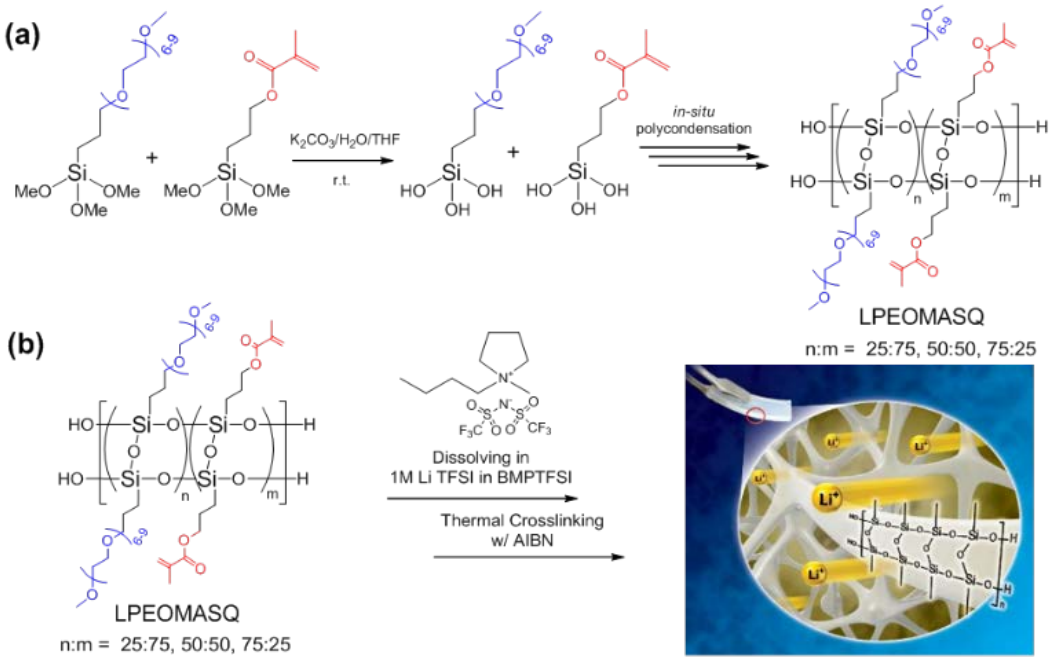

Figure 3.1. (a) Synthesis of LPEOMASQ series and (b) fabrication of PEGylated hybrid ionogels

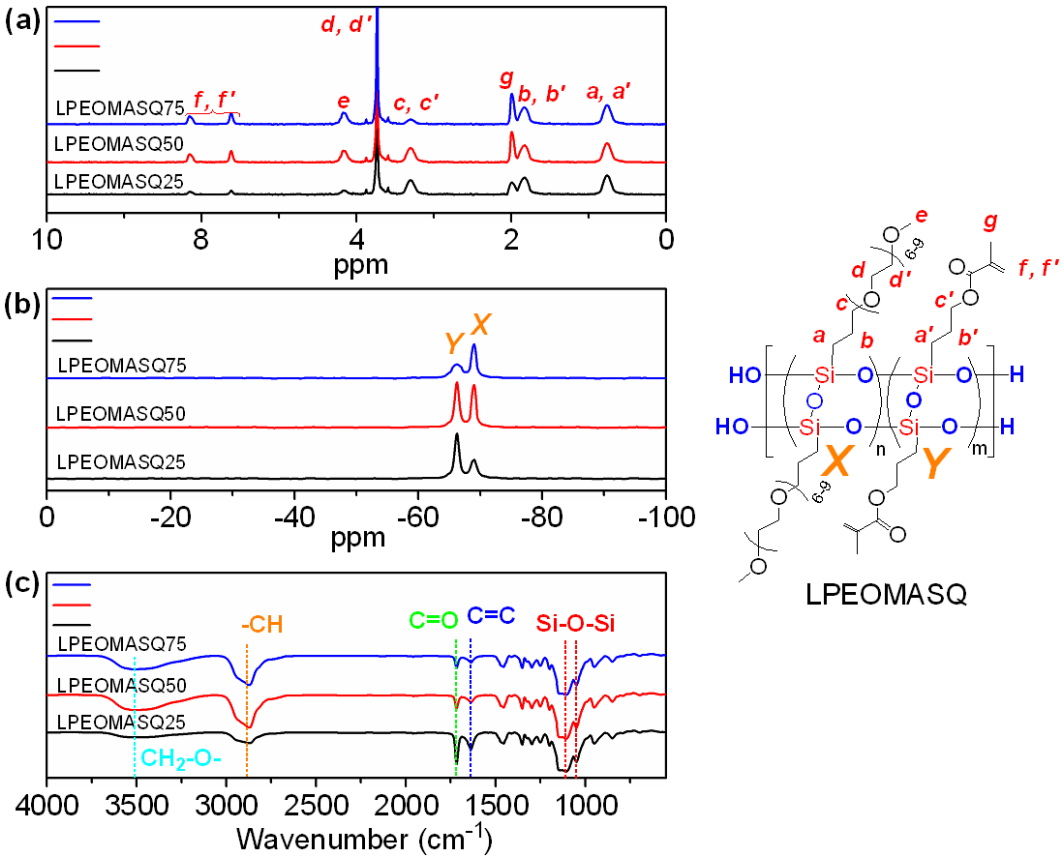

Figure 3.2. (a) ^{1}H NMR, (b) ^{29}Si NMR, and (c) FTIR spectra for PEGylated LPSQs

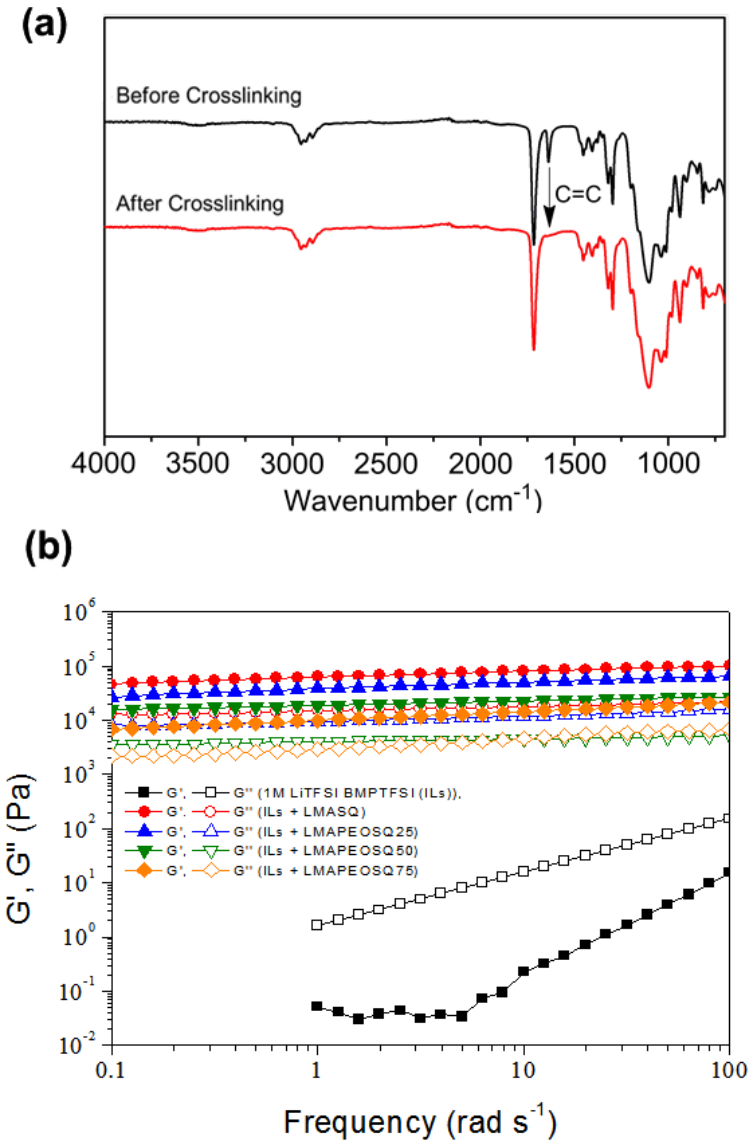

Figure 3.3. (a) FTIR spectra of LPEOMASQ75 5 wt % before and after cross-linking, (b) rheological properties of IL and hybrid ionogels.

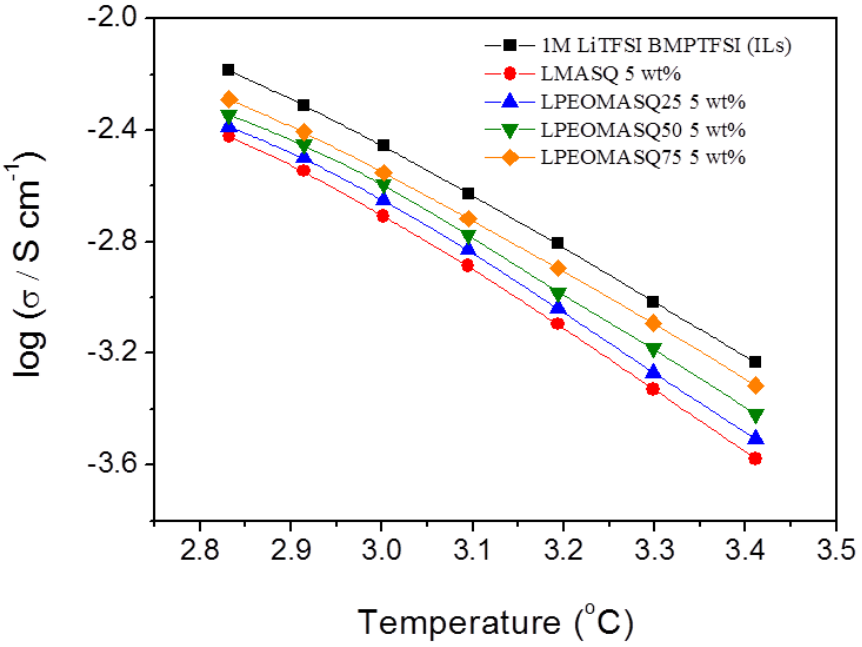

Figure 3.4. Temperature dependent ionic conductivities for the IL and hybrid ionogels.

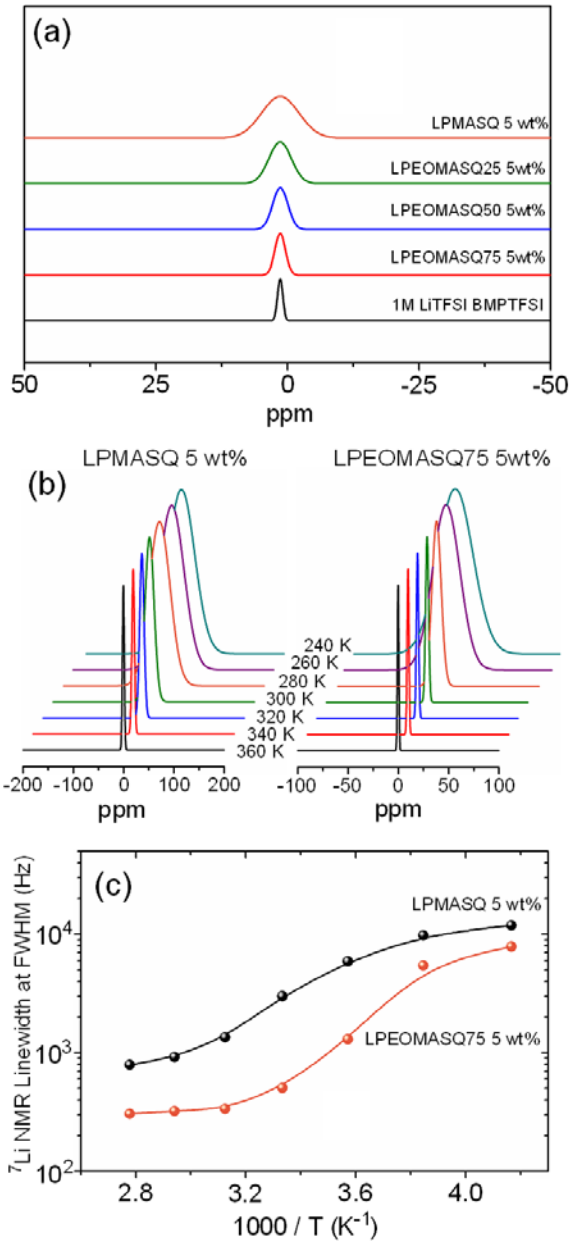

Figure 3.5 (a) Solid-state ^{7}Li NMR spectra for the IL and hybrid ionogels, (b) temperaturedependent solid-state ^{7}Li NMR spectra of LPMASQ 5 wt% and LPEOMASQ75 5 wt%, and (c) ^{7}Li NMR linewidth summary.

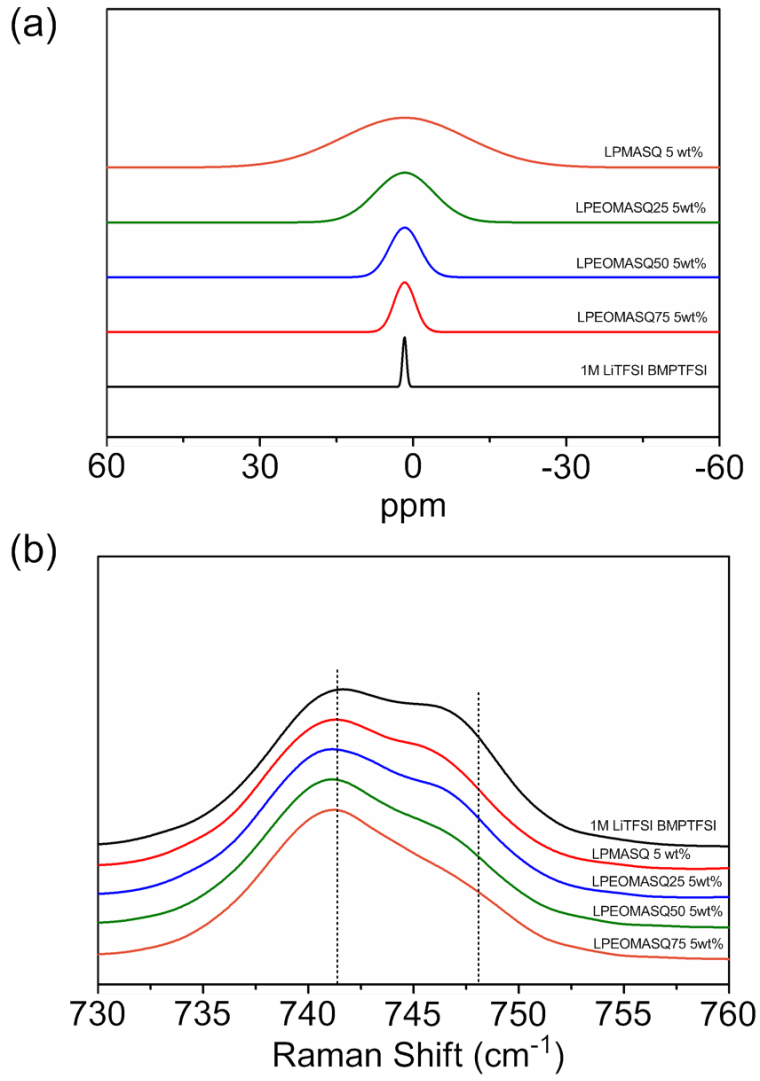

Figure 3.6. (a) Solid-state ^{19}F NMR spectra at room temperature and (b) Raman spectra.

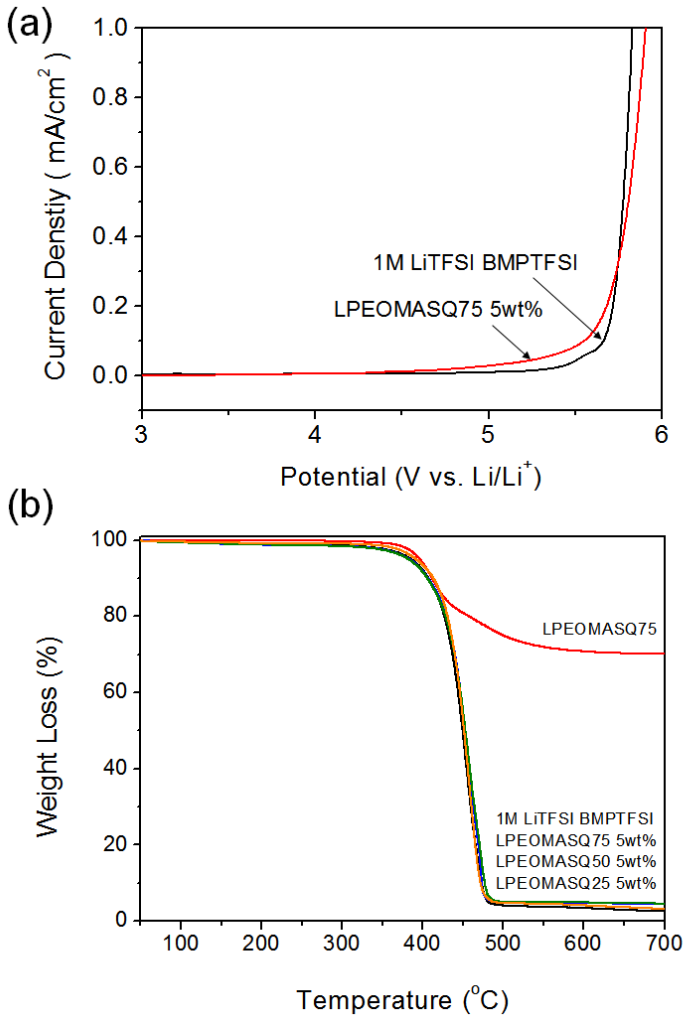

Figure 3.7. (a) Linear Sweep Voltamogram of BMPTFSI and LPEOMASQ75 5 wt% Hybrid Ionogel and (b) TGA Thermograms of 1M LiTFSI BMPTFSI, and hybrid ionogels.

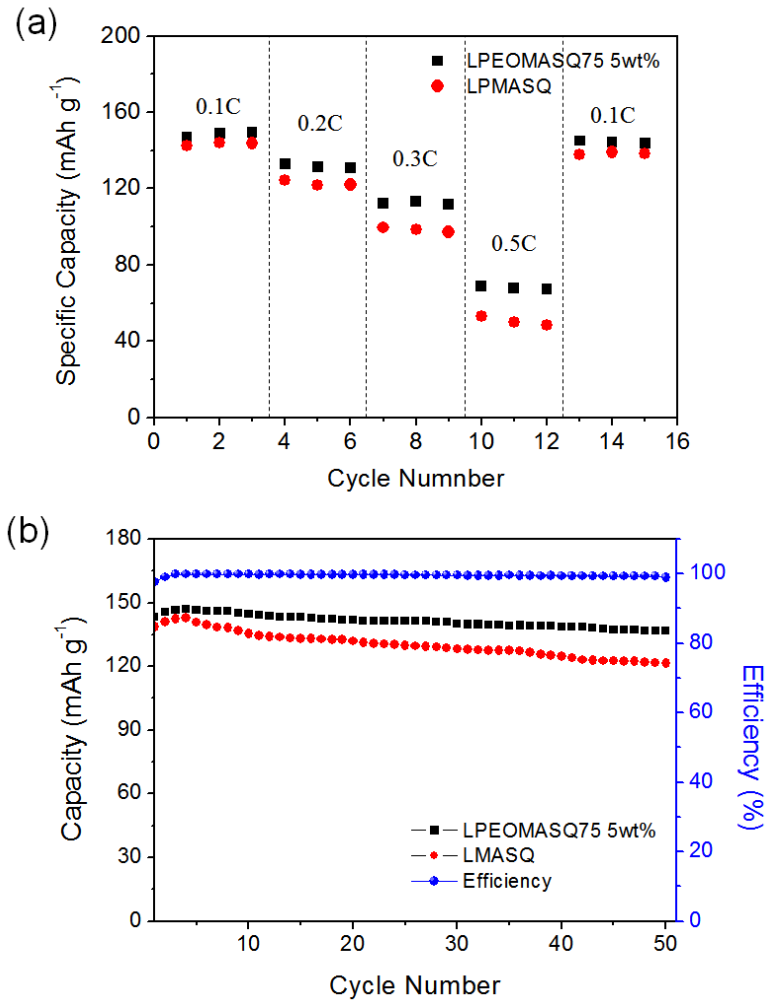

Figure 3.8. (a) Discharge capacities at various C-rates for LiFePO4/hybrid ionogel/Li cells and (b) cyclabilty of PEGylated hybrid ionogels.

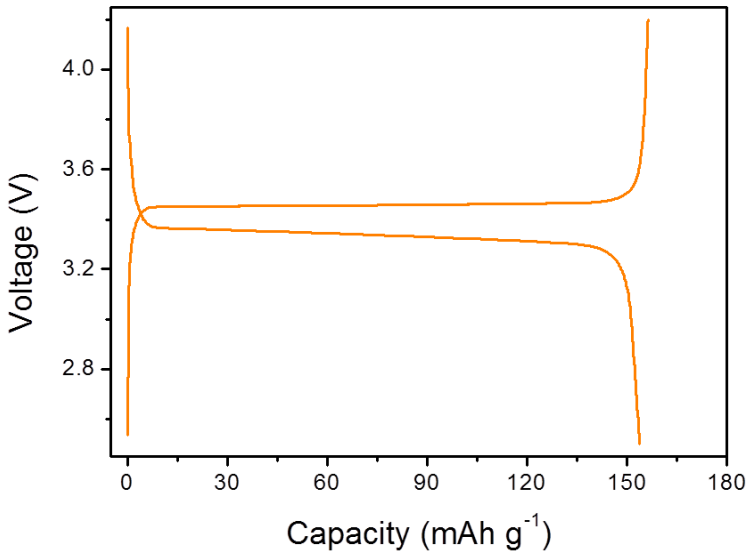

Figure 3.9. Representative charge-discharge profile of cell fabricated with 1M LiTFSI BMPTFSI.

Chapter 4

Multifunctional Mesoporous Ionic Gels and Scaffolds Derived from Polyhedral Oligomeric Silsesquioxanes

4.1. Introduction

A new methodology for fabrication of inorganic-organic hybrid ionogels and scaffolds is developed through facile crosslinking and solution extraction of a newly developed ionic polyhedral oligomeric silsesquioxane with inorganic core. Through design of various cationic tertiary amines as well of cross-linkable functional groups on each arm of the inorganic core, high performance ionogels are fabricated with excellent electrochemical stability and unique ion conduction behavior, giving superior lithium ion battery performance. Moreover, through solvent extraction of the liquid components, hybrid scaffolds with well-defined interconnected mesopores are utilized as heterogeneous catalysts for the CO_2-catalyzed cycloaddition of epoxides. Excellent catalytic performances, as well as highly efficient recyclability are observed when compared to other previous literature materials.

Inorganic metal oxide templates with well-defined architectures have been widely studied for advanced applications in energy, [1, 2] environment, [3] electronics, [4] medicine, [5, 6] and in some other sectors. Through realization of concepts such as pore-structure engineering and chemical modifications, versatile materials have been reported for various next generation applications. Most of

these inorganic templates are fabricated through one of these two methods: the use of block copolymer self-assembly [7,8] or the use of structural directing agents, such as surfactants,[9] followed by pyrolysis. These studies have detailed the wide-spread utility in the ability to form well-defined nano- to micropores with a high degree of regularity and diverse morphologies. Moreover, chemical treatments of these inorganic templates with silane coupling agents have imbued new functionalities for the next generation of advanced applications. [10, 11] However, these methods for fabrication of inorganic templates limit their scopes to heterogeneous processing. For applications requiring complete solution processability, the use of inorganic scaffolds derived from these methods can be considered unpractical approach.

Polyhedral oligomeric silsesquioxanes, commonly known as POSS, are consisting of silicon oxide, 3-dimensional polyhedrons with organic functional groups radially stemming outwards from the vertices. The well-defined inner inorganic core provides the smallest particle of silica known so far with sizes ranging from 1 to 3 nm, depending on the polyhedron size. The most common POSS is octahedron (T8-POSS).[12] An extensive library of new compounds has been reported for a plethora of applications through various chemical treatment of the organic functional group –R.[13-15] POSS can be considered as an ideal candidate for inorganic scaffolds due to several traits, including solution

processability, having well-defined inorganic core, and organic functionality.[12] In fact, the formation of porous inorganic scaffolds using POSS materials without the use of structure-directing agents or polymers has recently been reported.[13,15,16]

Solidified ionic liquids or ionogels have a myriad of unique functions, including high ionic conductivity, CO_2 capture ability, and catalytic properties.[17-20] The widespread interest in using these ionic functions stems from their outstanding thermal, electrochemical, and nonvolatile properties.[21] However, the fact that ionic liquids are actually liquids, limits their recyclability, recovery, and mechanical properties. As such, ionic liquid-supported materials are of immense interest to material scientists for practical applications in electrochemical cells and catalysts.

In this work, we studied a facile route to prepare ionic inorganic–organic hybrid scaffolds with well-defined mesopores through synthesis of a series of crosslinkable ionic POSS materials. We investigated the electrochemical performance of the ionogels prepared through crosslinking of the ionic POSS materials in an ionic liquid media and examined the catalytic performance of the hybrid supported mesoporous ionic POSS scaffolds through subsequent solvent extraction of the liquid phase (Scheme 1). Introduction of an ionic function at the molecular level to the POSS core makes these materials completely solution-

processable. The fabrication methods to produce ionogels and scaffolds offer a bottom-up approach for preparation of functional porous materials for energy and environmental applications..

4.2. Experimental

Materials.

1-methylimidazole (Aldrich, 99%), 2-bromobutane (Aldrich, 99%), 1-methylpyrrolidine (Aldrich, 99%), 1-iodobutane (Aldrich, 99%), chloropropyltrimethoxysilane (Gelest, 98%), propylene oxide (Aldrich, 99%), styrene oxide (Aldrich, 99%), allyl glycidyl ether (Aldrich, 99%), glycidyl methacrylate (Aldrich, 99%), and acetonitrile (J.T. Baker, HPLC grade) were vacuum distilled prior to use. Other solvents were of HPLC grade (J.T. Baker), were used as received. Azobisisobutryonitrile (AIBN) (Aldrich, 99%) was recrystallized from solution in MeOH prior to use. Irgacure 184 (BASF) was used as received. Ethylene oxide (Hanhwa chemicals, 99%) was used as received.

Synthesis of 1-ethyl 3-methyl imidazolium bis (trifluromethanesulfonyl) imide, (EMITFSI).

In a dry 500 mL round-bottom flask, stoichiometric amounts of 1-methylimidazole (48.4 g, 0.59 mol) and 2-bromobutane (64.3 g, 0.59 mol) were added to 250 mL of ethyl acetate and magnetically stirred at room temperature for

24 h. The product was repeatedly washed with ethyl acetate and filtered until pure white salt of EMIBr was obtained. EMIBr was then dissolved in deionized water and mixed with a stoichiometric amount of LiTFSI dissolved in deionized water. The organic phase was extracted with methylene chloride and subsequently dried at 100 °C for 24 h to remove any residual water. The resulting EMITFSI had less than 100 ppm H_2O as measured with Karl Fischer method. Ionic liquid solutions of 1 M LiTFSI in 1-ethyl 3-methyl imidazolium bis(trifluromethanesulfonyl)imide-(EMITFSI) were made through dissolving LiTFSI at 60 °C for 24 h and drying at 100 °C overnight prior to use.

Synthesis of *N*-butyl-*N*-methylpyrrolidinium bis (trifluoromethylsulfonyl) imide (BMPTFSI).

In a dry 500 mL round-bottom flask, stoichiometric amounts of 1-methylpyrrolidine (50 g, 0.59 mol) and 1-iodobutane (108 g, 0.59 mol) were added to 250 mL ethyl acetate and magnetically stirred at room temperature for 24 h. The product was repeatedly washed with ethyl acetate and filtered until pure white salt of BMPI was obtained. BMPI was then dissolved in deionized water and mixed with a stoichiometric amount of LiTFSI dissolved in deionized water. The organic phase was extracted with methylene chloride and subsequently dried

at 100 °C for 24 h to remove any residual water. The resulting BMPTFSI had less than 100 ppm H_2O as measured with the Karl Fischer method. Ionic liquid solutions of 1 M LiTFSI in BMPTFSI were made via dissolving LiTFSI at 60 °C for 24 h and drying at 100 °C overnight prior to use.

Synthesis of T8-Chloropropyl POSS (1).

First, a solution of concentrated HCl (5 mL) in MeOH (150 mL) was prepared in a 250 mL jacket flask equipped with a condenser and magnetic stir bar. To this solution, 3-chloropropyltrimethoxysilane (15 g, 0.075 mol) was added dropwise at room temperature with vigorous stirring. After addition of 3-chloropropyltrimethoxysilane, the solution was stirred at room temperature for 2 h. Stirring was then stopped and the solution was left at room temperature for another 48 h. Afterwards, di-n-butyltin dilaurate (0.15 g, 0.24 mol) was added and the reaction solution was stirred for another 48 h at room temperature, when a white crystalline precipitate appeared. The solution was filtered to collect the crystals, washed copiously with methanol, and subsequently dried in a vacuum oven set at 40 °C overnight. Yield of the reaction was measured as 3.68 g, 38%.

General Procedure for Metathesis Reactions with T8-chloropropyl POSS.

In a flame-dried 50 mL round bottom flask with a magnetic bar, T8-chloropropyl POSS (2) (1 g, 4.62 mmol chloropropyl equiv) was dissolved in 10 mL of dry DMF. After T8-chloropropyl POSS was completely dissolved, 1-vinylimidazole (0.52 g, 5.54 mmol) was added under N_2 (g) flow. The brown reaction mixture was then heated to 40 °C and vigorously stirred for 48 h when the reaction mixture turned to light orange, an indicative for the quaternization of imidazole moieties. After confirming that all of the chloropropyl groups were converted to propyl vinylimidazolium chloride groups via ^{1}H NMR examination, the reaction mixture was left to cool down at room temperature. Following partial evaporation of the volatiles, the reaction mixture was precipitated in 100 mL of cold acetone to give I-POSS-1a with a good yield (88%).

General Procedure for Ion Exchange.

The anion exchange method adopted in this study was a modified literature procedure. Typically, I-POSS-1a (1 g, 4.62 mmol imidazolium chloride equiv) was dissolved in 15 mL of deionized water. In another vial, LiTFSI (1.45 g, 5 mmol) was dissolved in 10 mL of deionized water. In this solution, the first

solution containing I-POSS-1a was precipitated very slowly with vigorous stirring. After stirring for 20 min, the solution was filtered off to give I-POSS-1b as a light brown glassy solid with a good yield (80%)

General Procedure for Fabrication of I-POSS-G Series.

I-POSS-1b was dissolved in a solution of 1 M LiTFSI in 1-ethyl-3-methylimidazolium bis(triflurometha nesulfonyl)imide (EMITFSI) to make IL solutions of 2, 5, and 10 wt %. To these solutions, AIBN (1 wt %, with respect to I-POSS) was added and stirred to make homogeneous solutions. Thermal curing was carried out at 70 °C for 3 h to facilitate full gelation, producing homogeneous and non-leaking gels. Identical procedures were carried out for triallylammonium-functionalized I-POSS-2b with 1-butyl-1-methylpyrrolidinium bis(triflurometha nesulfonyl)imide (BMPyrTFSI) as ionic liquid solution. UV-curing was also possible through the addition of Irgacure 184 as photoinitiator instead of AIBN, and gels were obtained through mild UV-irradiation of 3 J cm^{-2}.

General Procedure for Fabrication of I-POSS-S Series.

The obtained gels of I-POSS-G series (~ 5 g) were dispersed in THF (30

mL) and sonicated for 30 min at 40 °C. Afterwards, the liquid components were decanted. This procedure was repeated at least 5 times to ensure all of the ionic liquid was solvent extracted. Following mild treatment at 70 °C to completely dry the white powdery material, I-POSS-S series were obtained as fine white powders. No further chemical or mechanical treatments were required.

General Procedure for Catalytic Examinations.

To a predetermined amount of I-POSS-S, either neat epoxide or 400 mM of its solution in degassed acetonitrile was added to a custom built high pressure stainless steel reactor. After tightly sealing the reactor, a stainless steel gas line attached to CO_2 gas (99.999% purity) was fixed to the reactor and pressure was set at 110 psi and temperature at 110 °C. After a certain time, the reaction solution was filtered and the conversion to cyclic carbonate was measured with gas chromatography technique. For recyclability examinations, the filtered I-POSS-S scaffold powders were dried at 80 °C for 1 h prior to use.

Characterization.

Fourier transform infrared spectra were recorded with a Perkin-Elmer FT-IR system Spectrum-GX. Number average molecular weight (Mn) and molecular weight distributions (Mw/Mn) of polymers were determined using a JASCO PU-2080 plus SEC system equipped with a refractive index detector (RI-2031 plus), UV detector (λ = 254 nm, UV-2075 plus), and a Viscotek SLS apparatus using THF as the mobile phase at 40 °C with a flow rate of 1 mL min^{-1}. The samples were separated through four columns (Shodex-GPC KF-802, KF-803, KF-804, KF-805). ^{1}H NMR and ^{29}Si NMR spectra were recorded in $CDCl_3$ at 25 °C using a Varian Unity INOVA (1H: 300 MHz, 29Si: 59.6 MHz). Static solid-state ^{7}Li NMR spectra were obtained on a Varian INOVA (^{1}H: 400 MHz, ^{7}Li: 155.45 MHz) with spinning frequency held constant at 10 kHz with a pulse delay time of 4 s. Samples were packed into 7.5 mm zirconia rotors and sealed with KeI-F short caps. Thermal gravimetric analysis was carried out with a TA instrument (TGA 2950) at a heating rate of 10 °C min^{-1} under a N_2 atmosphere. Rheological properties were examined using a rheometer (Advanced Rheometric Expansion System, ARES) instrument with cone-plate geometry (25 mm diameter). All rheological measurements were performed in the linear viscoelastic region under a N_2 atmosphere. Surface area, pore volume and size distribution were measured

with N_2 adsorption method at 77 K using a BET instrument (ASAP 2010, Micromeritics). I-POSS-S series were dried at 70 °C prior to examinations. SEM and EDX mapping images were taken using a SEM Inspect F50 instrument.

The ionic conductivity was determined using a complex impedance analyzer (Bio-Logics, VMP3) over a frequency range from 1 Hz to 1 MHz at an AC amplitude of 10 mV. The electrochemical stability of the gel polymer electrolytes was examined using a linear sweep voltammetry system. In the experiments, a stainless steel working electrode was used with Li metal as both the counter and reference electrodes. The voltage was swept at a scan rate of 1.0 mV s^{-1}. Electrochemical measurements of the gel polymer electrolyte were conducted using 2032 coin cells consisting of a separator, Li metal, and a LiFePO4 cathode (containing 90 wt % $LiFePO_4$, 5 wt % carbon black, and 5 wt % PVDF). All the cells were assembled in an argon-charged glove box. After fabrication, the cells with pregel solution were subjected to thermal crosslinking for 3 h at 70 °C. The galvanostatic charge–discharge experiments were carried out in the voltage range of 2.5–4.2 V using a battery cycler (Wonatech, WBCS3000) at 50 ^{o}C. Cationic transference numbers were obtained through AC impedance method with the steady-state current technique.

4.3. Results and Discussion

We followed a literature procedure to synthesize T8-Chloropropyl POSS. [22] The Menshutkin reactions [23] with vinyl imidazole and triallylamine resulted in crosslinkable ionic POSS with two different quaternary ammonium chloride structures, named as Ionic POSS 1a and 2a. Subsequent ionic exchange with LiTFSI yielded TSFI– anion structures, named as Ionic POSS 1b and 2b (Figure 4.1(a)). All of the Ionic POSS materials were observed well soluble in organic solvents and were characterized with ^{1}H NMR, ^{13}C NMR, ^{29}Si NMR, and FT-IR techniques to examine their chemical structures (Figure 4.2). The ionic groups introduced to the cubic siloxane core were designed such that crosslinking function with vinyl or allyl groups was possible through mild thermal or UV treatments (Figure 4.3).

Using the obtained Ionic POSS 1b and Ionic POSS 2b products, we were able to completely solidify ionic liquid solutions, 1 M LiTFSI in EMITFSI or 1 M LiTFSI in BMPTFSI, with analogous cation structures at concentrations as small as 2 wt %. We were able to convey the solid gel-like properties via examination of the dynamic viscoelastic properties of I-POSS-G series (Figure 4.4). A pronounced plateau region of G′ and greater G′ than G″ in all frequencies

demonstrated a dynamic shift from the liquid to solid-like state due to the formation of an interconnected network structure. [24, 25]

First, the electrochemical properties of I-POSS-G materials were examined. Due to the miniscule amounts of Ionic POSS cross-linker required to fully solidify the ionic liquid solutions, the ionic conductivity (Figure 4.5) of I-POSS-G2b was exceptionally large, showing minimal depreciation relative to the neat ionic liquid. Moreover, compared with ionogel fabricated with MMA–POSS without any ionic group at identical cross-linker concentration of 5 wt %, the I-POSS-G2b gel exhibited larger ionic conductivity values at all temperatures. We attributed these observations to two main factors: (1) contribution of the molecular-level ionic function of Ionic POSS, and (2) the formation of interconnected network structure with well-defined mesopores, which will be discussed later. To probe the first hypothesis, we conducted single pulse solid-state ^{7}Li NMR experiments. As shown in Figure 4.6, the ^{7}Li NMR linewidths for I-POSS-G2b at 2, 5, and 10 wt % were significantly sharper than those of the MMA–POSS ionogels It indicates that the dynamic environment of the lithium ions was coupled with the ionic groups of network structure, and the system with ionic groups contains a larger concentration of mobile lithium ions than the system without ionic groups. We speculate that the incorporation of ionic species into the network structure resulted in the contrary effects on each cations and

anions, as attractive interactions arose from cationic moieties of the network structure and mobile $TFSI^-$ anions induced an increase in the concentration of ionic association in the vicinity of tethered ammonium cations, restricting the movement of the $TFSI^-$ anions. The mobility of lithium cations, on the other hand, was relatively slightly impaired by the cationic groups on the network structure. This is considered as a result of repulsive interaction between lithium cations and cationic network structure, which could help the ionic dissociation, leading to minimization of lithium ion mobility depreciation.

The mobility of ionic species was further investigated through combination of AC impedance method with steady-state current technique.[26] (Figure 4.7) The measured t_{Li+} values were 0.38 and 0.26 for I-POSS-G2b and MMA–POSS 5 wt % ionogel, respectively at room temperature, which is in good agreement with the lithium NMR examination results. The larger t_{Li+} value observed for ionic POSS gel again suggests that the tethered cationic groups may interact with the counter TFSI anions, allowing a relatively fast movement of lithium ions, whereas the MMA–POSS network only served as a physical support to maintain the mechanical robustness.

Prior to evaluating the electrochemical cell performances, the electrochemical stability and thermal stability of I-POSS-G series were confirmed via using linear sweep voltammetry (LSV) measurements (Figure 4.8) and TGA

(Figure 4.9), respectively. Lithium ion batteries fabricated with LiFePO4/I-POSS-G2b/Li structure were used to characterize the electrochemical performance of as-prepared hybrid ionogels. The rate capabilities of cells were examined and compared between two cross-linker systems, as presented in Figure 4.10(a). The cells were charged at a current density of 0.1 C and discharged at various current densities, ranging from 0.1 to 1 C. As shown, both cells delivered a similar discharge capacity in the initial cycle. However, upon increasing the current density, the cell with I-POSS-G2b exhibited noticeable improvement in capacity retention compared with the cells containing MMA–POSS ionogels. Moreover, the difference in discharge capacities between both the electrolyte systems continuously increased with increasing current density. The improvement of rate capability for cells with I-POSS-G2b could be ascribed to their higher ionic conductivity and transference number of lithium ions, which possibly mitigate the increase in cell polarization derived from an increase in IR drop, resulting in enhancement of electrochemical performance.

Moreover, the cycling performances of cells were further evaluated at a constant charge/discharge current rate of 0.1 C/0.1 C. Figure 4.10(b) presents the discharge capacity and coulombic efficiency as a function of cycle number. As expected, the cells containing I-POSS-G2b ionogels provided highly stable cycling performance with a large coulombic efficiency of nearly 99%. A specific

discharge capacity of 147 mA h g^{-1} was still retained after 50th cycles, which corresponds to 95% of its largest discharge capacity. This observation was in stark contrast with the cells fabricated with MMA–POSS ionogels that started to show a precipitous drop in specific capacity retention around 25 cycles.

In addition to the superior electrochemical properties of Ionic POSS Gels (I-POSS-G series), we were able to obtain fine white powders characterized to be well-defined mesoporous Ionic Scaffolds (I-POSS-S series) through facile solvent extraction with THF solutions of I-POSS-G series. These ionic scaffolds, as shown in Figure 4.11, exhibited a mesoporous structure with particle-like morphology, characteristic of inorganic sol–gel derived oxide materials, with the EDX mapping of I-POSS-S2a. The experimental observations revealing that the atomic distribution of Si, O, C, and N (Figure 4.10(b–e)) were exceptionally homogeneous distributed throughout, indicating the molecular level functionalization of the ionic groups to the inorganic core. With consideration of mix-cure-extraction method of fabrication for the synthesized Ionic POSS materials, the well-defined particle size distribution and mesoporous structure are attributed to the well-defined silica cube of POSS.

BET analyses of these porous ionic scaffolds revealed surface areas of 891 and 938 m^2 g^{-1} for I-POSS-S1b and I-POSS-S2b, respectively (Figure 4.10(f)). These large surface areas, which are similar to those have reported for

mesoporous oxides, coupled with the well-defined 7.2 and 6.3 nm pore size and narrow pore-size distribution for POSS-S1b (Figure 4.10(g)) and I-POSS-S2b, respectively, led us to investigate the use of these materials as heterogeneous catalysts for the CO_2 cycloaddition of epoxides. In this reaction, the cationic quaternary ammonium group tethered to the POSS core would coordinate with the epoxide, followed by ring-opening/oxidation with CO_2, giving the cyclic carbonate under neutral and mild conditions. [27-31]

The use of heterogeneous ionic liquid-supported catalysts for the CO_2 cycloaddition of epoxides has been extensively studied because of CO_2 having a notorious reputation of having no particular use in the chemical industry except for being one of the most abundant waste products produced, and of its harmful effects as a greenhouse gas contributing to global warming.[27-29] Use of CO_2 as a valuable reagent for the chemical syntheses of cyclic carbonates[30, 31] not only helps to recycle CO_2 but the formed cyclic carbonates through these reactions are currently ubiquitous in the battery/capacitor electrolyte industry. These cyclic carbonates, such as ethylene carbonate and propylene carbonate, are pervasively used as solvents to dissolve inorganic salts for non-aqueous electrolyte systems. [32]

Therefore, in addition to the epoxide precursor substrates of ethylene oxide and propylene oxide to form ethylene carbonate and propylene carbonate,

respectively, we investigated the heterogeneous ionic liquid-supported catalytic activity of our Ionic POSS Scaffolds (I-POSS-S) series with an extensive list comprising of simple to functional epoxides for CO_2 cycloaddition reactions. As presented in Table 4.1, the conversions for all of the various solvent-free reaction conditions and solution conditions were observed to be exceptionally high for the cycloaddition reactions with epoxides, as shown in Figure 4.12. Even when comparing the conversion rates and turnover frequency values with reports results (tabulated in Table 1), our I-POSS-S scaffolds revealed equal or better conversion performance under milder reaction conditions of lower CO_2 pressures or lower temperatures, as reflected in entries 1–8. This exceptional catalytic performance offers high accessibility of active ionic sites within the hybrid scaffold due to the well-defined mesopores between crosslinked inorganic cages.

The high catalytic activity independent of substituent group is also noteworthy. As shown, all of the tested epoxides provided conversion rates greater than 90%, even when the bulkiness of the epoxide substituent group increased from hydrogen for propylene oxide to methacryl for glycidyl methacrylate. Moreover, in addition to the exceptionally high conversions for all of the examined epoxide substrates, the turnover frequency for solvent-free and solution reaction systems were greater than previous reports of ionic-liquid supported heterogeneous catalyst systems (Table 4.1), making them highly applicable for

industrial use as well. When comparing the two different cation groups of imidazolium chloride and trialkylammonium chloride for I-POSS-S1a and I-POSS-S2a, respectively, we noticed that I-POSS-S1a exhibited slightly better catalytic performance (Figure 4.12). This observation was in part due to the higher CO_2-philic character of imidazolium heteroaromatic ring structure.

The overall exceptional catalytic activities of products have been attributed to several factors. First, a well-defined and interconnected porous structure facilitates substrate diffusion, as described previously, [33] allowing for high and easy access of the substrates to the POSS-core tethered ionic group. This high porosity and large surface area, derived from the interstitial space between POSS cubes chemically crosslinked with cationic ammonium groups of I-POSS-S1a and I-POSS-S2a, may facilitate diffusion of epoxides for optimal catalytic activity. Second, the pore diameters of 7.2 and 6.3 nm respectively for I-POSS-S1a and I-POSS-S2a are ideal for catalytic diffusion of various substrates, as several previous studies have reported that pore with diameters of larger than 4 nm are optimal for ionic liquid-supported heterogeneous CO_2 cycloaddition reaction systems.[33] We were also able to imbue high ionic content (~ 4 mmol g–1 I-POSS-S) to the inorganic matrix through functionalization of the ionic groups directly to the inorganic core, allowing for fast access of the substrate epoxides for catalytic activity.

We also examined the recyclability of I-POSS-S catalysts. As shown in Figure 4.12(c), both I-POSS-S1a and I-POSS-S2a materials exhibited exceptional performance with minimal to no depreciation in catalytic conversion of ethylene oxide to ethylene carbonate, as the total catalytic conversion degree of decrease was only about 5%, rendering these materials highly applicable as nanocatalysts for the CO_2 conversion of epoxides to cyclic carbonates. Other reactions are currently being investigated for these fully hybrid nanocatalysts.

4.4. Conclusion

In conclusion, a new methodology for fabrication of inorganic–organic hybrid ionogels and scaffolds was developed through facile crosslinking/solution extraction of an Ionic POSS material. Fabricated ionogels exhibited excellent electrochemical stability with unique ion conduction behavior, giving superior lithium ion battery performance. The heterogeneous catalyst application of the solvent extracted hybrid ionic scaffolds revealed that the well-defined interconnected porous structure allowed for unparalleled catalytic performance.

4.5. References

[1] Y. Lu, S. K. Das, S. S. Moganty and L. A. Archer, Adv. Mater, (2012) 24, 4430-4435.

[2] Z. Tu, P. Nath, Y. Lu, M. D. Tikekar and L. A. Archer, Accounts Chem. Res. (2015) 48, 2947-2956.

[3] M. Pera-Titus, Chem. Rev. (2014) 114, 1413-1492.

[4] M.-G. Kim, M. G. Kanatzidis, A. Facchetti and T. J. Marks, Nat. Mater. (2011) 10, 382-388.

[5] J. L. Townson, Y.-S. Lin, S. S. Chou, Y. H. Awad, E. N. Coker, C. J. Brinker and B. Kaehr, Nat. Commun. (2014) 5.

[6] I. I. Slowing, B. G. Trewyn and V. S. Y. Lin, J. Am. Chem. Soc. (2007) 129, 8845-8849.

[7] T. N. Hoheisel, K. Hur and U. B. Wiesner, Prog. Polym. Sci. (2015) 40, 3-32.

[8] A. G. Slater and A. I. Cooper, Science (2015) 348.

[9] S. A. Bagshaw and T. J. Pinnavaia, Angew. Chem. Int. Ed., 1996, 35, 1102-1105.

[10] E. Phillips, O. Penate-Medina, P. B. Zanzonico, R. D. Carvajal, P. Mohan,

Y. Ye, J. Humm, M. Gönen, H. Kalaigian, H. Schöder, H. W. Strauss, S. M. Larson, U. Wiesner and M. S. Bradbury, Sci. Transl. Med. (2014) 6, 260ra149-260ra149.

[11] T. Selvam, A. Machoke and W. Schwieger, Appl. Catal. A: Gen. (2012) 445–446, 92.

[12] D. B. Cordes, P. D. Lickiss and F. Rataboul, Chem.l Rev. (2010) 110, 2081-2173.

[13] Z. Li, D. Wu, Y. Liang, R. Fu and K. Matyjaszewski, J. Am. Chem. Soc. (2014) 136, 4805-4808.

[14] A. S. Lee, S.-S. Choi, H. S. Lee, K.-Y. Baek and S. S. Hwang, Dalton Trans. (2012) 41, 10585-10588.

[15] S. Wang, L. Tan, C. Zhang, I. Hussain and B. Tan, J. Mater. Chem. A (2015) 3, 6542-6548.

[16] M. Seino, W. Wang, J. E. Lofgreen, D. P. Puzzo, T. Manabe and G. A. Ozin, J. Am. Chem. Soc. (2011) 133, 18082-18085.

[17] A. I. Horowitz and M. J. Panzer, Angew. Chem. Int. Ed. (2014) 53, 9780-9783.

[18] J. Le Bideau, L. Viau and A. Vioux, Chem. Soc. Rev. (2011) 40, 907-925.

[19] J. Yuan, D. Mecerreyes and M. Antonietti, Prog. Polym. Sci. (2013) 38, 1009-1036.

[20] J. Sun, W. Cheng, W. Fan, Y. Wang, Z. Meng and S. Zhang, Catal. Today (2009) 148, 361-367.

[21] R. D. Rogers and K. R. Seddon, Science (2003) 302, 792-793.

[22] B. Marciniec, M. Dutkiewicz, H. Maciejewski and M. Kubicki, Organometallics (2008) 27, 793-794.

[23] A. W. T. King, J. Asikkala, I. Mutikainen, P. Järvi and I. Kilpeläinen, Angew. Chem. Int. Ed. (2011) 50, 6301-6305.

[24] A. S. Lee, J. H. Lee, S. M. Hong, J.-C. Lee, S. S. Hwang and C. M. Koo, RSC Adv. (2015) 5, 94241-94247.

[25] J. H. Lee, A. S. Lee, J.-C. Lee, S. M. Hong, S. S. Hwang and C. M. Koo, J. Mater. Chem. A (2015) 3, 2226-2233.

[26] D. Bansal, F. Cassel, F. Croce, M. Hendrickson, E. Plichta and M. Salomon, J. Phys. Chem. B (2005) 109, 4492-4496.

[27] A. Y. Hoekstra and T. O. Wiedmann, Science (2014) 344, 1114-1117.

[28] S.-g. Lee, Chem. Commun. (2006) 1049-1063.

[29] C. P. Mehnert, Chem.– A Eur. J. (2005) 11, 50-56.

[30] X. Zheng, S. Luo, L. Zhang and J.-P. Cheng, Green Chem. (2009) 11, 455-458.

[31] Y. Xiong, Y. Wang, H. Wang and R. Wang, Polym. Chem. (2011) 2, 2306-2315.

[32] K. Xu, Chem. Rev. (2004) 104, 4303-4418.

[33] H. Li, P. S. Bhadury, B. Song and S. Yang, RSC Adv. (2012) 2, 12525-12551.

[34] Z.-Z. Yang, Y.-N. Zhao, L.-N. He, J. Gao and Z.-S. Yin, Green Chem. (2012) 14, 519-527.

[35] Y. Xie, Z. Zhang, T. Jiang, J. He, B. Han, T. Wu and K. Ding, Angew. Chem. Int. Ed. (2007) 46, 7255-7258.

[36] S. Udayakumar, V. Raman, H.-L. Shim and D.-W. Park, Appl. Catal. A: Gen.(2009) 368, 97-104.

Table 4.1. Catalytic activity of I-POSS-S series for the CO_2 cycloaddition of various epoxides.

Entry	–R	Catalyst type	Catalyst amount [g]	Reaction aime [h]	Conversion [%][c]	Selectivity [%][c]	TOF [h^{-1}][d]	Literature values	
								Conversion [%]	TOF [h^{-1}]
1[a]	–H	I-POSS-S1a	0.5	6	88	91.3	35.7	99[34] Note: CO_2 Pressure 3× this study, temperature 120 °C.	33.3
2[a]	–H	I-POSS-S2a	0.5	6	84	84.1	27.7		
3[b]	–H	I-POSS-S1a	0.5	10	96	95.1	21.1	–	–
4[b]	–H	I-POSS-S2a	0.5	10	93	94.2	18.1	–	–
5[b]	–CH_3	I-POSS-S1a	0.5	10	95	93.1	21.1	97.4[35] Note: CO_2 Pressure 8× this study	19.8
6[b]	–CH_3	I-POSS-S2a	0.5	10	93	94.9	17.9		
7[b]	–C_6H_5	I-POSS-S1a	0.5	10	94	92.8	20.6	79.1[35] Note: CO_2 Pressure 8× this study	16.7
8[b]	–C_6H_5	I-POSS-S2a	0.5	10	91	94.3	17.7		
9[b]	–$CH_2OCH_2CHCH_2$	I-POSS-S1a	0.5	10	86	95.7	18.6	55.1[36] Note: Identical conditions	11.9
10[b]	–$CH_2OCH_2CHCH_2$	I-POSS-S2a	0.5	10	82	92.4	16.2		
11[b]	–$CH_2OCOCCH_2CH_3$	I-POSS-S1a	0.5	10	85	92.8	18.8	–	–
12[b]	–$CH_2OCOCCH_2CH_3$	I-POSS-S2a	0.5	10	83	91.4	16.0	–	–

[a] Solvent-free conditions; temperature: 110 °C; CO_2 pressure: 110 psi.

[b] Solution conditions: [Epoxide]: 400 mM in MeCN

[c] Determined by gas chromatography.

[d] Turnover frequency (TOF) = # mol_{conv} / # $mol_{ionic\ group}$ / reaction time

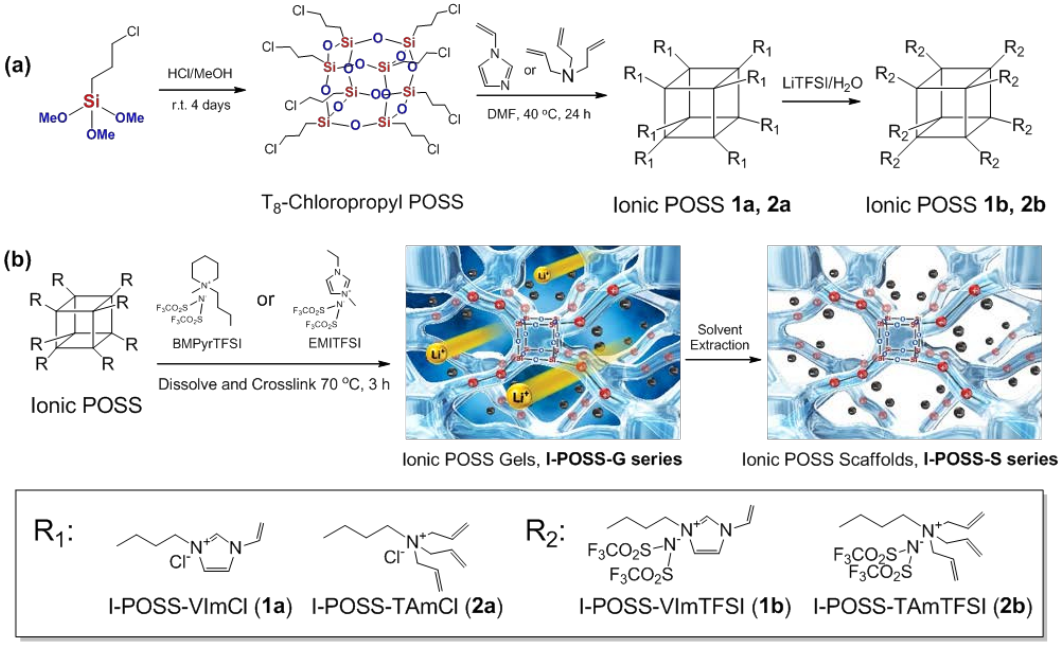

Figure 4.1. (a) Synthesis of Ionic POSS. (b) Fabrication of Ionic POSS Ionogels (I-POSS-G) and Ionic POSS Scaffolds (I-POSS-S) series.

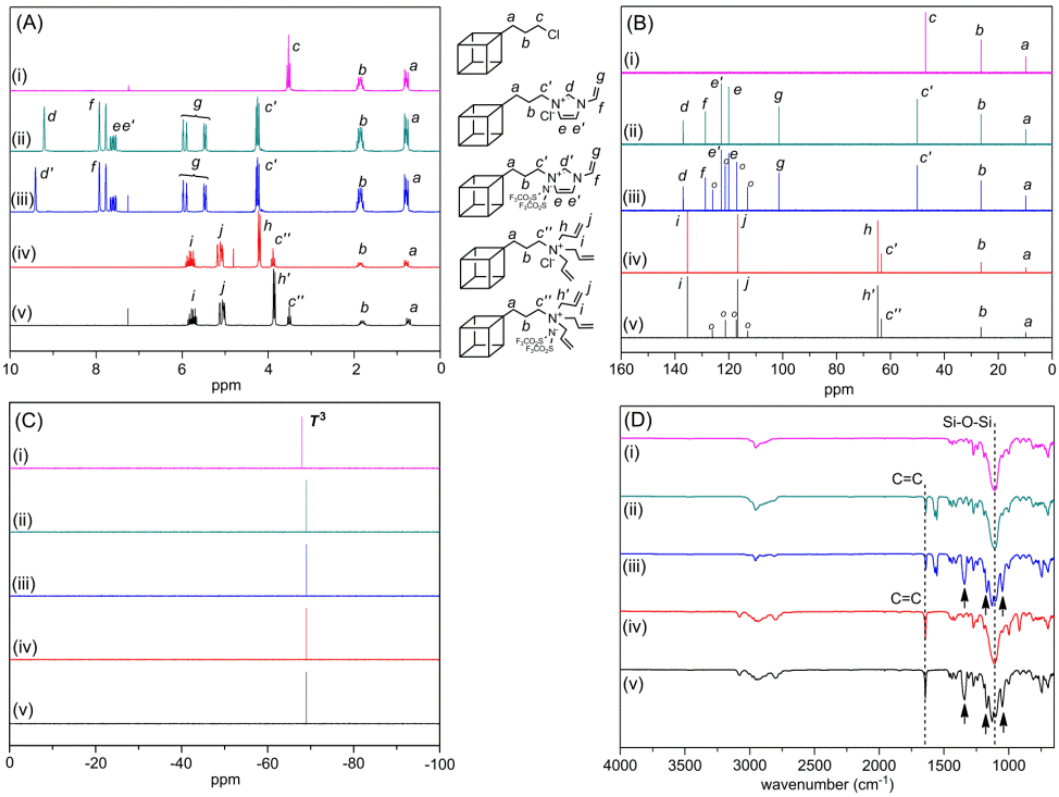

Figure 4.2. (A) ^{1}H NMR, (B) ^{13}C NMR, (C) ^{29}Si NMR, and (D) FTIR spectra for T8-Chloropropyl POSS, I-POSS-VIm, I-POSS-TAmCl, I-POSS-VImTFSI, and I-POSS-TAmTFSI with spectral assignments. Note: the cube represents the [SiO1.5]8 core.

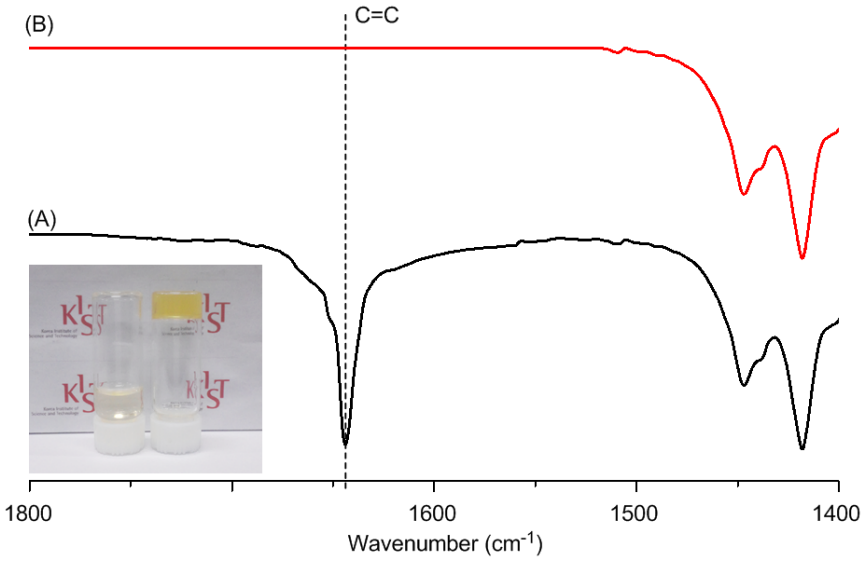

Figure 4.3. FTIR spectra of I-POSS-G1b 5 wt % (A) before and (B) after thermal curing with inset photograph showing the complete solidification of the neat ionic liquid.

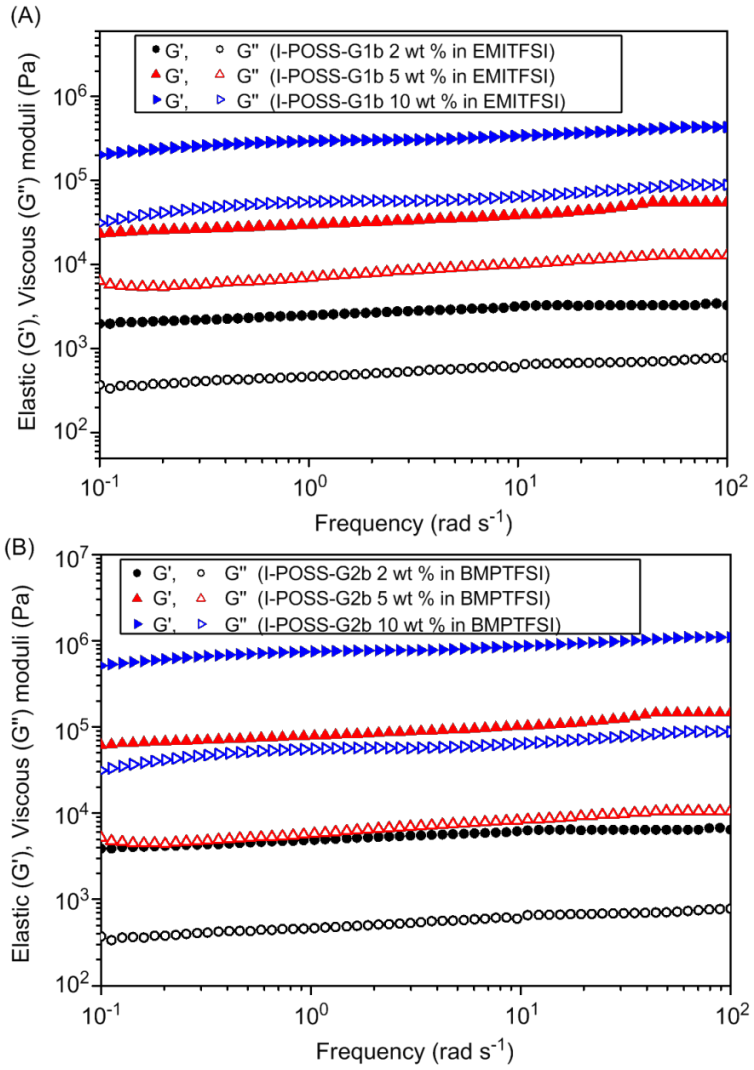

Figure 4.4. **Rheological properties of (A) I-POSS-G1b and (B) I-POSS-G2b series as a function of I-POSS concentration.**

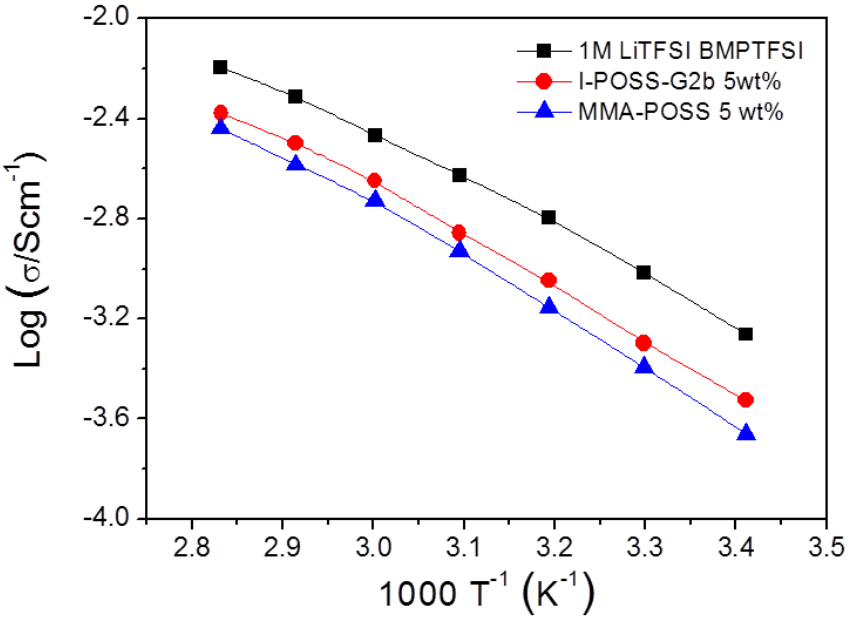

Figure 4.5 Temperature dependence of ionic conductivity.

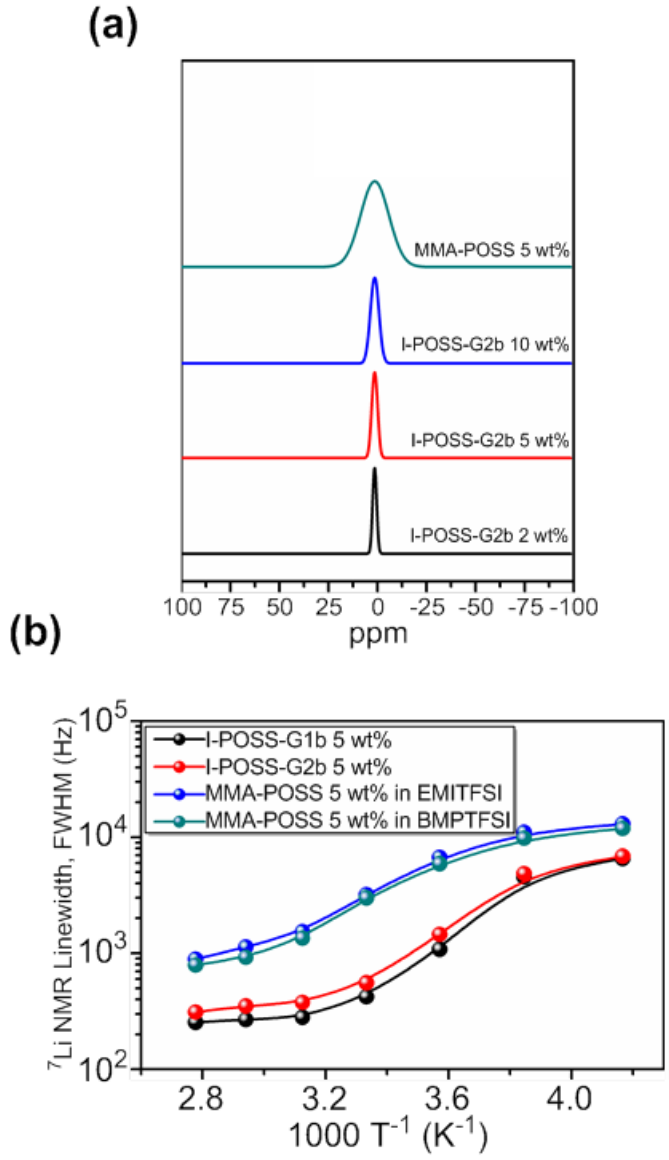

Figure 4.6. (a) Static solid-state ^{7}Li NMR spectra at room temperature. (b) Linewidth summary for temperature dependent static solid-state ^{7}Li NMR spectra.

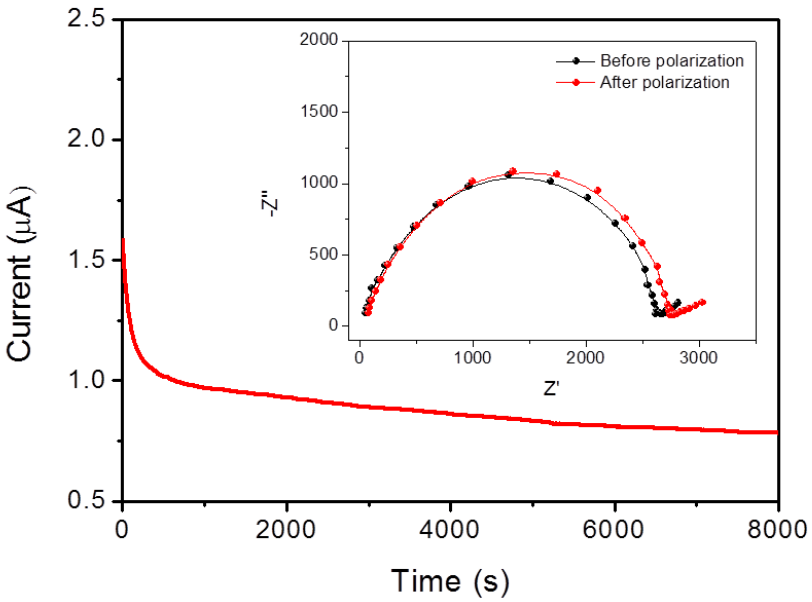

Figure 4.7. Chronoamperometric curve of Li/I-POSS-G1b/Li cell after a 10 mV dc pulse and impedance response (inset) of the same cell before and after dc polarization

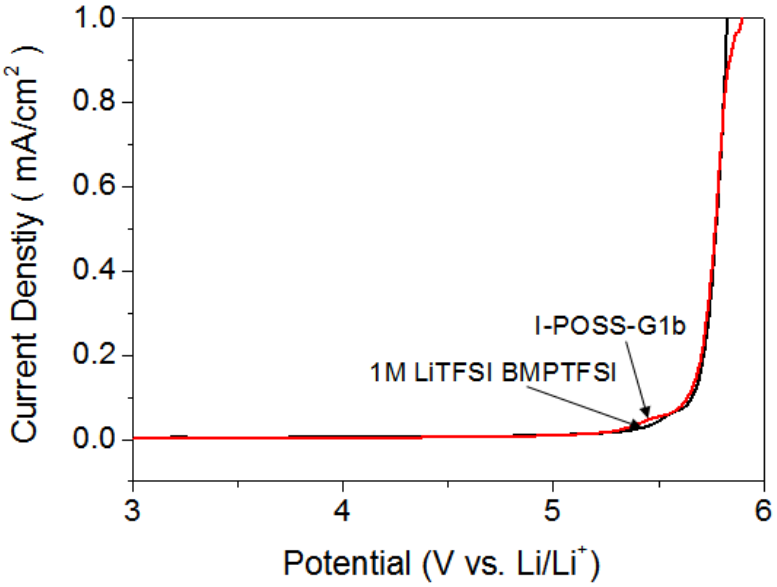

Figure 4.8. Linear sweep voltammetry of the neat ionic liquid, 1 M LiTFSI BMPTFSI and I-POSS-G1b.

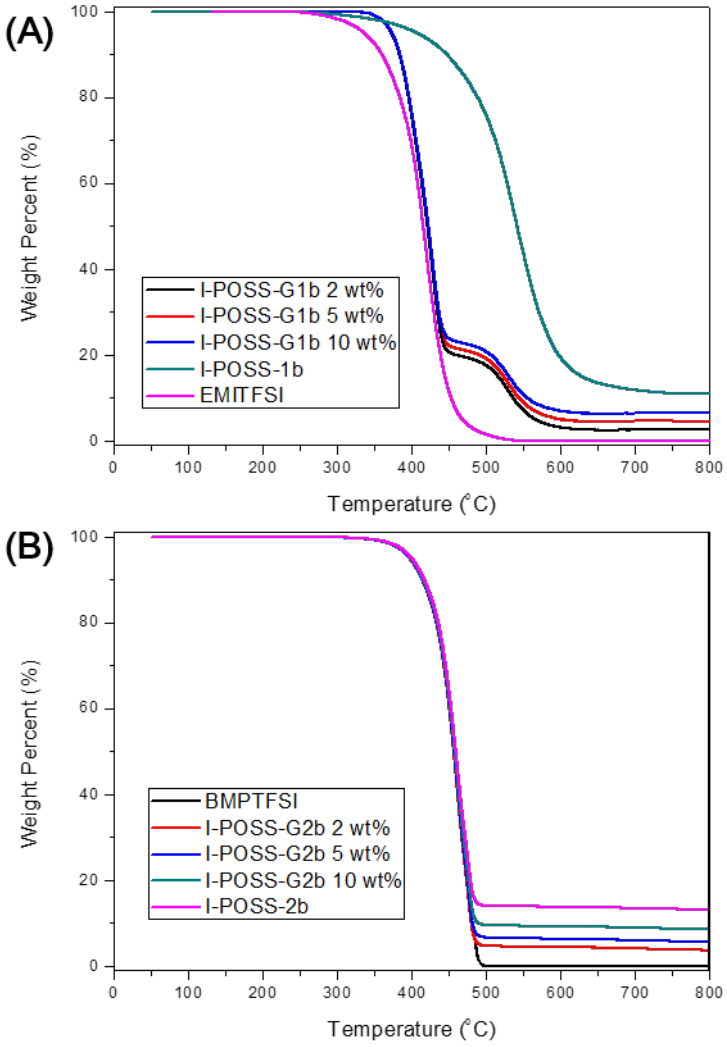

Figure 4.9. TGA thermograms of (A) EMITFSI with corresponding I-POSS-G1b gels and (B) BMPTFSI with corresponding I-POSS-G2b gels.

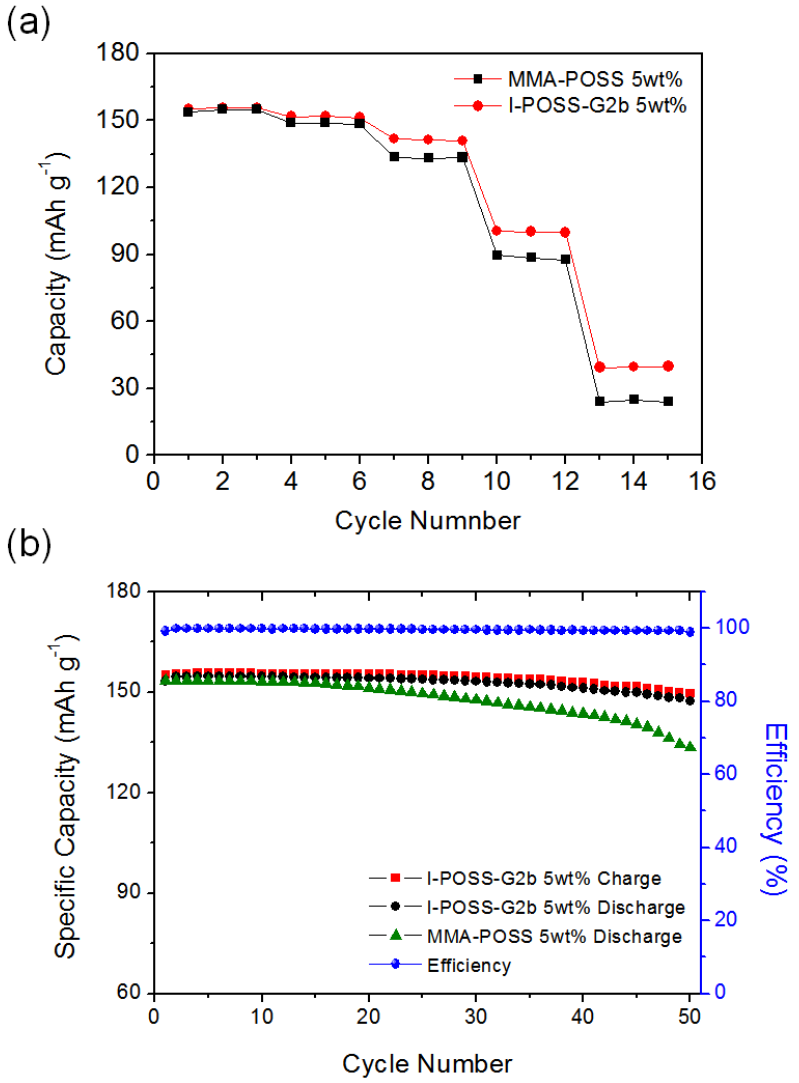

Figure 4.10. C-rate performance for Li/Gel/LiFePO4 LIB Cells. e) LIB cyclability tests for IL, I-POSS-G-2b 5 wt % and MMA–POSS 5 wt % gels.

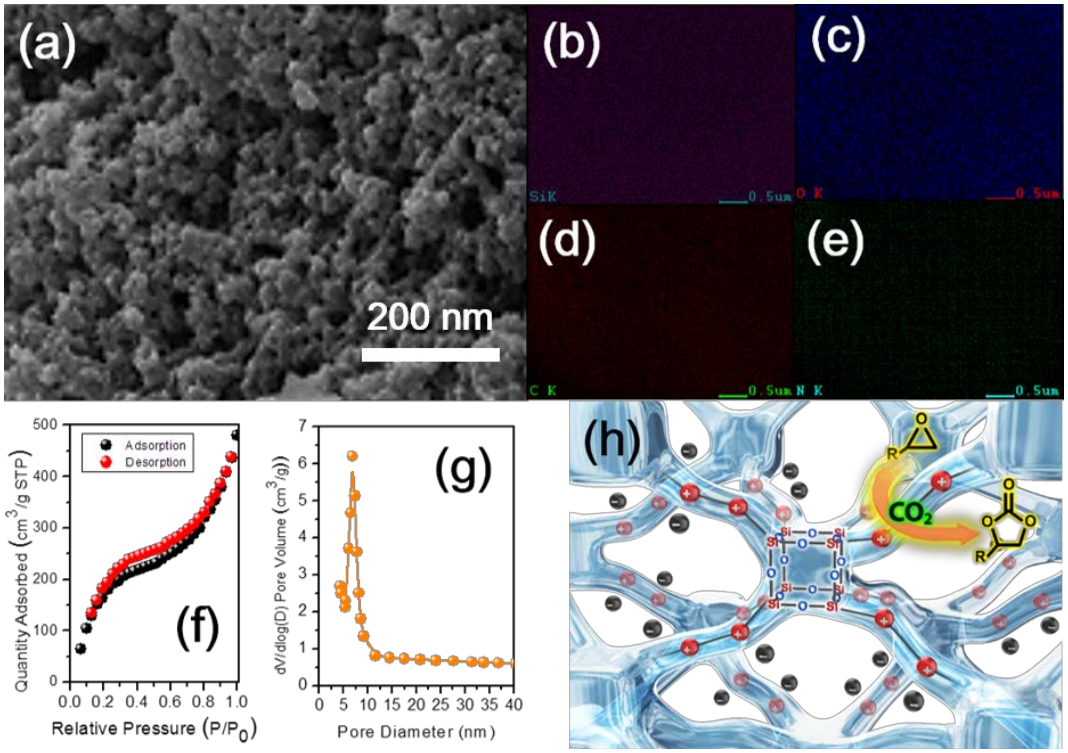

Figure 4.11. (a) SEM image of I-POSS-S2a. (b–e) EDX mapping images for atoms Si, O, C, N, respectively, (f) BET absorption-desorption isotherms, (g) Pore-size distribution of I-POSS-S1a, and(h) schematic of the CO_2 catalyzed cycloaddition of epoxides with the I-POSS-S series.

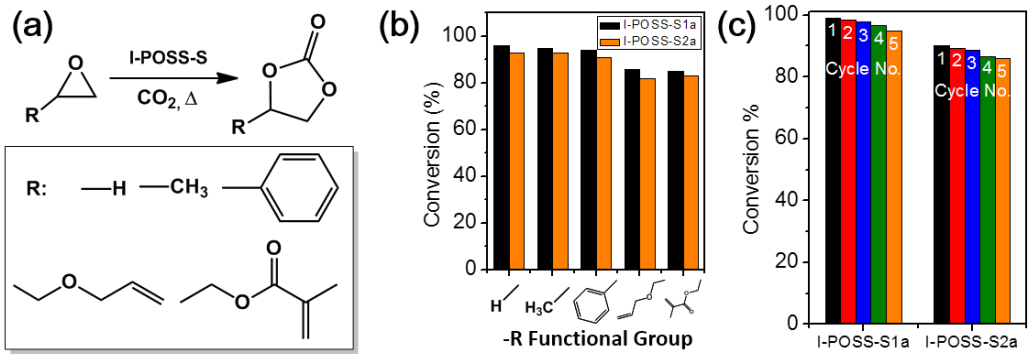

Figure 4.12. (a) CO_2 cycloaddition reaction scheme with I-POSS-S Series. (b) Conversions for all epoxide substrates evaluated in this study, [epoxide] = 400 mM in MeCN, 110 °C, CO_2 pressure: 110 psi. (c) Conversions of ethylene oxide to ethylene carbonate after recycling for 5 cycles..

Chapter 5

Facilitated Ion Transport in Smectic-like Ordered Ionic Liquid Crystals

5.1. Introduction

The structures and properties of self-assembled materials can be predicted using the structural motifs of precursors. For example, the structural motifs of phospholipids with hydrophilic phosphate head groups and hydrophobic hydrocarbon chains comprises the double layered structures of cell membranes.[1] In material science, various self-assemblies have been adopted and exploited for predictive design, including molecular crystals, colloids, lipid bilayers, microphase-separated polymers, and self-assembled monolayers.[2-4] Recently, the ion transport behavior in self-assembled ionic liquid (IL) crystals with complex structures (i.e., columnar,[5-7] smectic,[8-12] and bicontinuous cubic phases[13-16]) have been studied extensively, as the structures of IL crystals have been considered as highly promising media for efficient and selective transport of ions. Conventional ILs include a bulky cation with either a long alkyl chain[17-21] or a rigid mesogenic unit[7, 15, 22, 23] to induce a self-assembled ionic liquid crystal phase through either hydrophilic/phobic interactions between charged ionic heads and long alkyl chains pendant to the cation of the IL, or steric interactions between mesogen groups. The self-assembled IL crystals reveal predominately solid-like viscoelastic behavior because of their high degree of

structural order.[2, 24] The bulkiness of ions combined with solid-like viscoelasticity behavior restrict the transport of the mobile ions in the self-assembled IL crystals, which jeopardize their utilization in future electrochemical devices such as lithium batteries, capacitors, and solar cells.[25, 26]

Herein, we report novel ionic mixtures of an imidazolium-based room temperature IL containing ethylene oxide functionalized phosphite anion with a lithium salt that was able to self-assemble into smectic-like ordered IL crystals. Two key features in this work are the unique origin of the smectic order of the ionic mixtures and the facilitated ion transport behavior in the ordered IL crystal. We discovered that these IL crystals self-assembled truly through Coulombic interactions between ion species, not through the well-known hydrophilic/phobic interaction between ion heads and pendant groups or the steric interaction between mesogenic moieties. Furthermore, unprecedentedly, the smectic-like order in the IL crystal ionogel facilitates ion transport.

5.2. Experimental

Materials.

1-Methylimidazole and dimethylphosphite were purchased from Sigma-Aldrich Chemical Co. (Youngin, Republic of Korea). 2-(2-(2-Methoxyethoxy)ethoxy)ethanol and LiTFSI (lithium bis(trifluoromethanesulfonyl)imide) were purchased from TCI Co. (Tokyo, Japan). All chemicals were used as received without further purification.

Synthesis of 1, 3-Dimethylimidazolium methylphosphite ([DMIm][MP])

The Ionic liquid of [DMIm][MPEGP] was synthesized through two-step synthesis reactions: 1) synthesis of 1,3-Dimethylimidazolium methylphosphite [DMIm][MP] followed by 2) coupling reaction between a phosphite-containing molecule [DMIm][MP] and an ether-containing molecule 2-(2-(2-methoxyethoxy)ethoxy)ethanol. First, the reagents 1-Methylimidazole (8.2 g, 0.1 mole) and dimethylphosphite (11.0 g, 0.1 mole) were dissolved in a 100 mL round-bottomed flask and stirred for 12 h at 120 °C. After cooling to room

temperature, the reaction mixture was washed with 30 mL of ethyl acetate three times and dried under vacuum to obtain a pale yellow viscous liquid (yield: 86%). Elemental analysis calcd (%) for $C_6H_{13}N_2O_3P$: C, 37.50; H, 6.82; N, 14.58; O, 24.98; P, 16.12. Found: C, 37.19; H, 6.85; N, 14.46; O, 25.30. 1H NMR (400 MHz, D_2O, 25 °C): δ 3.37 (d, 3H, PO–CH_3); 3.73 (s, 6H, N–CH_3); 5.87, 7.46 (d, 1H, P–H); 7.35 (d, 2H, CHN); 8.51 (s, 1H, NCHN).

Synthesis of 1, 3-dimethylimidazolium (2-methoxy(2-ethoxy(2-ethoxy(2-ethoxy))))ethylphosphite ([DMIm][MPEGP]).

[DMIm][MP] (9.6 g, 50 mmol) and 2-(2-(2-methoxyethoxy)ethoxy)ethanol (16.4 g, 0.1 mole) were dissolved in a 100 mL round-bottomed flask and stirred for 12 h at 130 °C under vacuum. After cooling to room temperature, the reaction mixture was washed with diethyl ether three times and dried under vacuum to obtain a pale yellow viscous liquid (yield: 82%). Elemental analysis calcd (%) for $C_{12}H_{25}N_2O_6P$: C, 44.44; H, 7.77; N, 8.64; O, 29.60; P, 9.55. Found: C, 45.02; H, 7.84; N, 8.48; O, 29.81. 1H NMR (400 MHz, D_2O, 25 °C): δ 3.24 (s, 3H, O–CH_3); 3.43 (m, 2H, O–CH_2); 3.59 (m, 8H, O–CH_2); 3.85 (s, 6H, NCH_3); 3.89 (m, 2H, PO–CH_2); 5.91, 7.48 (d, 1H, P–H); 7.28 (d, 2H, CHN); 8.52 (s, 1H, NCHN).

General Procedure for Fabrication of Ionogels.

The ionic mixtures were prepared through dissolving LiTf2N in [DMIm][MPEGP]. The lithium salt content was varied between x = 0 and 3.0, where x corresponds to the molar ratio of the components (moles of LiTf2N / moles of [DMIm][MPEGP]).

Characterization.

The optical birefringence of the ionic mixtures was investigated through examination of sample in a tube located between crossed polarizers. DSC examinations were performed using a DSC 200-F3 instrument (NETZSCH Instruments) at a heating rate of 10 °C/min Synchrotron SAXS measurements were performed at the 4C1 SAXS beamline in the Pohang Light Source, Republic of Korea. The wavelength of the monochromatic X-ray beams was 0.6754 Å and the distance between sample and detector was 2 m. Temperature was controlled using a sample stage provided by Pohang Light Source. Rheological properties were examined using a rheometer (Advanced Rheometric Expansion System, ARES) instrument with cone-plate geometry. All rheological measurements were

performed in the linear viscoelastic region under an inert nitrogen atmosphere. The ionic conductivity was determined using a complex impedance analyzer (Bio-Logics, VMP3) over a frequency range from 0.1 Hz to 1 MHz at an AC amplitude of 10 mV. The electrochemical stabilities of the ionic liquids and ionic mixture were analyzed using cyclic voltammetry (CV) and linear sweep voltammetry (LSV) methods at ambient temperature. To obtain the cyclic voltammogram, a platinum working electrode of 1 mm diameter was used with a platinum rod as a counter electrode, and lithium metal as a reference electrode at a scan rate of 1.0 mV/s. In the LSV experiments, a stainless steel working electrode was used with lithium metal as both the counter and reference electrodes. The voltage was swept at a scan rate of 1.0 mV/s.

All NMR experiments were performed on a 600 MHz NMR spectrometer (Agilent Tech, USA) equipped with a 5 mm liquid NMR probe (Doty Scientific, USA), with a maximum gradient strength of ~31 T/m. The ^{31}P NMR spectra for these ionic mixtures were obtained using a single-pulse excitation with a 90 degree pulse of 12 μs at Larmor frequency of 242.93 MHz at ambient temperature. The ^{31}P chemical shift (δ) of 85% H3PO4 at 0 ppm was used as an external reference. The number of mobile ions was obtained from 1D liquid NMR spectra of ^{31}P, ^{7}Li and ^{19}F for $[MPEGP]^{-}$, Li^{+}, and $TFSI^{-}$ ions, respectively, at ambient temperature. The Stejskal-Tanner equation, $S(g) = S(0)exp[-D(\gamma g\delta)^2(\Delta-\delta/3)]$,

where S(g) and S(0) are the echo heights at the gradient strengths of g and 0, respectively, D is the diffusion coefficient, γ is ^{7}Li, ^{1}H and ^{19}F gyromagnetic ratios, respectively, Δ, i.e. The diffusion delay is the time interval between the two bipolar pulse gradients and δ is the gradient length. The gradient strength was varied with 15 equal steps and the maximum gradient strength was chosen accordingly to an echo height at the maximum gradient between 0.4 ~ 25 T/m. The 90° pulse lengths 12, 5.5 and 7 μs were used for ^{7}Li, ^{1}H and ^{19}F, respectively. The gradient duration δ was 2~4 ms. The diffusion delay Δ varied 20 to 40 ms for ^{7}Li and ^{1}H PFG-NMR and fixed at 4 ms for ^{19}F PFG-NMR. From the preliminary test, the apparent diffusion coefficients as a function of Δ showed these lengths of Δ were long enough to reach the steady state diffusion in these samples.

5.3. Results and Discussion

The chemical structures for IL of [DMIm][MPEGP] ((1,3-dimethylimidazolium (2-methoxy(2-ethoxy(2-ethoxy(2-ethoxy))))ethylphosphite) and lithium salt of LiTFSI (lithium bis(trifluoromethanesulfonyl)imide) are presented in Figure 5.1 The [DMIm][MPEGP] compound, featuring an ethylene oxide chain grafted on the phosphite anion, was synthesized through two-step reactions, as illustrated in Figure 5.1. The transparent room temperature IL product of [DMIm][MPEGP] revealed no melting behavior, but a glass transition temperature at –67 °C (Figure 5.3). The ionic mixtures were prepared through dissolving LiTFSI in [DMIm][MPEGP]. The lithium salt content was varied between x = 0 and 3.0, where x corresponds to the relative amount of salt (moles of LiTFSI / moles of [DMIm][MPEGP]).

We first investigated the effect of LiTFSI concentration on the optical birefringence of ionic mixtures at room temperature. As presented in Figure 5.4(b), the neat IL and the ionic mixture of x = 0.1 were optically isotropic. Remarkably, when the ratio of LiTFSI increased to x = 0.4, the ionic mixture began to reveal optical birefringence. Upon increasing the amount of LiTFSI, the optical birefringence became stronger until x = 1.0, where the birefringence reached its

maximum. The optical birefringence was subsequently reduced with further increase in the amount of LiTFSI.

The synchrotron SAXS profiles for IL and ionic mixtures with varied amount of LiTFSI at room temperature are shown in Figure 5.5(a). The neat IL and the ionic mixture with low lithium salt concentration (x = 0.1) exhibited featureless SAXS patterns, confirming absence of any structural order. Meanwhile, the ionic mixtures with intermediate salt concentrations (x = 0.4 and 1.0) revealed characteristic scattering peaks, indicating the presence of structural regularity. The structural order began to appear at x = 0.4, became stronger until x = 1.0, and then was observed to weaken with further increase in lithium salt concentration. The sample of x = 1.0 with strongest structural order exhibited a set of peaks inclusive of three characteristic reflection peaks at small q values and a broad halo peak at large q values. The order of reflections at low q value can be indexed to 001, 002, and 003, corresponding to the reflection of a layered structure [27,28] with an interlayer spacing ($d = 2\pi/q^*$) of 4.36 nm. The broad and weak halo scattering at large q value demonstrates a statistical random intermolecular distance distribution. [29] The SAXS results indicate that the sample of x = 1.0 has a smectic-ordered liquid crystalline phase. The mixture of x = 3.0 (containing excess lithium salt) exhibited weak and broad scattering at small q values and a strong and broad halo scattering at large q values, demonstrating a weakly

segregated structure when compared with the mixture of x = 1.0. These observations were consistent with the trends observed in the optical birefringence results, indicating that the formation and evolution of mesostructures were primarily governed by the amount of LiTFSI. The neat IL and the ionic mixtures with low lithium salt concentrations form no structural order. Above the critical amount of LiTFSI (x = 0.4), the mixtures form a smectic-ordered liquid crystal phase, as illustrated in Figure 5.5(b). However, the presence of excess lithium salt in the mixture disrupts the structural order. Moreover, it should be noted that the ethylene oxide chains pendent to the negatively charged phosphite anions were not interdigitated and provided the hydrophilicity and flexibility to the IL crystal with layered regularity.

The changes of dynamic viscoelastic properties of the ionic mixtures as a function of angular frequency are shown in Figure 5.6(a). Neat IL and the ionic mixture with x = 0.1 behaved predominantly as a viscous liquid. The loss modulus G″ was observed to be greater than the storage modulus G′ and both G′ and G″ values exhibited linear frequency dependences. In contrast, for the samples with x = 0.4 and 1.0, G′ and G″ were frequency independent and G′ value was greater than G″, indicating predominantly solid-like viscoelastic behavior. [30,31] At this

stage, both G′ and G″ values increased with an increase in salt concentration. These observations clearly demonstrate that the ionic mixtures pass through a transition from the liquid-like to solid-like phases at around x = 0.4, indicating the formation of IL crystal ionogels. The gel strength increased with increased salt concentration until x = 1.0, and then decreased with further increase in lithium salt content. The gel behavior remained up to x = 1.4. Meanwhile, with further increase in LiTFSI concentration (x > 1.4), the mixtures recovered the fluidity of a viscous liquid, indicating relatively weak segregation compared with the ionogel samples. These observations were in good agreement with the polarized optical microscopy and SAXS examinations results.

The thermotropic phase transition behaviors of ionic mixtures are exhibited in Figure 5.6(b–d). As depicted in Figure 5.6(b), the ionogel with x = 0.4 revealed a sharp decrease in dynamic storage modulus at around 70 °C, indicating the presence of a phase transition from an ordered gel to a disordered liquid state. However, unlike the sample with x = 0.4, the ionogel with x = 1.0 continued to preserve the solid-like viscoelastic character even at very elevated temperatures. Similarly, thermo-responsive phase transition behaviors of samples of x = 0.4 and 1.0 were observed in the synchrotron SAXS experiments at various temperatures (Figure 5.6(c,d)). The intensity of characteristic reflection peaks for

the sample with x = 0.4 gradually decreased with increasing temperature, revealing a transition from an ordered to a disordered phase at 70 °C. In contrast, the respective SAXS peaks of the sample with x = 1.0 remained stable and nearly constant at temperatures beyond 150 °C (Figure 5.6(d)). The absence of thermotropic phase transition demonstrated that the smectic order of the x = 1.0 sample was extraordinarily stable, even at very elevated temperatures.

The ionic conductivities of neat IL and ionic mixtures as a function of temperature are shown in Figure 5.7(a). In general, the ionic conductivity increases with the increase in temperature. Moreover, the ionic conductivity of ILs decrease not only due to the addition of metal salts [32] (e.g., LiTFSI), but also through formation of ordered structures, [25, 26] because both factors can increase viscosity, retarding the mobility of ionic species. In this work, however, the ionic conductivity of the ionic mixtures appeared to follow an inverse relationship to the viscoelastic behavior of materials. The ionic conductivity increased with increases in lithium salt concentration until x = 1.0, and for this sample, which had the largest viscoelasticity character, the maximum ionic conductivity value was measured.

Based on the structural and ion-conducting experimental results, the ionic mixtures are classified into three different states as a function of LiTFSI

concentration: Phase I ($x < 0.4$), phase II ($0.4 \leq x \leq 1.4$), and phase III ($1.4 < x$), as illustrated in Figure 5.7(b). Ionic mixtures in phase I form isotropic structure without any structural order, resulting in optical isotropy and low viscosity liquid-like behavior. Ionic mixtures in phase II form robust smectic structural order, providing strong optical birefringence and solid-like ionogel behavior. The ionogel of sample $x = 1.0$ with strongest smectic order revealed the largest viscoelasticity. Ionic mixtures in phase III form weakly segregated structure, resulting in optical birefringence but viscous, liquid-like behavior. The ionic conductivity depended on the lithium salt concentration. Interestingly, the ionogel of $x = 1.0$ with the largest viscoelasticity revealed the largest ionic conductivity.

The exceptional phase and ion conduction behavior of the ionic mixtures raises two critical questions: What is the origin of the smectic order? Why do the smectic-ordered IL crystals with solid-like viscoelasticity exhibit faster ion transport behavior over the ionic mixtures with viscous liquid-like states?

The origin of the structural order of the self-assembled IL crystals studied in this work is unambiguously different from that of conventional IL crystals. Generally, IL crystals are self-assembled either through hydrophilic-phobic interactions between charged ion heads and long alkyl chain pendant groups [17-

21, 23], or through steric interactions between rigid mesogenic moieties in the molecular structure of ILs. [5-16] In this work, however, the room temperature IL of [DMIm][MPEGP] does not have any structural order itself as it does not contain any hydrophobic long alky chain or mesogenic unit. It does, however, contain a strong hydrophilic ethylene oxide pendant group on the anion. Interestingly, the smectic order appears in the ionic mixtures of [DMIm][MPEGP] and LiTFSI (in the limited range of x from 0.4 to 1.4). The strong dependency of phase behavior of ionic mixtures on the lithium salt concentration indicates that the smectic order is derived from a balance of electrostatic interactions among the mixed ionic species.

To better understand the cause of the structural order, the ^{31}P NMR chemical shift (δ) and P–H coupling constant (J_{PH}) of the phosphite anion of $[MPEGP]^-$ were examined. [33] As the results in Figure 5.8(a) show, the δ and J_{PH} depend on the LiTFSI content. The ionic mixture with x = 0.1 (in phase I) revealed almost the same δ and JPH value as the neat IL. In contrast, the ionic mixture with x = 1.0 (in phase II) exhibited a strong downfield shift in δ and a larger J_{PH} value compared with the neat IL. This enhancement of the J_{PH} value, accompanied by the large downfield shift in δ occurred mainly due to the strong electrostatic deshielding of the phosphite anion $[MPEGP]^-$ by Li^+ cation. [33] This observation offers compelling evidence that the smectic order of the x = 1.0

sample is attributed to the strong Coulombic interaction between Li^+ cations in the lithium salt and the oxygen atoms on the $[MPEGP]^-$ anion in the IL. The collapse of the characteristic ^{31}P resonance for the x = 3.0 sample is due to the local magnetic field distribution generated by the low degree of structural order, as observed in the SAXS profile (Figure 5.5(a)).

We also investigated the diffusion behavior of mobile ions using pulsed field gradient (PFG) NMR to discern the fast-ion transport behavior in the smectic-ordered ionogel. The ^7Li PFG spin-echo profiles of ionic mixtures with x = 0.1, 1.0, and 3.0 are shown in Figure 5.8(b). In PFG NMR, the echo signal is attenuated with the field gradient strength (g) due to loss of coherence caused by random bulk diffusion of ions; faster ion diffusion generates faster echo signal decay. [34] Figure 5.9(a, b) show the numbers and diffusion coefficients of [DMIm]+, $[MPEGP]^-$ and Li^+, and $TFSI^-$ mobile ions in the ionic mixtures obtained from 1H, ^1H, ^7Li, and ^{19}F PFG NMR examinations, respectively. The number of mobile ions was evaluated from the intensity of the 1-dimensional liquid NMR signals. The numbers of total mobile ions were similar regardless of LiTFSI concentration because both [DMIm][MPEGP] and LiTFSI are ionic materials. The ionic mixture with x = 1.0 revealed much faster echo decay than mixtures with x = 0.1 and x = 3.0. Diffusion coefficient was calculated through fitting of echo signal using the well-known Stejskal–Tanner (ST) equation: [35]

$$S(g) = S(0)exp[-Di(\gamma g\delta)^2(\Delta-\delta/3)] \quad (1)$$

where S(g) and S(0) are the echo heights at the gradient strengths of g and 0, respectively, Di is diffusion coefficient of i mobile ion, and γ is gyromagnetic ratio. In equation (1), Δ is the diffusion delay, which is the time interval between the two pulse gradients, and δ is the gradient length, and the area of gradient pulse, $q = (2\pi)^{-1}\gamma g\delta$. For the systems studied here, the diffusion coefficients vary with LiTFSI concentration and the diffusion coefficients of mobile ions showed a maximum value in phase II. Figure 5.9(c) presents the variation of ionic conductivity (σ_D) calculated using the Nernst-Einstein equation: [36]

$$\sigma_D\ (\mathrm{S/cm}) = \frac{e^2}{k_B T}(n_{Li}D_{Li} + n_{TFSI}D_{TFSI} + n_{DMIm}D_{DMIm} + n_{MPEGP}D_{MPEGP}) \quad (2)$$

where n_i and D_i are the number and diffusion coefficient of the ions, respectively. The calculated σ_D revealed the same LiTFSI content dependency as that found for the diffusion coefficients. The maximum value for σ_D was observed in phase II, which was consistent with the measured ionic conductivity (σ_{mea}) (as shown in

Figure 5.7). These PFG NMR observations show that larger ion conductivity in phase II is caused by faster diffusion behavior of mobile ions in the smectic order, not by the commonly stipulated reasons such as the number of mobile ions and the viscoelastic properties of the materials. [37]

The unique facilitated ion transport in the smectic order may be attributed to the presence of hydrophilic and flexible ethylene oxide chains on the phosphite anion. As Kishimoto et al. reported, [38] ethylene oxides chains are very flexible and compatible with ions. The mobile ions are capable of diffusing three orders of magnitude faster along the planes of ethylene oxide domains rather than along the out of plane direction, as the flexible and hydrophilic ethylene oxide chains constitute a single layer of layered lamellae structure.

Additionally, it should be noted that the PFG spin-echo profile for sample of x = 1.0 in Figure 5.8(b) also exhibits strong NMR diffraction behavior appearing as echo minima and maxima as the field gradient increases. [39-41] The NMR diffraction behavior appears when the mesostructure in a material influences the diffusion behavior of the mobile ions. Thus, this information is a clear indication of the presence of smectic order in the IL crystal.

Finally, the electrochemical stabilities of the ionogel systems studied here were evaluated using the linear sweep voltammetry technique. No significant

oxidative decomposition was observed at below 5.0 V in the anodic region (Supplementary Figure 5.10), indicating that the prepared IL crystals were electrochemically stable up to 5.0 V, which could be useful in high-voltage electrochemical devices. [42]

5.4. **Conclusion**

In summary, we have demonstrated a novel ionic mixture consisting of an imidazolium-based IL containing ethylene oxide functionalized phosphite anion and a lithium salt that self-assemble into smectic-ordered IL crystal ionogels through strong Coulombic interaction between Li^+ cations of the lithium salt and the phosphite anions of the ionic liquid. The IL crystal showcases unique facilitated ion transport, resulting in enhanced ionic conductivity over their liquid-phase counterparts due to the smectic ordering that provides a facilitated ion transport pathway. Large ionic conductivity, remarkable electrochemical stability, and viscoelastic robustness of the IL crystal ionogels provide promising opportunities for their future electrochemical applications.

5.5. References

[1] A. J. Verkleij, R. F. A. Zwaal, B. Roelofsen, P. Comfurius, D. Kastelijn and L. L. M. van Deenen, Biochim. Biophys. Acta. (1973) 323, 178-193.

[2] T. Kato, Science (2002) 295, 2414-2418.

[3] G. M. Whitesides and M. Boncheva, Proc. Natl. Aca. Sci. (2002) 99, 4769-4774.

[4] G. M. Whitesides and B. Grzybowski, Science (2002) 295, 2418-2421.

[5] H. Shimura, M. Yoshio, K. Hoshino, T. Mukai, H. Ohno and T. Kato, J. Am. Chem. Soc. (2008) 130, 1759-1765.

[6] M. Yoshio, T. Kagata, K. Hoshino, T. Mukai, H. Ohno and T. Kato, J. Am. Chem. Soc.(2006) 128, 5570-5577.

[7] M. Yoshio, T. Mukai, H. Ohno and T. Kato, J. Am. Chem. Soc. (2004) 126, 994-995.

[8] B. Soberats, M. Yoshio, T. Ichikawa, S. Taguchi, H. Ohno and T. Kato, J. Am. Chem. Soc. (2013) 135, 15286-15289.

[9] B. Soberats, E. Uchida, M. Yoshio, J. Kagimoto, H. Ohno and T. Kato, J. Am. Chem. Soc. (2014) 136, 9552-9555.

[10] T. Mukai, M. Yoshio, T. Kato, M. Yoshizawa and H. Ohno, Chem.

Commun. (2005), 1333-1335.

[11] S. Yazaki, M. Funahashi, J. Kagimoto, H. Ohno and T. Kato, J. Am. Chem. Soc. (2010) 132, 7702-7708.

[12] K. Kishimoto, M. Yoshio, T. Mukai, M. Yoshizawa, H. Ohno and T. Kato, J. Am. Chem. Soc. (2003) 125, 3196-3197.

[13] R. L. Kerr, S. A. Miller, R. K. Shoemaker, B. J. Elliott and D. L. Gin, J. Am. Chem. Soc. (2009) 131, 15972-15973.

[14] T. Ichikawa, M. Yoshio, A. Hamasaki, J. Kagimoto, H. Ohno and T. Kato, J. Am. Chem. Soc. (2011) 133, 2163-2169.

[15] T. Ichikawa, M. Yoshio, A. Hamasaki, T. Mukai, H. Ohno and T. Kato, J. Am. Chem. Soc. (2007) 129, 10662-10663.

[16] T. Ichikawa, M. Yoshio, A. Hamasaki, S. Taguchi, F. Liu, X.-b. Zeng, G. Ungar, H. Ohno and T. Kato, J. Am. Chem. Soc. (2012) 134, 2634-2643.

[17] J. N. A. Canongia Lopes and A. A. H. Pádua, J. Phys. Chem. B (2006) 110, 3330-3335.

[18] J. D. Holbrey and K. R. Seddon, Dalton Trans. (1999), 2133-2140.

[19] C. M. Gordon, J. D. Holbrey, A. R. Kennedy and K. R. Seddon, J. Mater. Chem. (1998) 8, 2627-2636.

[20] A. Triolo, O. Russina, H.-J. Bleif and E. Di Cola, J. Phys. Chem. B (2007) 111, 4641-4644.

[21] Y. Wang and G. A. Voth, J. Am. Chem. Soc. (2005) 127, 12192-12193.

[22] Y. Gao, J. M. Slattery and D. W. Bruce, New J. Chem. (2011) 35, 2910-2918.

[23] K. Binnemans, Chem. Rev. (2005) 105, 4148-4204.

[24] T. Kato, Y. Hirai, S. Nakaso and M. Moriyama, Chem. Soc. Rev. (2007) 36, 1857-1867.

[25] A. Eisele, K. Kyriakos, R. Bhandary, M. Schonhoff, C. M. Papadakis and B. Rieger, J. Mater. Chem. A (2015) 3, 2942-2953.

[26] S. Taguchi, T. Matsumoto, T. Ichikawa, T. Kato and H. Ohno, Chem. Commun. (2011) 47, 11342-11344.

[27] A. E. Bradley, C. Hardacre, J. D. Holbrey, S. Johnston, S. E. J. McMath and M. Nieuwenhuyzen, Chem. Mater. (2002) 14, 629-635.

[28] M. Yang, B. Mallick and A.-V. Mudring, Cryst. Growth Des. (2013) 13, 3068-3077.

[29] D. K. Yoon, Y. H. Kim, D. S. Kim, S. D. Oh, I. I. Smalyukh, N. A. Clark and H.-T. Jung, Proc. Natl. Aca. Sci. (2013) 110, 19263-19267.

[30] Q. Wang, J. L. Mynar, M. Yoshida, E. Lee, M. Lee, K. Okuro, K. Kinbara and T. Aida, Nature (2010) 463, 339-343.

[31] M. Yoshida, N. Koumura, Y. Misawa, N. Tamaoki, H. Matsumoto, H. Kawanami, S. Kazaoui and N. Minami, J. Am. Chem. Soc. (2007), 129,

11039-11041.

[32] S. Seki, Y. Ohno, Y. Kobayashi, H. Miyashiro, A. Usami, Y. Mita, H. Tokuda, M. Watanabe, J. Electrochem. Soc. (2007), 154, A173-A177.

[33] F. R. Spitz, J. Cabral and P. Haake, J. Am. Chem. Soc. (1986), 108, 2802-2805.

[34] W. S. Price, Concepts in Magn. Reson. (1997) 9, 299-336.

[35] E. O. Stejskal and J. E. Tanner, J. Chem. Phys. (1965) 42, 288-292.

[36] I. Nicotera, C. Oliviero, W. A. Henderson, G. B. Appetecchi and S. Passerini, J. Phys. Chem. B (2005) 109, 22814-22819.

[37] T. Ueki and M. Watanabe, Macromolecules (2008) 41, 3739-3749.

[38] K. Kishimoto, T. Suzawa, T. Yokota, T. Mukai, H. Ohno and T. Kato, J. Am. Chem. Soc. (2005) 127, 15618-15623.

[39] Y. Saito, T. Umecky, J. Niwa, T. Sakai and S. Maeda, J. Phys. Chem. B (2007) 111, 11794-11802.

[40] K. Hayamizu, E. Akiba and W. S. Price, Macromolecules (2003) 36, 8596-8598.

[41] P. T. Callaghan, A. Coy, D. MacGowan, K. J. Packer and F. O. Zelaya, Nature (1991) 351, 467-469.

[42] M. Armand, F. Endres, D. R. MacFarlane, H. Ohno and B. Scrosati, Nat. Mater. (2009) 8, 621-629.

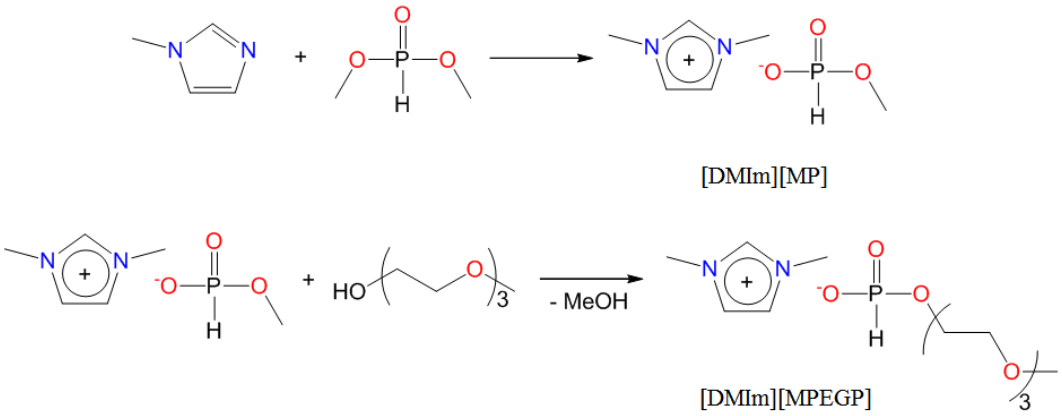

Figure 5.1. Reactions scheme for the synthesis of [DMIm][MP] and [DMIm][MPEGP] compounds

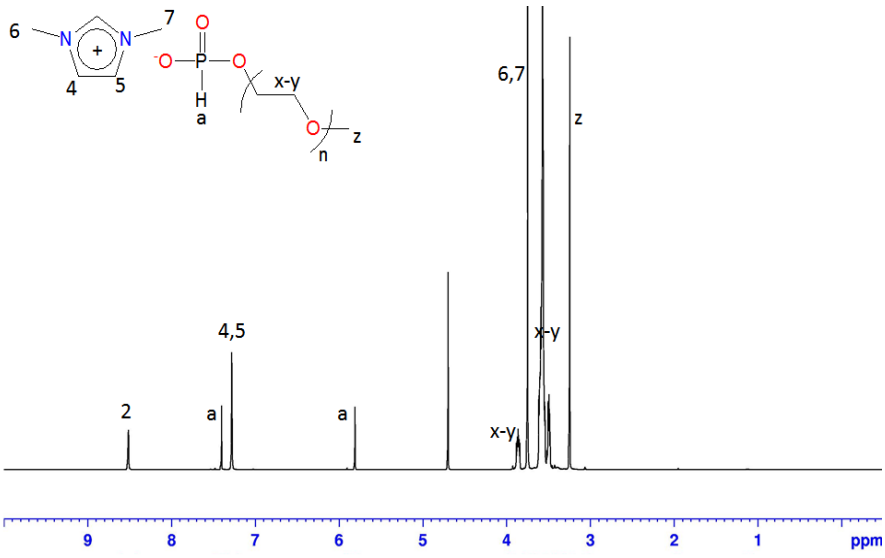

Figure 5.2. 1H NMR spectra of [DMIm][MPEGP]

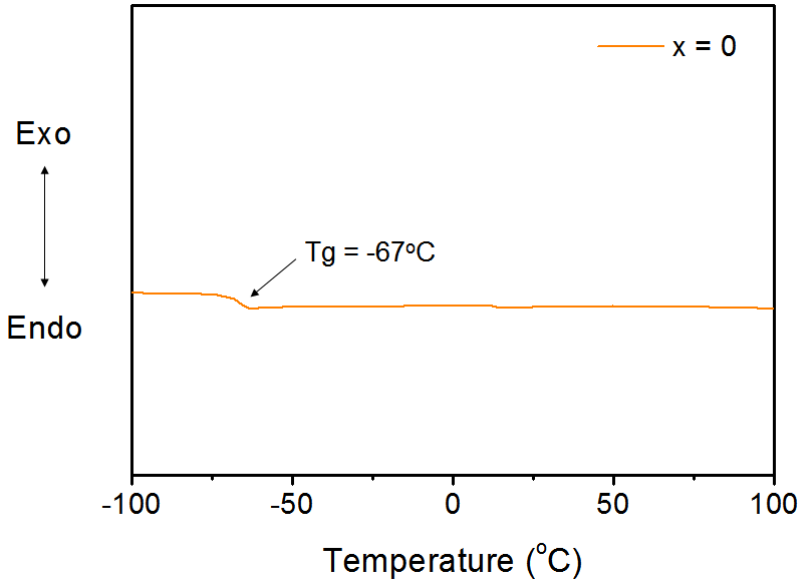

Figure 5.3. Differential scanning calorimeter (DSC) thermogram of neat [DMIm][MPEGP].

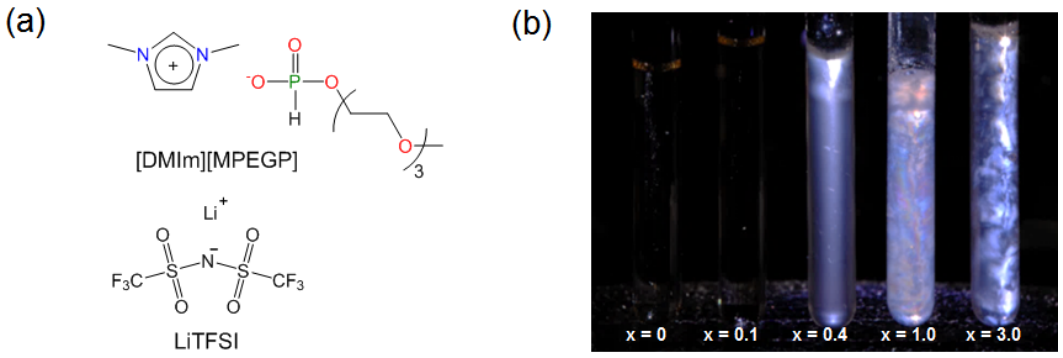

Figure 5.4. (a) Chemical structures of [DMIm][MPEGP] and LiTFSI. (b) Photographs of ionic mixtures of [DMIm][MPEG200] and LiTFSI with various salt concentrations between crossed polarizers at room temperature.

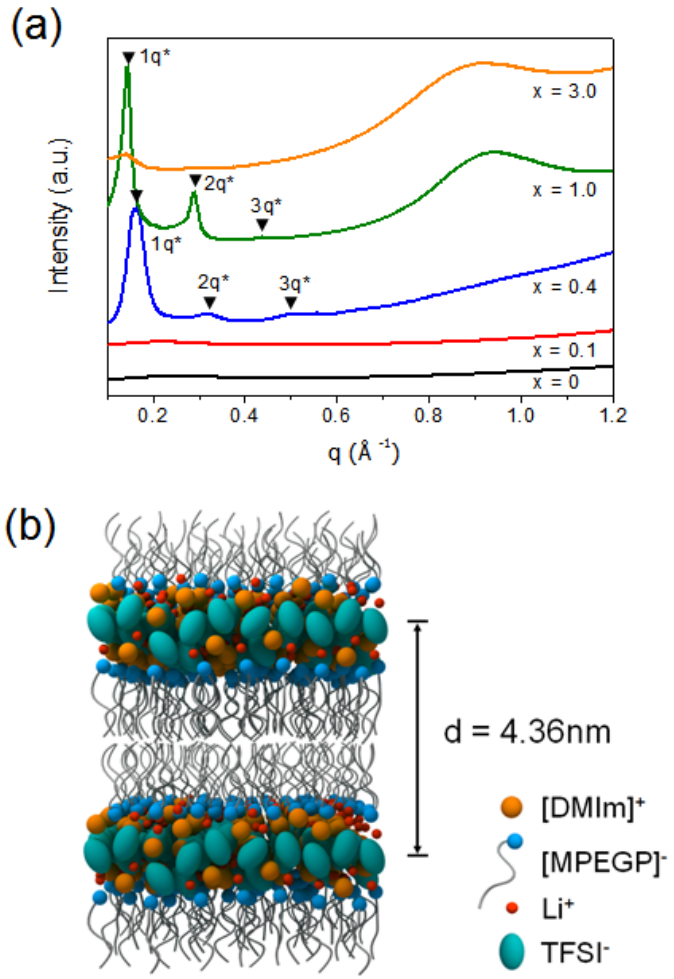

Figure 5.5 (a) SAXS curves of ionic mixtures at various salt concentrations at room temperature. (b) Schematic illustration of the mesostructure for [DMIm][MPEGP] and LiTFSI mixture.

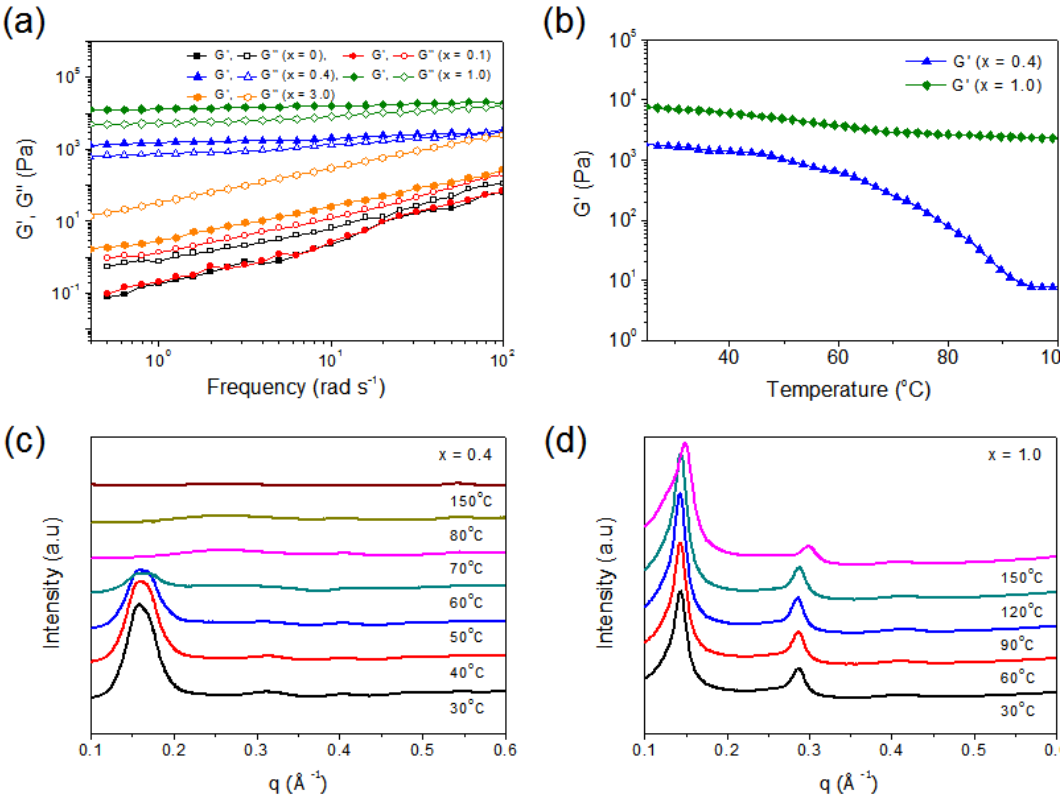

Figure 5.6 (a) Dynamic viscoelastic properties of IL and ionic mixtures with various salt concentrations. (b) Temperature sweep of viscoelastic properties of ionic mixtures with x = 0.4, and 1.0 (c) and (d) SAXS curves of x = 0.4 and 1.0 samples at various temperatures, respectively..

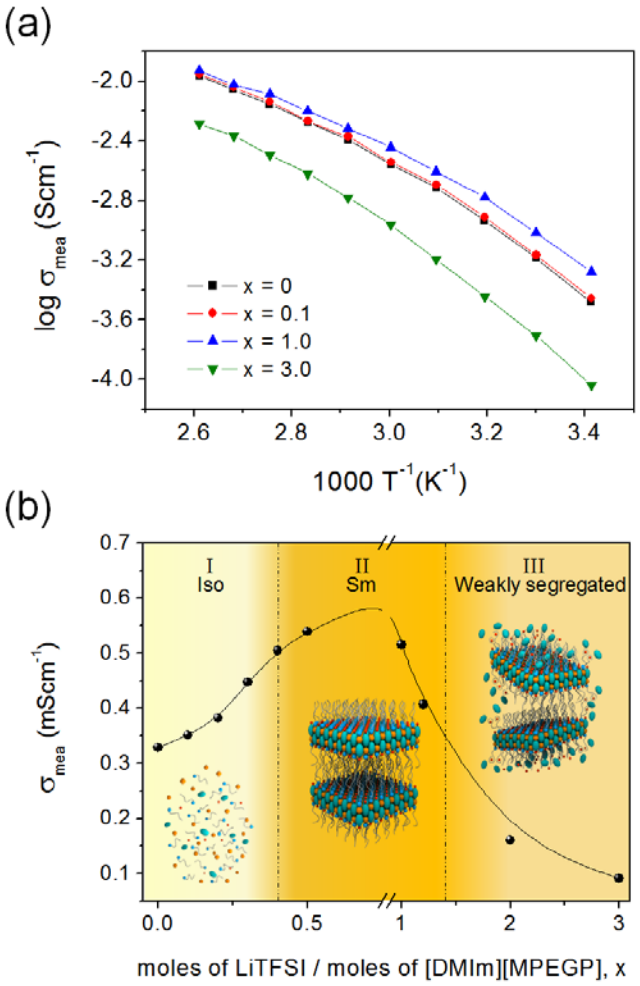

Figure 5.7 (a) Temperature dependent ionic conductivities of IL and ionic mixtures at various salt concentrations. (b) Phase diagram and ionic conductivity of [DMIm][MPEGP] and LiTFSI ionic mixtures as a function of relative salt concentration (x) at 20 °C.

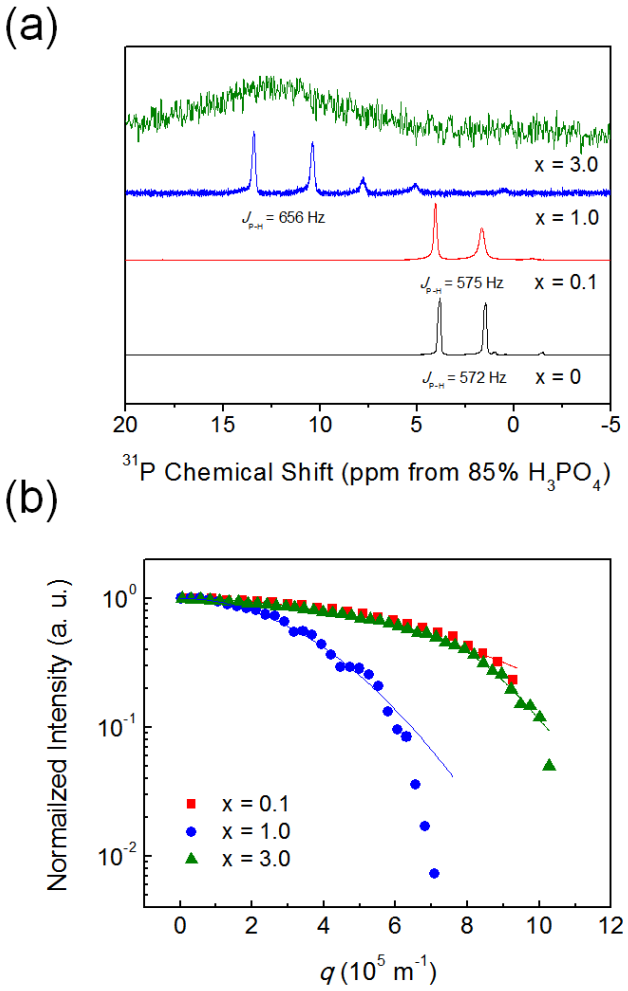

Figure 5.8. (a) ^{31}P NMR resonance spectra of the ionic mixtures at various relative salt concentrations. b) ^{7}Li PFG-echo profile of ionic mixtures of x = 0.1, 1.0, and 3.0

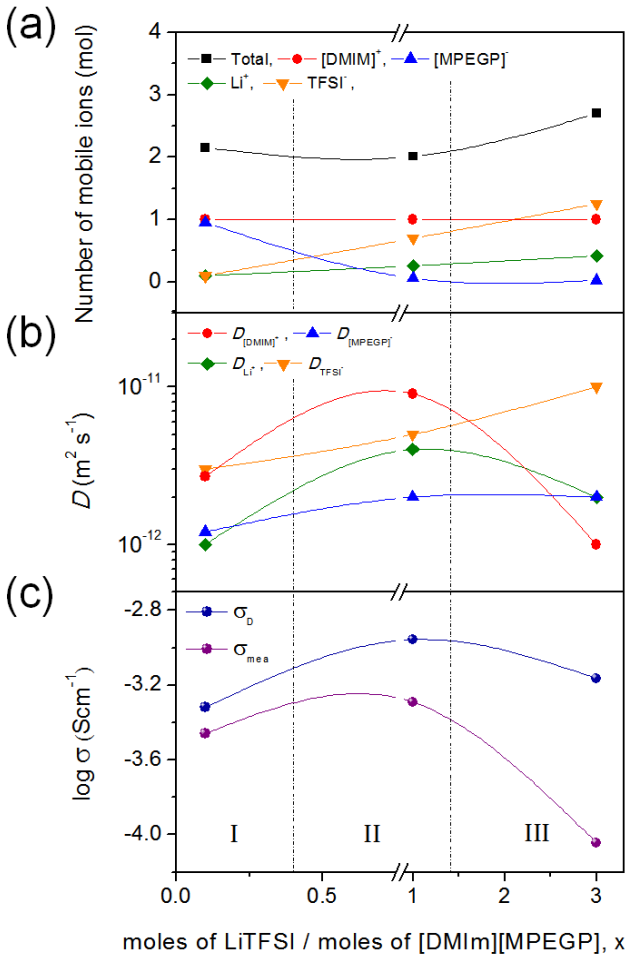

Figure 5.9. (a) Number of mobile ions, (b) diffusion coefficient of mobile ions, and (c) measured ionic conductivity (σ_{mea}) and calculated ionic conductivity (σ_D) using the Nernst-Einstein equation.

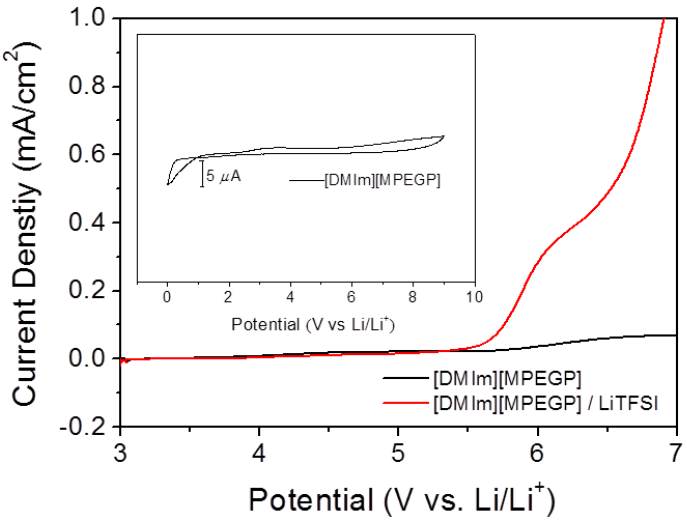

Figure 5.10. Linear sweep voltammograms of [DMIm][MPEGP] and [DMIm][MPEGP]/ LiTFSI mixture, with an inset of figure showing the cyclic voltammogram for [DMIm][MPEGP].

초 록

본 연구에서는 가교성 폴리실세스키옥산과 이온성 액체를 포함하는 이온겔 전해질의 합성 및 분석, 그리고 리튬 전지로의 응용에 대하여 기술하였다. 첫째로, 염기 촉매 하에서 진행된 축합반응을 이용하여, 다수의 가교성 메타크릴 작용기를 함유하는 고분자량의 사다리형 폴리실세스키옥산 (LPMASQ)을 합성하였다. 완전히 축합된 형태의 본 고분자는 미 반응물인 실란올을 고분자 사슬 말단에만 포함하여, 높은 열적, 전기화학적 안정성과 내산성을 나타내었다. 또한 다수의 가교성 메타크릴 작용기는 서로 쉽게 반응하여 공유결합으로 연결될 수 있게 하였다. 상기의 독특한 고분자의 구조적 특성은 높은 사슬간의 가교효율과 빠른 겔화 반응을 가능하게 하였다. 단지 2 wt%의 미량의 LPMASQ만으로 이온성 액체 전해질 용액이 겔화되었으며, 이를 통해 균일하고, 열적, 기계적으로 안정한 유/무기 복합 이온겔 전해질을 제조할 수 있었다. 더욱이, 이온겔 전해질은 높은 이온전도도와 전기화학적 안정성을 가져 높은 쿨롱효율과 싸이클 특성을 나타내는 리튬 전지

용 전해질로 적용이 가능하였다.

둘째, 앞서 합성된 유/무기 복합 이온겔 전해질의 이온 전도 특성을 개선하기 위하여, 다양한 PEO 작용기 조성을 포함하는 새로운 사다리형 폴리실세스키옥산 공중합체들을 합성하였다. 같은 함량의 가교성 폴리실세스키옥산들을 이온성 액체와 혼합하고 열을 가하여 가교 구조를 형성하였으며, 이를 통해 기계적으로 안정된 유/무기 복합 이온겔 전해질들을 준비하였다. 다양한 분광학적 분석을 통해, PEO 작용기를 가지는 폴리실세스키옥산이 포함된 이온겔 전해질들은 메타크릴 작용기만을 가지는 폴리실세스키옥산을 함유하는 이온겔 전해질보다 우수한 이온 전도 특성을 나타냄을 확인하였다. PEO 작용기의 도입은 이온겔 전해질의 해리된 이온들의 수와 확산속도 증가와 밀접한 상관관계를 가지고 있었다. 이어진 리튬 전지응용에서 PEO 작용기를 가지는 폴리실세스키옥산이 포함된 유/무기 복합 이온겔 전해질은 앞선 연구에서 제조된 이온겔 전해질에 비해 개선된 리튬 전지 성능을 나타내었다.

셋째, 이온성 작용기가 포함된 폴리헤드랄 실세스키옥산을 합성하였다. 가교 반응이 가능한 다양한 양이온성 3차 아민들이 무기 실세스키옥산에 기능화되었으며, 이를 이온성 액체와 혼합 후 열 가교반응을 통

해 유/무기 복합 이온겔 전해질을 제조하였다. 본 유/무기 복합 이온겔 전해질은 높은 전기화학적 안정성과 이온 전도특성을 나타내었다. 더욱이, 양이온성 가교구조는 이온겔 전해질의 음이온과 정전기적으로 상호작용하여 확산속도를 감소시키는데 반해, 리튬 양이온의 이동도를 증가시켰다. 리튬 이온 전지 응용결과 높은 쿨롱효율 및 싸이클링 특성을 나타내었다. 또한, 이온겔을 이루는 이온성 액체의 추출을 통해 미세기공 구조를 가지는 지지체를 준비하였다. 이온성 기능기를 가지는 지지체들은 이산화탄소를 에폭사이드로 전환하기 위한 불균일계 촉매로 활용되었으며, 높은 촉매효율과 재활용 특성을 나타내었다.

마지막으로, 에틸렌 옥사이드가 기능화된 포스파이트 음이온을 가지는 이온성 액체가 합성하였다. 본 이온성 액체와 리튬염과의 혼합 결과 자기조립구조를 가지는 이온겔 전해질을 제조할 수 있었으며, 분광학적 분석을 통해 스멕틱 액정과 유사한 구조를 가짐을 확인하였다. 본 자기조립구조는 각 이온들간의 친수/소수성 상호작용과 분자 사슬간의 입체장해 효과가 아닌 정전기적인 인력에 의해 형성되었다. 특이하게도, 단독 이온성 액체보다 이온겔 상태에서 우수한 이온 전도특성을 나타내었으며, 내부 나노구조체의 발달에 따라 이온전도도가 증가하였다. 각 액정상 집합체들이 이루는 구조체들은 이온의 전달을 촉진하였다. 이에

따라, 본 물질은 새로운 이온겔로서, 높은 이온전도도, 전기화학적, 기계적 안정성을 가진 고기능성 전해질로 다양한 에너지 분야에서 적용 가능하다.

주요어: 유/무기 복합 물질, 겔 고분자 전해질, 이온성 액체, 이온겔, 실세스키옥산, 이온성 액정, 리튬 전지

학번: 2012-31301 성명: 이진홍